INL/EXT-21-64168

Light Water Reactor Sustainability Program

Scalable Technologies Achieving Risk-Informed Condition-Based Predictive Maintenance Enhancing the Economic Performance of Operating Nuclear Power Plants

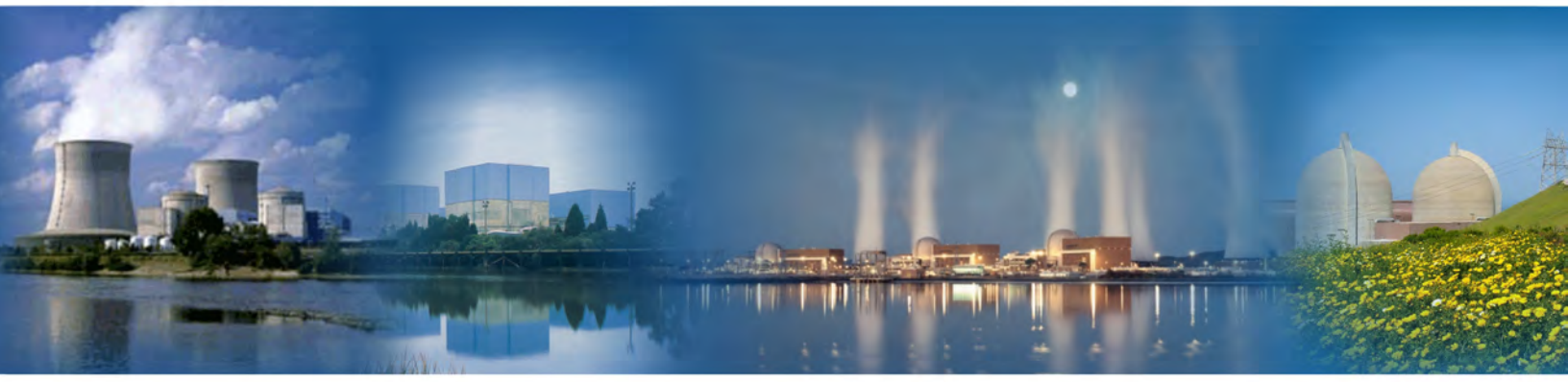

August 2021

U.S. Department of Energy

Office of Nuclear Energy

INL/EXT-21-64168

Scalable Technologies Achieving Risk-Informed Condition-Based Predictive Maintenance Enhancing the Economic Performance of Operating Nuclear Power Plants

Vivek Agarwal, Koushik A. Manjunatha, Andrei V. Gribok, Torrey J. Mortenson, Han Bao, Randall Reese, Thomas Ulrich, and Ronald L. Boring

Harry Palas
Public Services Enterprise Group, Nuclear LLC

August 2021

Prepared for the
U.S. Department of Energy
Office of Nuclear Energy

ABSTRACT

The primary objective of the research presented in this report is to develop scalable technologies deployable across plant assets and the nuclear fleet in order to achieve risk-informed predictive maintenance (PdM) strategies at commercial nuclear power plants (NPPs). Over the years, the nuclear fleet has relied on labor-intensive, time-consuming preventive maintenance (PM) programs, driving up operation and maintenance (O&M) costs to achieve high capacity factors. A well-constructed risk-informed PdM approach for an identified plant asset was developed in this research, taking advantage of advancements in data analytics, machine learning (ML), artificial intelligence (AI), physics-informed modeling, and visualization. These technologies would allow commercial NPPs to reliably transition from current labor-intensive PM programs to a technology-driven PdM program, eliminating unnecessary O&M costs.

The work presented in the report is being developed as part of a collaborative research effort between Idaho National Laboratory and Public Service Enterprise Group (PSEG) Nuclear LLC. This report (1) reflects the results of work by LWRS program researchers on the PSEG-owned Salem and Hope Creek nuclear power plants (NPPs); (2) presents the utilization of circulating water system (CWS) heterogeneous data and fault modes from both the Salem and Hope Creek NPP sites in order to develop salient fault signatures associated with each fault mode; (3) describes the integration of component-level predictive models into a robust, system-level model enabled by federated-transfer learning; (4) describes the development of a physics-informed model of the circulating water pump (CWP) and motor; (5) develops a scalable risk and economic model; and (6) outlines the development of a user-centric visualization application.

The outcomes presented in this report lay the foundation and provide a much-needed technical basis for focusing on the explainability and trustworthiness of ML- and AI-based technologies as part of future research.

Page intentionally left blank

EXECUTIVE SUMMARY

In support of the U.S. Department of Energy Office of Nuclear Energy's priorities for the existing nuclear fleet, research, development, and deployment of scalable, cost-effective technologies enabling risk-informed predictive maintenance (PdM) in commercial nuclear power plants (NPPs) were conducted. Implementation of a scalable, risk-informed PdM program is critical for long-term safe, economical operation of NPPs, leveraging automation to achieve efficiency gains and enhanced reliability of plant systems. Over the years, the nuclear fleet has relied on labor-intensive, time-consuming preventive maintenance (PM) programs to operate and maintain plants systems in order to achieve high capacity factors, leading to high operation and maintenance (O&M) costs. Research, development, and demonstration of scalable technologies through public/private partnerships and application of advanced machine learning (ML) techniques have paved the way for deploying a risk-informed PdM program that has otherwise proven elusive thus far. This notable outcome involves working with the commercial nuclear power industry to develop a deployable risk-informed PdM strategy that is achieved by integrating three scalable technologies: (1) advanced data analytics to continuously monitor and analyze data for the identified plant system, (2) a federated-transfer learning predictive modeling approach coupled with risk models to assess the economics of automation; and (3) a user-centric visualization tool that helps plant personnel understand results and make informed decisions. Specifically, INL partnered with the Public Service Enterprise Group (PSEG) Nuclear, LLC to develop technologies and publish a report describing how deploying a risk-informed PdM strategy can enable the nuclear industry to achieve substantial cost savings and enhance its economic competitiveness in the energy market. A demonstration of some of these scalable technologies was implemented into a cloud-based centralized nuclear digital platform developed by PKMJ Technical Services LLC (now part of Westinghouse Electric Company). Comprehensive implementation of scalable technologies is envisioned for their nuclear digital platform, enabling industry-wide adaptation and implementation in the near future.

The notable contributions captured in the report are as follows:

- Reflect the results of work by Light Water Research Sustainability (LWRS) program researchers on the PSEG-owned Salem and Hope Creek NPPs.
- Present the utilization of circulating water system (CWS) heterogeneous data and fault modes from both the PSEG Nuclear, LLC plant sites in order to develop salient fault signatures associated with each fault mode. The ML diagnostic/prognostic models utilize these fault signatures to automatically determine the condition (*healthy* vs. *unhealthy*) of the CWS—a determination otherwise performed by subject matter experts at plant sites and/or monitoring and diagnostic (M&D) centers. The developed approach automatically categorizes a specific fault mode with a high degree of confidence, thereby offsetting the time-consuming, labor-intensive practices of the PM program.
- Achieve integration of component-level predictive models into a robust system-level model enabled by federated-transfer learning. Federated learning (FL) is a decentralized approach to ML: collecting data from CWS components across different units to develop robust models that are combined for representation in the ML algorithm (i.e., "model"). Transfer learning (TL) is an approach that allows application of a developed "model" to different but related systems within the same plant site, or to the same system (i.e., CWS) at different plant sites. This advancement is a *first-of-a-kind application* of federated-transfer learning in the nuclear industry.
- Develop a detailed, physics-informed model of a CWS motor and pump (M&P) set to capture the dynamics of CWS operation. This modeling approach provides the ability to simulate data associated with fault modes for which minimal or no evidence is available in historical plant process data, enabling the generation of comprehensive fault signatures to achieve robust predictive models.

- Achieve the coupling of a three-state Markov chain risk model and a prognostic model, using a proportional hazards model to derive probabilities reflecting NPP states (i.e., full-load operation, derate, and trip). These state probabilities are used to understand the *economics of automation* achieved by transitioning from a time-consuming, labor-intensive, cost-prohibitive PM program to a risk-informed PdM strategy.
- Outline the development of a user-centric visualization that provides the right level of information, in the right format, to the right person. The human-system interface (HSI) design, based on user-centric visualization guided principles, uses the design inputs provided by users from the PSEG-owned Salem and Hope Creek plants. This approach also focused heavily on ensuring that the ML models were transparent and explainable to skeptical users by implementing human-centered artificial intelligence concepts. The inputs were collected via a series of structured virtual interviews, and an initial prototype was evaluated in a second round of similar interviews. A representative user-centric HSI was developed using the Microsoft PowerBI platform.

The scientific accomplishments achieved under this notable outcome stem from developing innovative scalable technological solutions that signify advancements in (1) online asset monitoring, (2) data analytics, (3) modeling and simulation (M&S), (4) risk assessment methodologies, and (5) user-centered design strategies. These advancements are leading the transformation of the nuclear industry to adopt risk-informed PdM strategies. This adoption would drive automation, efficiency gain, enhanced reliability of plant systems, and substantial cost savings via dramatic reductions or elimination of unnecessary time-consuming, labor-intensive maintenance activities, thus helping nuclear power achieve economic competitiveness in the energy market. Transferring the scalable technologies to an industrial partner like PKMJ Technical Services LLC would enable their implementation into a cloud-based digital platform and broaden the possible implementation of technologies for use by industry to achieve the greatest return on investment, based on economies of scale.

The scalable risk-informed PdM research summarized in this report will continue through further planned activities under the Technology Enabled Risk-Informed Maintenance Strategy project. Specifically, future work will focus on the explainability and trustworthiness of ML- and AI-based technologies. These important, challenging aspects must be addressed prior to adoption by the nuclear industry. In parallel, LWRS researchers, in collaboration with industrial partners, will develop the technical requirements for an AI/ML data architecture, as well as analytics capabilities that support the implementation of the necessary trustworthy, explainable methodologies within a centralized digital platform.

ACKNOWLEDGEMENTS

This report was made possible through funding from the U.S. Department of Energy (DOE)'s Light Water Reactor Sustainability program. We are grateful to Alison Hahn of DOE and Bruce P. Hallbert and Craig A. Primer at Idaho National Laboratory (INL) for championing this effort. We thank John M. Shaver and Nikki M. Peterson at INL for the technical editing and formatting of this report. We thank Barry Pike III and Lauren M. Perttula of RED, Inc. for some of the graphics contained in the report. We would also like to thank Dillon Brennan at the PSEG-owned Hope Creek plant for his valuable technical contributions.

Page intentionally left blank

CONTENTS

FIGURES

TABLES

Page intentionally left blank

ACRONYMS

AI	artificial intelligence
CM	corrective maintenance
CWP	circulating water pump
CWS	circulating water system
DOE	Department of Energy
DP	discharge pressure
DT	differential temperature
eSOMS	Electronic Shift Operations Management System
FL	federated learning
HCAI	human-centered artificial intelligence
HSI	human-system interface
INL	Idaho National Laboratory
LWR	light water reactor
LWRS	Light Water Reactor Sustainability
M&D	monitoring and diagnostic
M&P	motor and pump
M&S	modeling and simulation
MA	motor axial
MIB	motor inboard
MOB	motor outboard
MK	multi-kernel
ML	machine learning
NN	neural networks
NPP	nuclear power plant
O&M	operation and maintenance
PDF	probability density function
PdM	Predictive maintenance
PM	Preventive maintenance
PSEG	Public Service Enterprise Group
PSD	power spectral density
R&D	research and development
RMSE	root mean square error
SV	support vector

SVM	support vector machine
TERMS	Technology-Enable Risk-informed Maintenance Strategy
TL	transfer learning
VSN	vibration sensor node
WO	work order
XAI	explainable artificial intelligence

SCALABLE TECHNOLOGIES ACHIEVING RISK-INFORMED CONDITION-BASED PREDICTIVE MAINTENANCE ENHANCING THE ECONOMIC PERFORMANCE OF OPERATING NUCLEAR POWER PLANTS

1. INTRODUCTION AND MOTIVATION

The primary objective of the research presented in this report is to develop scalable technologies that are deployable across plant assets and the nuclear fleet to achieve risk-informed predictive maintenance (PdM) strategies at commercial nuclear power plants (NPPs). Over the years, the nuclear fleet has relied on labor-intensive, time-consuming preventive maintenance (PM) programs, driving up operation and maintenance (O&M) costs to achieve high capacity factors. A well-constructed, risk-informed PdM approach for an identified plant asset has been developed in this research, taking advantage of advancements in data analytics, machine learning (ML), artificial intelligence (AI), physics-informed modeling, and visualization. These technologies would allow commercial NPPs to reliably transition from the current labor-intensive PM programs to a technology-driven PdM program (see Figure 1), thus eliminating unnecessary O&M costs.

Figure 1. Transition from a PM program to a risk-informed PdM program.

There is an immediate need to reduce the O&M costs (bundled with the labor-intensive PM program) associated with the current domestic fleet of NPPs (94 operating units). Operating in a market selling wholesale electricity for $22/MWh becomes unsustainable with current (as of 2019) total average operating costs for the entire fleet at $30.42/MWh (Figure 2). Prices for producing energy by nuclear plants have reduced since 2015 (Figure 2) but remain high compared to other energy sources. In addition, the global energy market trends are driven heavily by the abundant reserves of natural gas and the declining costs of renewable energy systems.

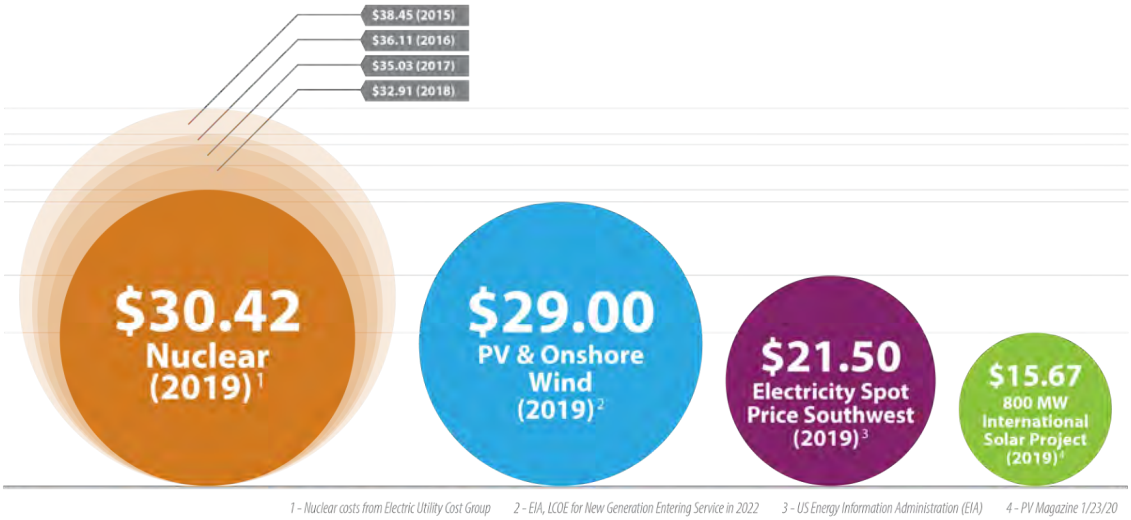

Figure 2. Total average operating costs ($/MWhr) for different energy sources.

Nuclear O&M costs involve manually performed inspection, calibration, testing, and maintenance of plant assets at periodic frequencies, along with time-based replacement of assets, irrespective of condition. This has resulted in a costly, *labor-centric business model*. Fortunately, technologies exist (advanced sensor, data analytics, and risk assessment methodologies) for enabling the transition to a *technology-centric business model* that will significantly reduce PM activities, driving down costs since labor is a rising cost and technology is a declining cost. This transition will also enable NPPs to maintain high capacity factors (and perhaps even achieve higher ones) while still significantly reducing O&M costs.

The scalability of the risk-informed PdM strategy presented in this report was developed by Idaho National Laboratory (INL), in collaboration with Public Service Enterprise Group (PSEG) Nuclear, LLC. To develop initial scalable methods, models, and visualization schemes, the circulating water system (CWS) at the PSEG-owned Salem and Hope Creek NPPs was selected as the identified plant asset. The CWS, an important non-safety-related system, is omnipresent across the fleet of existing light water NPPs. Traditionally, most PdM approaches in the nuclear industry are developed at the component level [1-5]. This approach is not holistic, and presents challenges when scaled to the system or plant level. Furthermore, it prevents NPP sites from reaping the maximum benefits in terms of automation, optimization of labor and material resources, cost savings, etc. The research approach presented in this report addresses these limitations.

The research and development (R&D)—along with notable outcomes—reported here are part of the Technology Enabled Risk-Informed Maintenance Strategy (TERMS) project sponsored by the U.S. Department of Energy (DOE)'s Light Water Reactor Sustainability (LWRS) program. The LWRS program is an R&D program conducted in close partnership with industry to provide the technical foundations for licensing, managing, and economically operating the current fleet of NPPs. To achieve both program and pathway goals [6], a series of pilot projects are underway to develop and demonstrate new technologies that can affect transformative change in NPP operations and support.

The TERMS pilot project is developing the necessary technologies and methodologies to achieve performance improvements through a transformative transition to PdM. This research is designed to help nuclear industry officials understand the benefits of advanced data analytics and risk methodologies in eliminating unnecessary costs associated with labor-intensive, time-based PM programs at NPPs. To deliver this message and enable the transition to risk-informed PdM across plant systems and the nuclear fleet, the report presents the scalability R&D activities performed on the CWS at two plant sites.

The challenges facing the industry are clearly understood by regulators, operators, and vendors alike, but particular roadblocks make changes difficult to implement. The PdM R&D plan [7] laid the foundation for real-time condition assessment of plant assets. Successful execution of this plan will result in the development of a deployable PdM program for plant use, enhancing safety, reliability, and the economics of operation.

1.1 Framework to Scale the Risk-Informed Predictive Maintenance Strategy

These R&D efforts focus on the optimization and automation of maintenance activities as an essential part of the industry's strategy for modernizing and sustaining the existing fleet of operating light water reactors. Previous R&D focused on outlining a framework to achieve scalable, risk-informed PdM strategies [8]. Specifically, implementation of technologies to ensure scalability across plant systems and the nuclear fleet is critical to the deployment of a risk-informed PdM strategy at commercial NPPs. For this research, *scalability is defined as expanding the capabilities of a target entity to meet current and future application-specific requirements*. "Entity" in this context is defined as an element of the suggested framework shown in Figure 3.

The elements of the framework shown in Figure 3 include data generation and governance, methodologies, visualization, infrastructure, and organizational alignment. For details on each element (i.e., entity) of the framework, refer to [9]. All elements of the framework must be reliable, acceptable, maintainable, and secure. Furthermore, each element should be flexible, modular, and simple, with an appropriate level of redundancy.

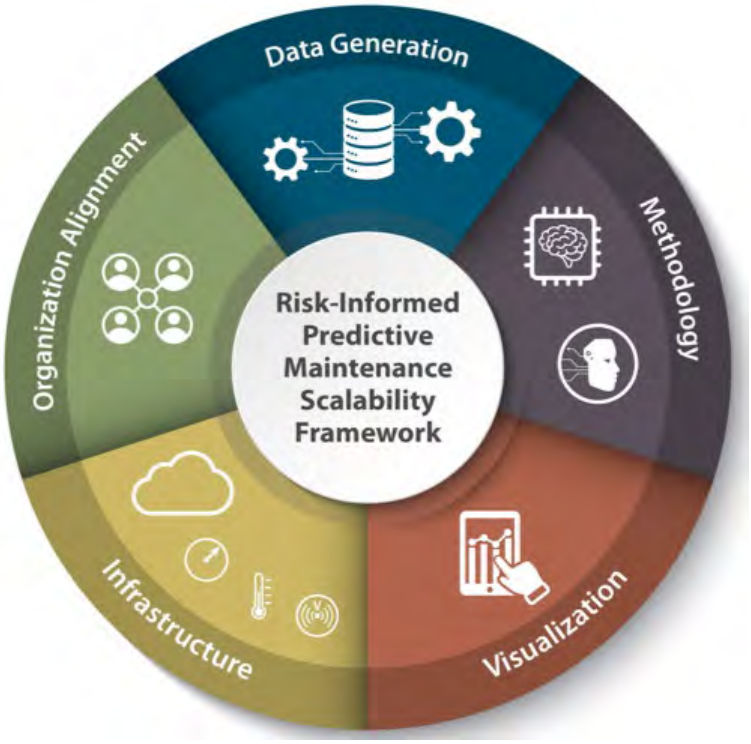

Figure 3. A framework to scale the risk-informed predictive maintenance strategy.

1.2 Research Approach and Contributions

For the identified plant system (i.e., CWS, in this research), the approach (shown in Figure 4) to develop a scalable, deployable, risk-informed PdM strategy for PSEG's Salem and Hope Creek plants is followed. This aligns with the scalable framework presented in Figure 3.

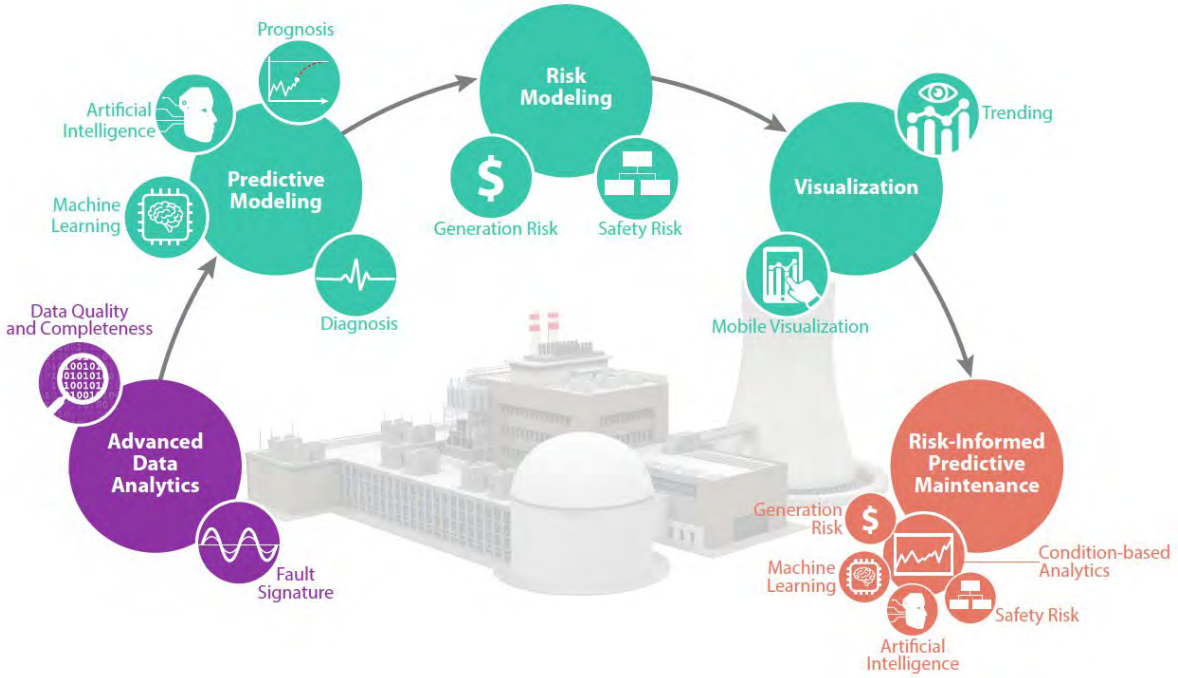

Figure 4. R&D approach enabling a risk-informed PdM strategy adoptable by commercial NPPs for an identified plant asset.

To follow the approach in Figure 4, significant analysis of the heterogeneous data (plant process data, vibration data, work order [WO] data, set-point information, and replacement/repair data) collected at different temporal and spatial resolutions is performed initially, and corroborated to ensure data completeness. In addition, data analysis includes addressing data quality issues such as missing values, outliers, duplicate values and timestamps, and bad data resulting from instrumentation errors or incorrect manual entries. The cleaned dataset is used to develop fault signatures for CWS faults of interests.

A fault signature is a unique set of features associated with a specific fault mode. Fault signatures are used to develop predictive models (i.e., diagnostic and prognostic). ML approaches such as support vector machines (SVMs) and neural networks (NNs) utilize these fault signatures to automatically and accurately estimate a CWS's current state of health. Based on the estimate, a prognosis can be performed to understand the CWS's future state of health, based on forecasted values of the fault signatures. This allows the plant system engineer to prepare for specific actions and resources needed to address the issue and prevent a forced shutdown scenario.

The diagnostic and prognostic model outputs are integrated with a generation risk modeling approach. The CWS is a non-safety system and does not impact plant safety. However, the operational efficiency of the CWS impacts the power generation capability of the plant unit. Integrating time and state of health into static risk models enables dynamic risk assessment, which, in turn, is used to estimate the economic benefits of condition-based maintenance strategies.

Each previous stage of the approach generates a different type of information of interest to various plant staff, including but not limited to monitoring and diagnostic (M&D) center staff, system engineers, maintenance and engineering staff, planners, and utility corporate staff. Thus, it is important to design a user-centric visualization interface that provides correct information, in the right format, at the right time, to the right person.

When seamlessly integrated, these stages of the approach result in a scalable, deployable, risk-informed PdM strategy. The research advancements and innovations achieved by following the approach (laid out in Figure 4) are the notable contributions captured in this report. These include:

- Utilize CWS heterogeneous data and fault modes from both the PSEG plant sites to develop salient fault signatures associated with each fault mode. The resulting ML diagnostic/prognostic models utilize these fault signatures to automatically determine the CWS's condition (i.e., *healthy* vs. *unhealthy*)—a task otherwise performed by subject matter experts at plant sites and/or M&D centers. The developed approach automatically categorizes a specific fault mode with a high degree of confidence, offsetting the time-consuming, labor-intensive practices of the PM program.
- Integrate component-level predictive models into a robust system-level model enabled by federated-transfer learning. Federated learning (FL) is a "decentralized" approach to ML: collecting data from CWS components across different units to develop robust models that are combined into an aggregated ML model. The transfer learning (TL) approach enables application of the developed aggregated model to different but related systems within the same plant site, or to the same system (i.e., CWS) at different plant sites. This advancement is a *first-of-a-kind application* of federated-transfer learning in the nuclear industry.
- Develop a detailed, physics-informed model of a circulating water pump (CWP) and motor set to capture the dynamics of CWS operation. This modeling approach offers the ability to simulate data associated with fault modes for which minimal or no evidence is available in historical plant process data, enabling generation of comprehensive fault signatures to achieve robust predictive models.
- Achieve the coupling of a three-state Markov chain risk model and a prognostic model by using a proportional hazards model to derive probabilities reflecting NPP states (i.e., full-load operation, derate, and trip). These state probabilities are used to understand the *economics of automation* achieved by transitioning from a time-consuming, labor-intensive, cost prohibitive PM program to a risk-informed PdM strategy.
- Outline the development of a user-centric visualization that provides the right level of information, in the right format, to the right person. The human-system interface (HSI) design, based on user-centric visualization guided principles, uses the design inputs provided by users from the PSEG-owned Salem and Hope Creek plants. This approach also focuses heavily on ensuring that the ML models are transparent and explainable to skeptical users by implementing human-centered artificial intelligence (HCAI) concepts. The inputs were collected via a series of structured virtual interviews, and an initial prototype was evaluated throughout a second round of similar interviews. A representative user-centric HSI was developed using the Microsoft PowerBI platform.

The scientific accomplishments achieved under this notable outcome stem from developing innovative scalable technological solutions that signify advancements in (1) online asset monitoring, (2) data analytics, (3) modeling and simulation (M&S), (4) risk assessment methodologies, and (5) user-centered design strategies. These advancements are leading the transformation of the nuclear industry to adopt risk-informed PdM strategies. This adoption would drive automation, efficiency gains, enhanced reliability of plant systems, and substantial cost savings via dramatic reduction or elimination of unnecessary, time-consuming, labor-intensive maintenance activities, thus helping nuclear power to

achieve economic competitiveness in the energy market. Transferring the scalable technologies to an industrial partner such as PKMJ Technical Services LLC would enable their implementation into a cloud-based digital platform and broaden the possible implementation of technologies for use by industry to achieve the greatest return on investment, based on economies of scale.

1.3 Report Layout

This report is organized as follows:

- Chapter 2 describes the heterogeneous CWS data analyzed to develop fault signatures for fault modes of interest for both the Salem and Hope Creek NPPs.
- Chapter 3 presents the details of the federated-transfer learning approach. Utilizing the Salem plant's CWS fault signatures, federated predictive models were developed using multi-kernel (MK) SVM and artificial NN approaches. The federated predictive models were used to assess the state of health of the Hope Creek CWS as part of TL.
- Chapter 4 presents the development of a detailed, physics-informed model of a CWS motor and pump (M&P) set in order to capture the dynamics of CWS operation. This model allows for generating simulated data for fault scenarios for which limited (or no) data were historically available.
- Chapter 5 describes the three-state plant-level Markov chain process to address the scalability of risk models. The risk model is coupled with the predictive model via a proportional hazard model in order to determine the real-time probabilities of being in any of the three states. These probabilities are then used to understand the economics of automation.
- Chapter 6 describes the development of a user-centric visualization. This approach also focuses heavily on ensuring that the ML models are transparent and explainable to skeptical users by implementing HCAI concepts.
- Chapter 7 summarizes the research accomplishments and presents a path forward in advancing R&D activities.

2. DATA ANALYTICS AND FAULT SIGNATURES

This chapter describes the CWS at the PSEG-owned Salem and Hope Creek NPPs, this CWS being the asset selected for demonstrating PdM. Heterogeneous data related to the CWS were made available from both plant sites. The data include plant process data, WO data, CWP and CWP motor replacement data, fault modes, and real-time vibration data. These heterogeneous data were analyzed to understand CWS operation and its relationship to power generation, then used to develop salient fault signatures for each fault mode of interest. These faults signatures were used to build predictive models to understand the state of health of the CWS (see Section 3).

2.1 Circulating Water System

The CWS is an important non-safety-related system. As the heat sink for the main steam turbine and associated auxiliaries, the CWSs at the Salem and Hope Creek NPPs are designed to maximize steam power cycle efficiency while minimizing any adverse impacts on the Delaware River [10]. An NPP CWS has two salient functions: strain the water before it is pumped through the condenser, and cool the steam in the condenser. The thermodynamic efficiency of the plant is largely determined by the operational effectiveness of the CWS, which must also comply with the constraints imposed by the Environmental Discharge Restrictions set by the state of New Jersey.

A CWS consists of the following major equipment [10]:

- Vertical, motor-driven circulating pumps (i.e., "circulators"), each with an associated fixed trash rack and traveling screen at the pump intake to filter out debris and marine life
- Main condenser (tube side only)
- Condenser waterbox air removal system
- Circulating water sampling system
- Screen wash system
- Necessary piping, valves, and instrumentation/controls to support system operation.

The Salem NPP (a two-unit pressurized water reactor) features six circulators at each unit. Schematic representations of the main condensers for Salem Units 1 and 2 are shown in Appendix A, in Figures A-1 and A-2, respectively. Each pair of waterboxes is named using the following convention: Unit #, Condenser #A, and Unit #, Condenser #B. Figure 5 shows the pair of waterboxes associated with condenser 1 of Unit 1 (i.e., 11A and 11B).

The Hope Creek NPP (a single-unit boiling water reactor) has four circulators. A schematic representation of the Hope Creek CWS is shown in Figure 6, and several distinct differences when compared to the Salem CWS can be seen. These include: (1) the water supply to the Hope Creek CWS comes from a cooling tower water basin, not directly from the Delaware River; (2) the Hope Creek CWS does not have traveling screens, but each circulator has a single-pump screen to prevent debris transmission to the waterboxes; and (3) the Hope Creek CWS has four circulators feeding six waterboxes via a common header, unlike the Salem CWS, in which each waterbox had its own circulator.

A general functional description of the Salem CWS, component integration, and design basis are found in [10]. This description is similar to that regarding the Hope Creek NPP, with minor differences in the integration as a result of previously highlighted changes in the design basis. The CWS equipment that most impacts the unit's gross load output are the CWPs and CWP motors. The number of CWPs operating together impacts the generated gross load. A derate is a percentage decrease in gross load, due to unavailability of plant assets supporting power generation. A trip is a reactor shutdown in which one or more plants assets are unavailable, leaving the plant unable to maintain safe reactor operation. An outage occurs when the reactor power is at zero for an extended period of time (though usually less than a month) to address scheduled fuel cycle maintenance. During this time, all the plant assets are non-operational, leading to an observable pattern in the plant gross load: labeled as operational, derate, trip, and outage. As the CWS is the focus of this report, distinctions between the derates and the trips caused by this system and other plant systems—for both the Salem and Hope Creek plants—are shown in Figure 7 and Figure 8 respectively. The patterns shown in these figures are observable across the entire domestic NPP fleet.

For the Salem NPP, a derate in the plant generation occurs when 1–3 CWPs in a unit are unavailable at any given time. The magnitude of the derate is mainly determined by the number of CWPs unavailable

at that specific time, along with some other minor factors. If 4–5 CWPs in a Salem unit are unavailable at any given time, the unit would trip.

For the Hope Creek NPP, a derate in plant generation occurs when 1–2 CWPs in the unit are unavailable at any given time. The magnitude of the derate is mainly determined by the number of CWPs unavailable at that specific time, as well as by some other minor factors. However, the impact of the CWS on Hope Creek's power generation is also influenced by the season. During the summertime period, the unit operates all four CWPs to maintain full power, and unavailability of even a single CWP would result in a derate. Outside this summertime period, the unit can maintain full power with three of the four CWPs operating (i.e., if the unit is operating all four CWPs outside the summertime period, one CWP can be removed for maintenance [or any other reason] without impacting [i.e., derating] the power generation [see Figure 9]). In Figure 9, the gross load values in blue represent all four pumps being run simultaneously, whereas the gross load values in red indicate only three pumps being run. The summer of 2014 is highlighted via a pink background. Note that, during summer, a derate occurs whenever a single pump goes offline. However, this is not the case for the non-summer months.

In addition, numerous gross load derates unassociated with any loss of Hope Creek CWPs were observed (i.e., all four pumps were fully operational, yet a drop in gross load occurred). These derates are attributable to plant systems at Hope Creek that are not part of the CWS. Further exploration of the cause of these gross load dips may be in order. In particular, the large derates in mid-2019 and early-2021 should be further examined. See Figure 10 for a plot of all the Hope Creek plant derates not attributable to the CWS. Red represents instances that occurred in summer, blue represents non-summer instances.

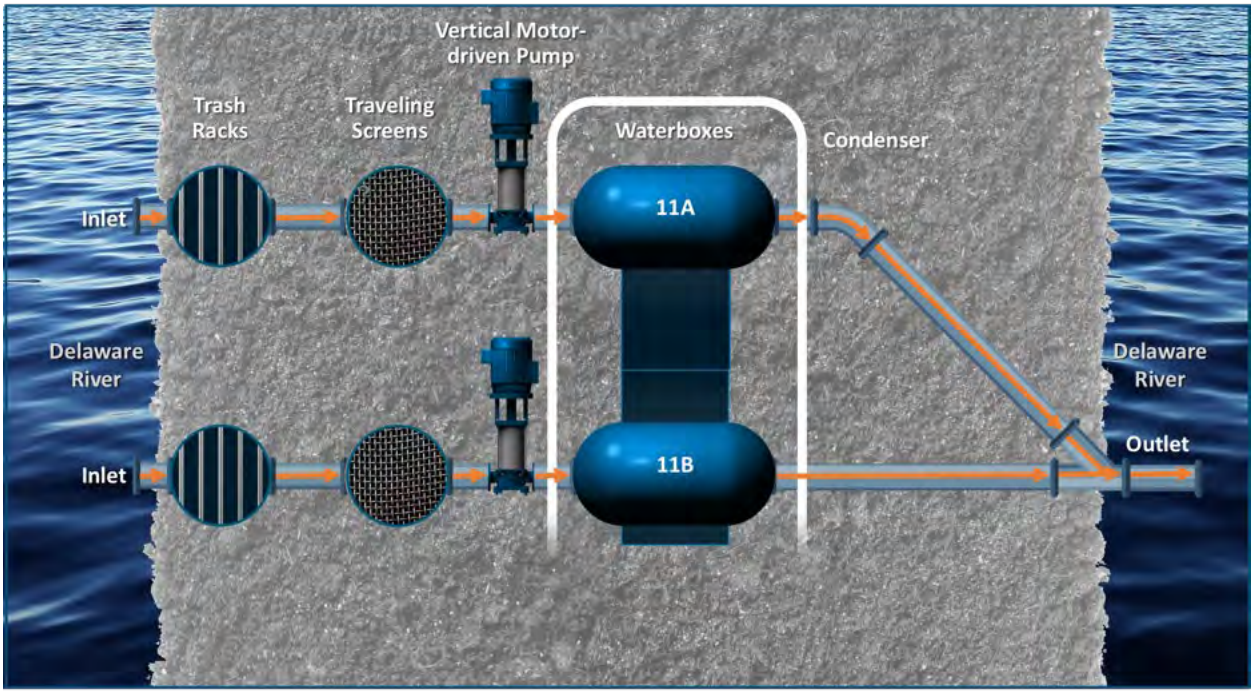

Figure 5. Schematic representation of the Salem CWS in Unit 1.

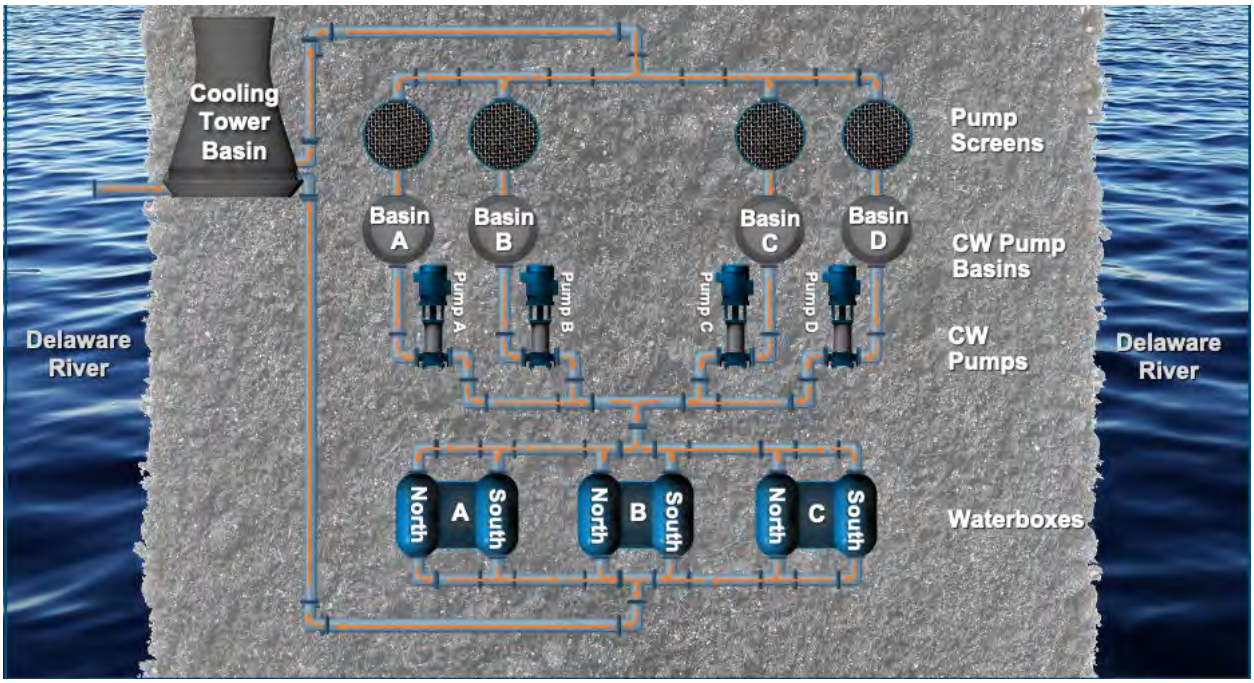

Figure 6. Schematic representation of the Hope Creek CWS.

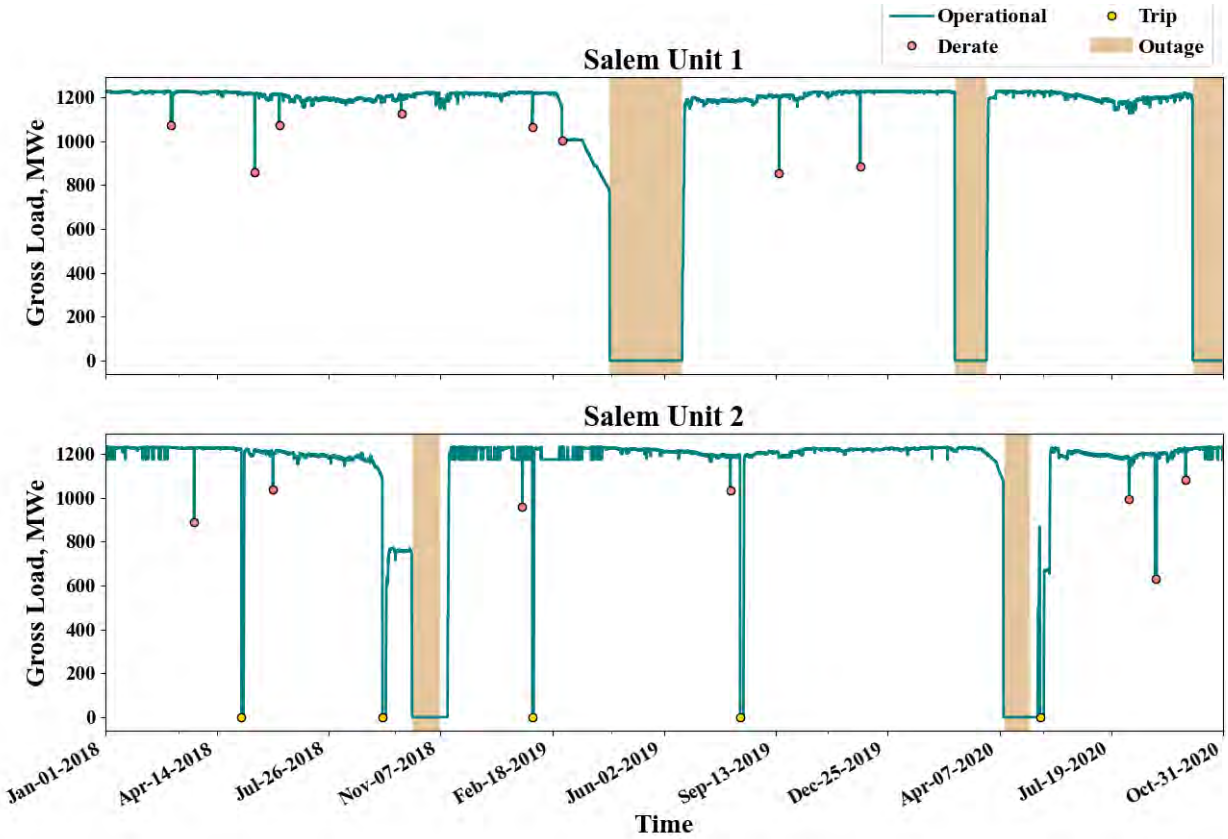

Figure 7. Relationship between number of CWP motors operating and gross load for Salem Units 1 (top) and 2 (bottom).

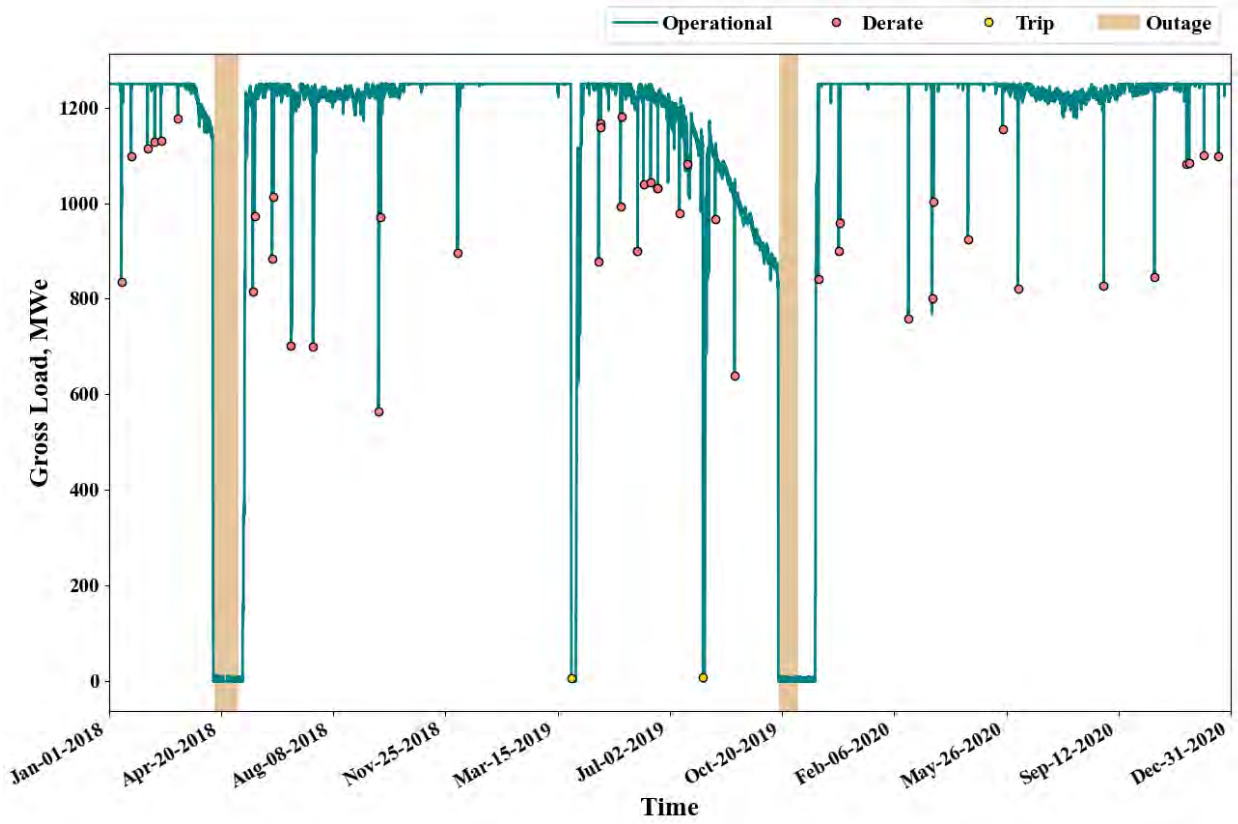

Figure 8. Relationship between number of CWP motors operating and gross load for Hope Creek.

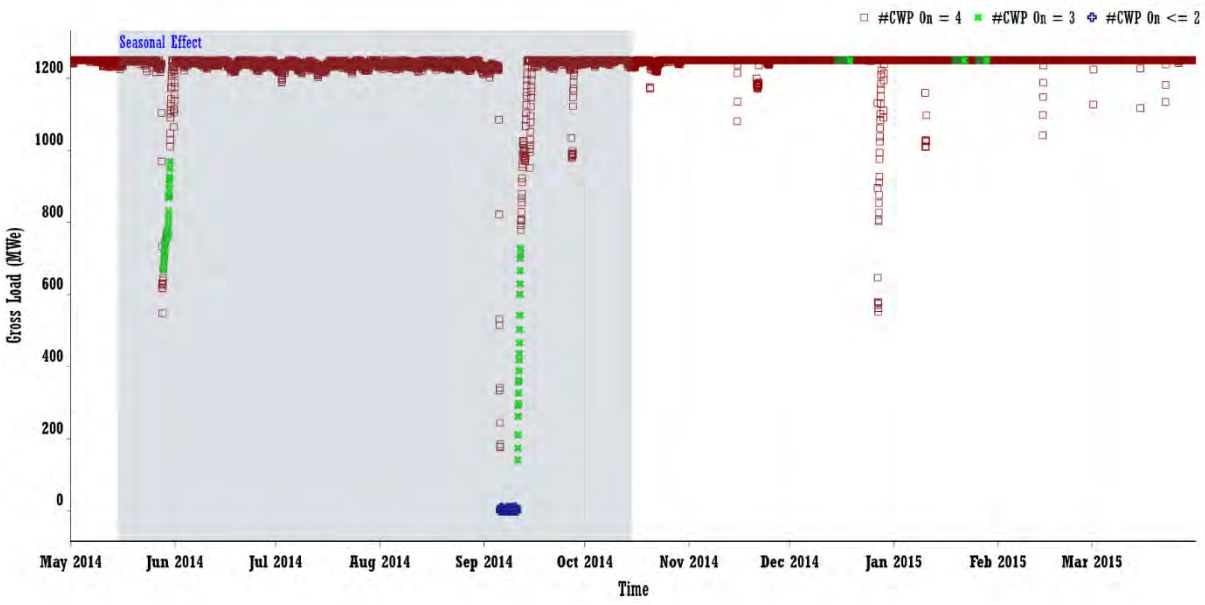

Figure 9. Seasonal impact on the number of pumps required to maintain full gross load at Salem.

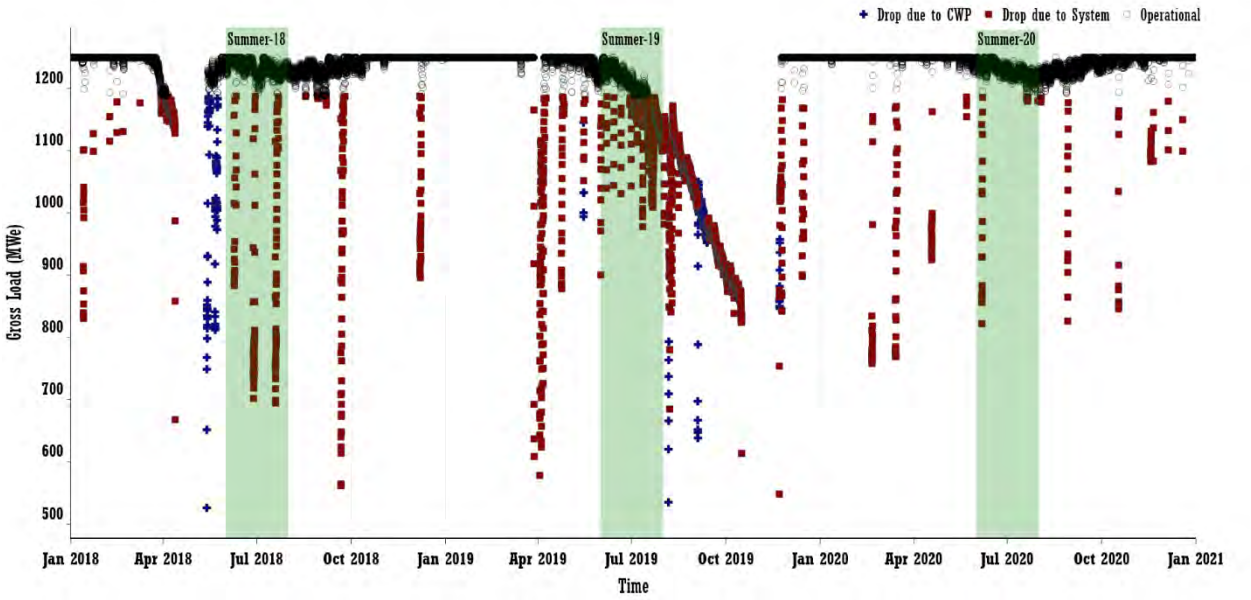

Figure 10. Decrease in Hope Creek gross load, due to CWS and non-CWS issues.

2.2 Circulating Water System Data

Presented here is a discussion on the data from the CWS in Salem Units 1 and 2 for the time period of January 2009 to December 2020, and from the Hope Creek CWS for the time period of January 2010 to May 2021. Data collected from the plant system contain metadata related to plant processes, maintenance logs, operator logs, and condenser information. Typical plant process data relevant to the CWS include gross load, river inlet/outlet temperatures, and motor-related information such as on-off duration/status, motor current, and temperature measurements at the motor stator and bearings. Condenser data include condenser backpressure, exhaust temperature, exhaust hood temperature, condensate hotwell temperature, and vacuum pump status. Additional datasets include river level, river inlet/outlet temperatures, operator actions, discharge header pressure, and ambient air temperature. The similarities and differences in the CWS data when comparing the Salem and Hope Creek NPPs are summarized in Appendix B, Tables B-1–B-6.

2.2.1 Salem Circulating Water System Data

The Salem Unit 1 and Unit 2 CWS process data are collected once per minute and stored in the Salem plant's OSIsoft Process Information system. Due to file size restrictions, the project team received CWS process data on an hourly frequency for both units, from 2009 to 2020. Since the start of the project, the data were shared periodically via a secured file portal and stored on a secure, INL-approved platform. Continuous CWP motor current data for both Units 1 and 2 are available only from September 2017 onward. Figure 11 shows a sampling of CWS process data for a Salem unit. Along with the process data, the CWP inlet pressure is collected every 12 hours in the electronic Shift Operations Management System (eSOMS).

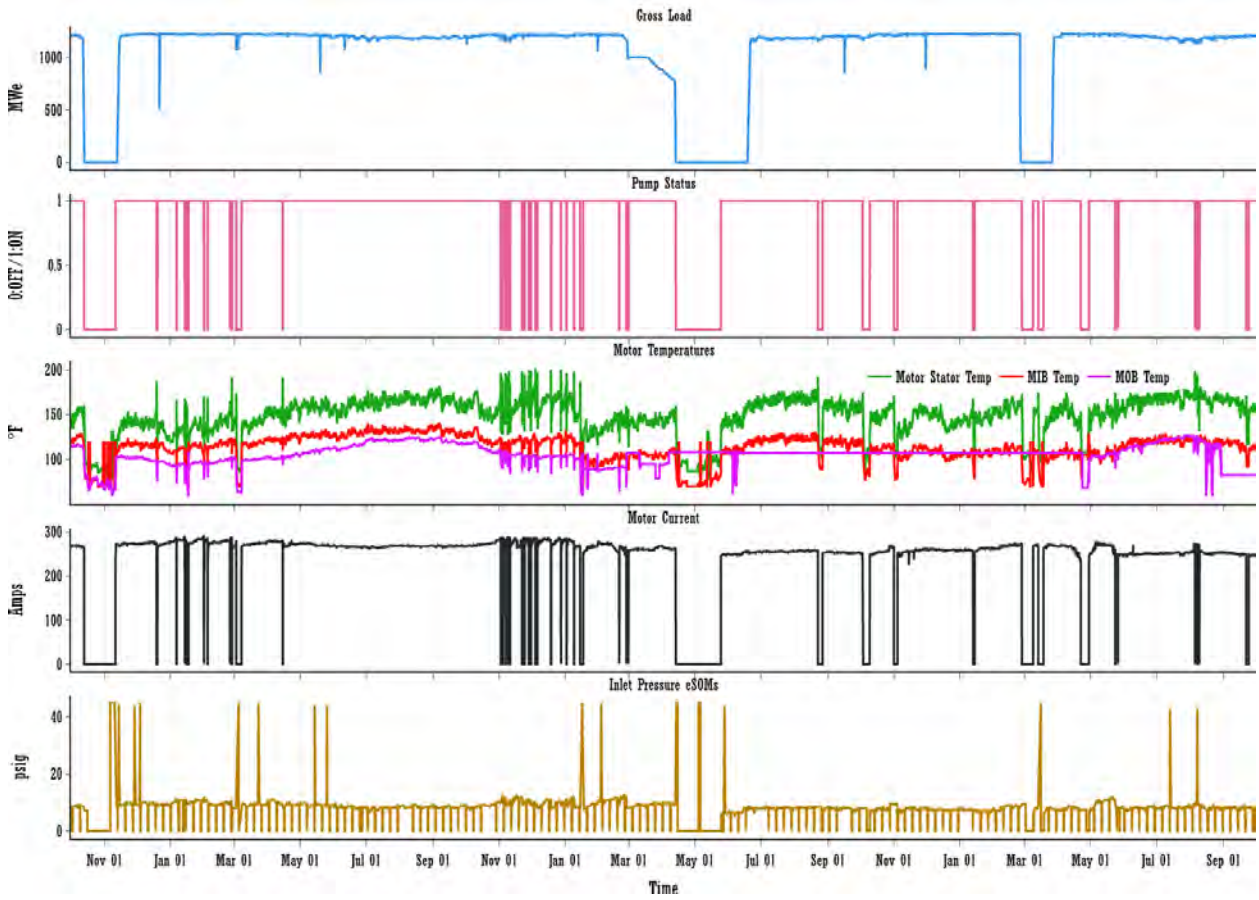

Figure 11. Sampling of CWS measurements from a Salem unit.

PSEG performs periodic vibration measurements on the CWP motors. PKMJ and INL worked with PSEG to install wireless vibration sensor nodes (VSNs) from KCF Technologies on the CWP motors of Salem Units 1 and 2, as described in [4]. Sixty VSN-3 sensor nodes [11] were installed across 12 Salem NPP CWP motors and the associated CWP bypass valves. Three wireless VSNs were installed on each CWP motor, and two were installed on each associated CWP bypass valve at the plant site. The three VSNs installed on the CWP motors measure motor axial (MA) vibrations, motor outboard (MOB) bearing vibrations, and motor inboard (MIB) bearing vibrations. The placement of the transducers on the CWP motors and the bypass valves can be found in [4,5]. Each VSN consists of a temperature sensor and two accelerometers sensitive to orthogonal in-plane motions. The VSNs were mounted on the plant asset via a magnetic base in the node.

The vibration data consist of metadata such as date (format: YYYY-MM-DD), time (format: Coordinated Universal Time), and sampling rate of the vibration signal. The vibration signal is collected for 3.2 seconds at a sampling rate of 512 samples/second. The vibration signal can be collected for different lengths of time and at higher sampling rates (up to 2,056 samples/second).

Installation of wireless VSNs enables continuous vibration monitoring of CWP motors, eliminating the need for periodic vibration-measurement PM. The collection of continuous vibration measurements, as part of the CWS process data, enhances the diagnosis and prognosis of CWP motor conditions. Figure 12 shows a representative vibration signal for both directions from the VSN located on the MA position.

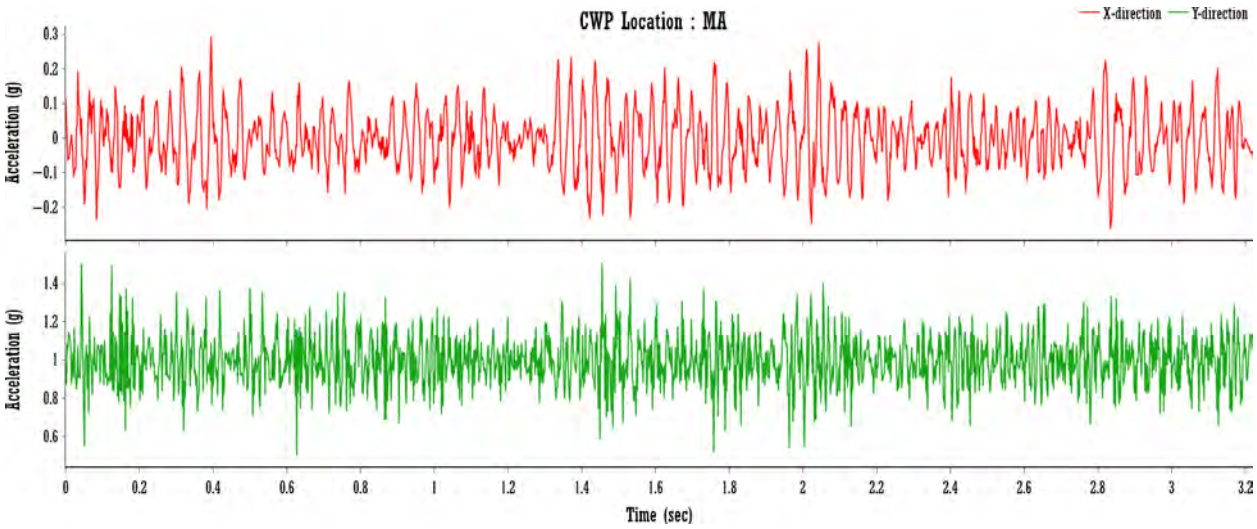

Figure 12. Vibration measurement collected at the MA location on a CWP motor for VSN directions x and y.

These vibration signals were initially made available to the project team via a secure KCF cloud platform [4]. PKMJ Technical Services later developed an application programing interface that enabled continuous download of vibration data between PKMJ and INL. For details on the application programing interface requirements, see [12].

2.2.2 Hope Creek Circulating Water System Data

The Hope Creek CWS data consist of hourly measurements spanning from January 1, 2010, to May 18, 2021. Overall plant status data include gross load in megawatts and a 15-minute average of the ambient outside temperature. Each of the four CWPs measurements include the basin level, discharge pressure (DP), motor winding temperature, vibration (see below), MA position, outbound and thrust bearing temperatures, and discharge valve position. The pump run status (on/off) is also recorded. Figure 13 shows a sampling of CWS process data from the Hope Creek plant.

We have intermittent vibration data for each of the four Hope Creek CWPs. The main periods of record are hourly recordings between January 16 and December 28, 2017, and November 5, 2019, and May 18, 2021. Three types of vibration data were recorded: inbound bearing radial vibration, MIB radial vibration, and MOB radial vibration. Each of these metrics was recorded in both the horizontal and vertical directions. An example plot of this data for a CWP (MIB radial vibration) is shown below in Figure 14. The status of a CWP is included; note that the dips in the vibration data directly relate to the pump being off. Vibration plots for bearing radial vibration and MOB vibration are similar.

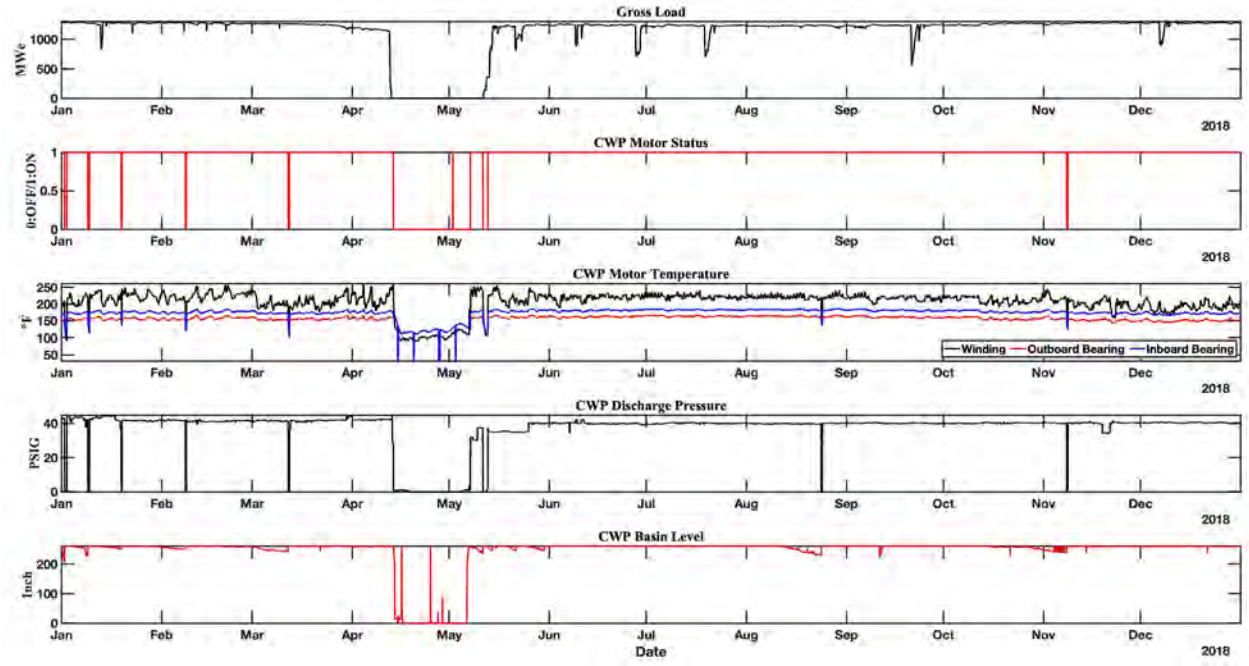

Figure 13. Sample process data from a Hope Creek CWP.

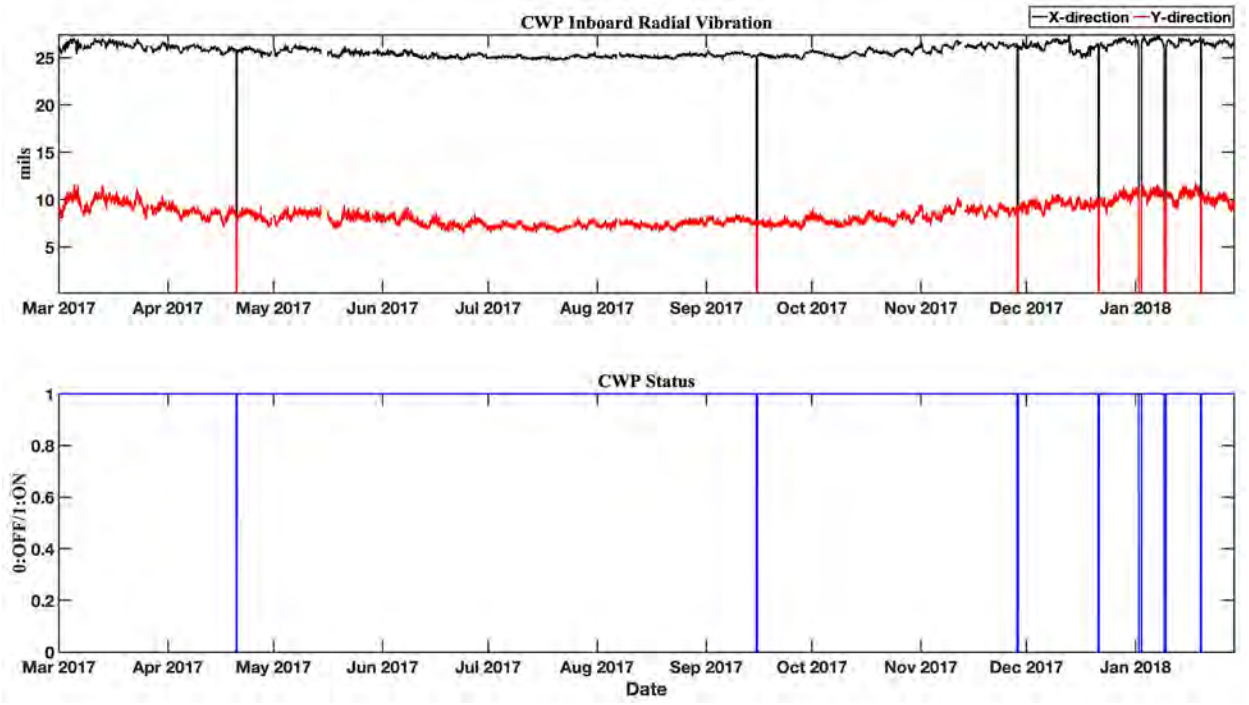

Figure 14. Example MIB radial vibration data for a Hope Creek CWP.

2.3 Fault Modes

The Salem and Hope Creek CWSs experienced several types of faults in the time span for which the data were analyzed. Salem and Hope Creek NPP system engineers and the staff at PSEG's M&D center

used their subject matter expertise, along with different process parameter alarm limits, to diagnose these faults and recommend mitigative actions. This is a reactive, unoptimized approach.

These faults (Table 1) are infrequent, but failure to diagnose them in a timely manner result in unexpected downtime, derates, or trips, causing a drop in gross load that, in turn, leads to foregone revenue (i.e., lost opportunities to generate electricity and revenue) and additional maintenance costs. Based on the period encompassing the data made available for analysis (i.e., 2008–2021 for Salem, and 2010–2021 for Hope Creek), some fault types resulted in multiple plant derates and trips (thus impacting plant generation), while others impacted plant generation only once, or not at all.

For these diagnosed faults, relevant CWS process data, vibration sensor data, and WO data associated with the CWS were used to develop a condition-based monitoring solution. The CWS WO data [4] were used to create an approximate timeline of when faults occurred and were corrected, in addition to a timeline of PM activities. The fault timeline is particularly important for identifying possible fault features relevant to the fault modes listed in Table 1. ML models can be used to make such diagnoses based on fault signatures.

Table 1. CWS faults observed at the Salem and Hope Creek NPPs.

Salem NPP CWS Faults	Hope Creek NPP CWS Faults
Waterbox fouling	Waterbox fouling
CWP diffuser	Heating, ventilation, and air conditioning inlet/outlet issue
CWP bellmouth	Motor bearing oil level
CWP shaft misalignment	CWP screen clogging
Clogging in air intake screens of the CW motors	CW motor bearing
Moisture and salt contamination of CW motor windings	
CW motor oil level (low)	

2.4 Fault Signatures

Fault signatures enable informed decision-making to prevent potential failure of the plant asset. They can also be used for root cause analysis if failure occurs. The different fault modes associated with a plant asset (i.e., the CWS, in this report [Table 1]) have unique, consistently identifiable fault signatures. In practice, fault signature identification and diagnosis are not straightforward and can benefit from analyses of historical data. Each detected fault signature for a particular degradation mode should have enhanced feature verification and confidence by selecting additional process and condition monitoring data that provides complimentary information.

Of the faults of interest (Table 1) examined during this project, only four fault types had multiple instances that resulted in CWP shutdowns. The multiple occurrences of these faults strengthen the fault signature analysis and its usage for training/testing ML algorithms. Waterbox fouling caused numerous instances of CWP shutdowns, even though this fault is not a pump or motor fault, but a system fault that may show symptoms affecting pump performance. The waterbox fault also occurred numerous times, allowing for development and testing of condition-based monitoring algorithms. Fault types with only a single instance of causing a CWP shutdown provided limited information for developing a fault signature and training ML algorithms. The potential fault signatures contained within the data are not readily

resolvable at this time. A potential way of addressing this sparseness in some of the fault signatures is to leverage simulated data generated from the first-principals model of the CWS M&P set (see Section 4). It is anticipated that, as ML technology matures for operational plant applications, these subtle faults will be identified.

This section of the report discusses two examples of waterbox fouling. The first is from the Salem NPP and the second from the Hope Creek NPP. The two examples highlight the similarities and differences in the fault signatures for waterbox fouling and are a perfect lead-in as to why federated-transfer learning is required for predictive modeling. (See Section 3 for further discussion on FL.)

The primary issue noted with the Salem CWS is fouling of the waterboxes by grass and debris. Fouling of the waterboxes typically occurs due to accumulation of grass/debris in the waterbox, resulting in condenser tube blockage and reduced circulator water flow. This is a unique and frequent issue at Salem; the Salem CWP intake comes directly from the Delaware River, which produces a significant quantity of grass/debris. The grassing season typically occurs between February 1 and May 31 [10]. Grassing often emerges from the river during high-wind conditions associated with storms. During these periods, the motor current can oscillate with river level changes. Operations monitors the waterbox motor current and inlet pressure, and schedules waterbox cleanings, based on deviations in motor current and inlet pressure when compared against historical baseline data. Waterbox fouling is typically identified via:

- Motor current increase (also, though far less frequently, motor current decrease)
- Inlet pressure increase
- Waterbox differential temperature (DT) increase
- Condenser thermal performance loss.

Figure 15 shows an instance of waterbox fouling diagnosed in Salem Unit 2's CWP 22B. An upward drift in DT and motor current was identified on July 23, 2018. Consequently, the gross load began to dip. Note that, in Figure 15, the CWP 22B motor current increased from 231 to 245 amps, and the DT increased from 14 to 16°F, with the gross load not trending as expected. The motor current and DT decreased to 220 amps and 14°F, respectively, following the waterbox cleaning on August 25, 2018, resulting in a 30–40 MWe improvement in gross load. The waterbox fault and approximate date of the shutdown were found by searching the WO database and narrative log information.

In the case of the Hope Creek NPP, waterbox fouling is not a major fault, yet still of interest. The cause of waterbox fouling for Hope Creek is once again debris (limited grassing) in the water circulated in and out of the cooling tower basin. Figure 16 shows an instance of waterbox fouling in Hope Creek waterbox A. Under normal operating conditions with no faults, the DP across the Hope Creek CWPs are, on average, 40–41 PSIG. Note that, in Figure 16, on around December 23, 2017, CWP A's DP began trending upward and goes above 43 PSIG. Following the DP trend, the DT across the north and south ends of waterbox A also trends upward in the same time period. These slow, steady increases in differential pressure and DT trends are indicative of waterbox fouling. Following a waterbox cleaning on around January 23, 2018, the DP reduced to near 41 PSIG, and the DT also stabilized.

These two examples show that different fault features can indicate the same fault. Developing a comprehensive fault signature for each fault mode is key to achieving scalable, accurate predictive models. For other CWP fault signatures, see reference [12].

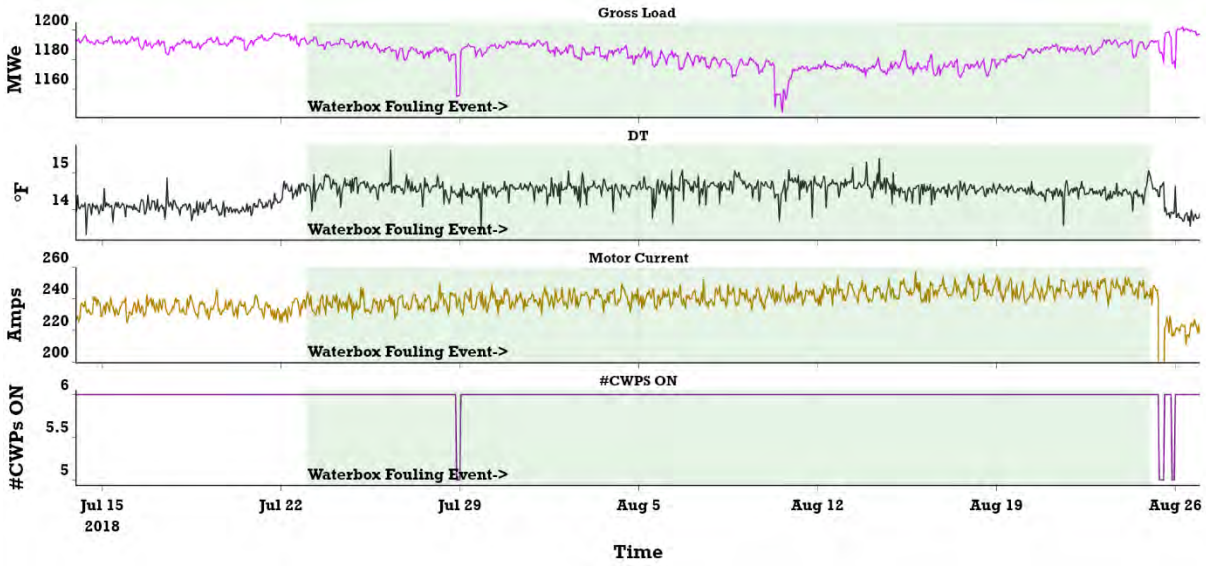

Figure 15. An example of changes to the CWS process data both before and after waterbox fouling at Salem Unit 2's waterbox 22B.

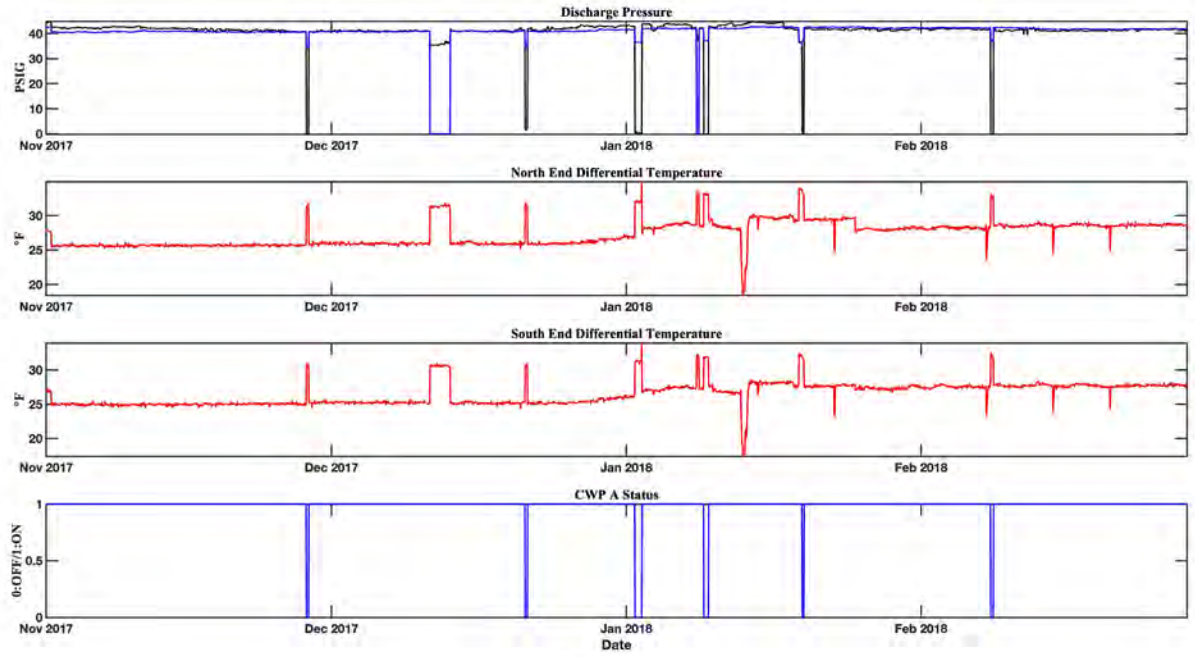

Figure 16. An example of changes to the CWS process data both before and after waterbox fouling at Hope Creek's waterbox A.

3. PREDICTIVE MODELING

In this chapter, the federated-transfer learning predictive modeling approach is described. The FL model was developed using the Salem CWS data. Two types of federated models were developed: MK SVM classifiers and NN models. The performance of federated models is compared with that of individual prediction models. The federated models were tested on the Hope Creek CWS data as part of a TL approach. Performance of federated-transfer models on the Hope Creek CWS data is also discussed.

3.1 Federated-Transfer Learning

To build ML-driven diagnostic and prognostic models, it is crucial to capture all the data patterns across every fault mode. For NPPs, building a comprehensive ML model is challenging because (1) faults are rare events, and it is highly unlikely for all the faults to occur in each component; (2) for a newly installed component/system or plant unit, it is infeasible to build AI models from scratch; (3) collecting all the data at a centralized location is limited by high bandwidth costs; (4) achieving low-latency, real-time decision support is crucial; and (5) privacy, security, legal, and commercial concerns restrict data sharing across different plants. Hence, the two approaches (i.e., FL [13,14] and TL [15,16]) discussed in the following subsection focus on (1) developing an individual component-level model using component-specific available data sources, (2) consolidating the knowledge gained from individual component models for a given plant asset into a master model, (3) using the master model to make diagnostic and prognostic estimations of the entire system, and (4) applying (i.e., transferring) the master model for diagnostic and prognostic estimations of similar plant systems, either at the same plant site or at different plants. A schematic representation of FL and TL is shown in Figure 17. FL is demonstrated on Salem Units 1 and 2, while the TL framework is demonstrated on the Hope Creek NPP.

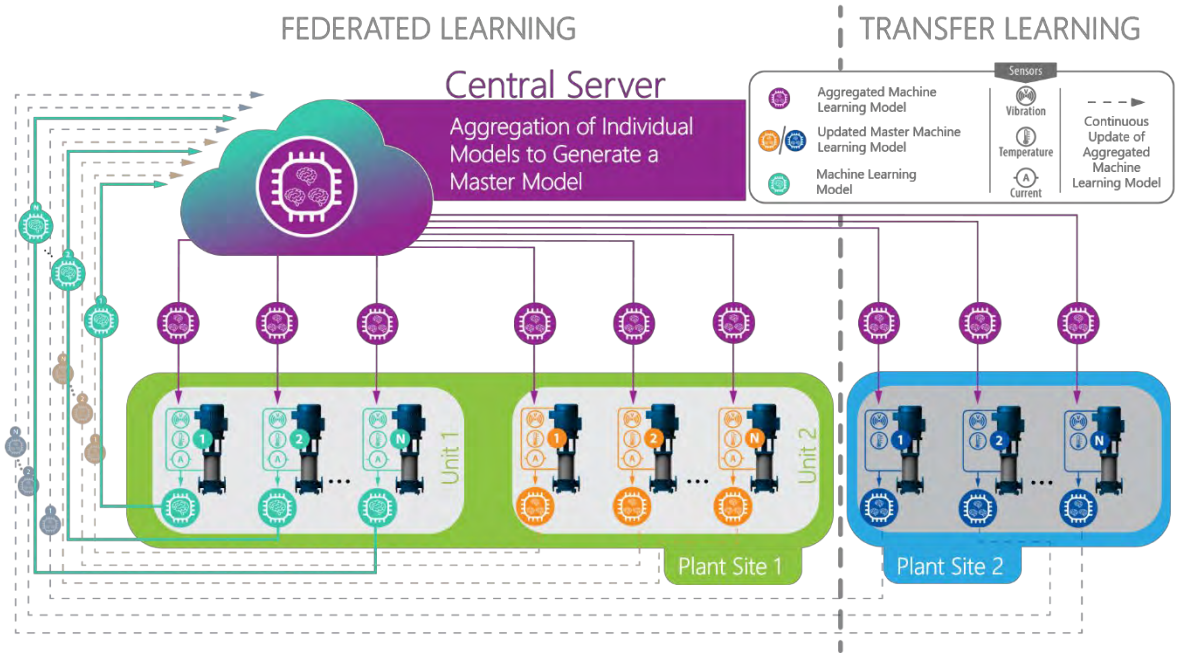

Figure 17. Schematic representation of the federated learning and transfer learning approaches.

3.2 Federated Learning Using Multi-Kernel Support Vector Machines

FL was demonstrated using an MK-based SVM [17] that classifies whether a CWP is in a *healthy* or *unhealthy* state. FL was demonstrated on the Salem NPP data, with each local model being developed for a pair of CWPs connected to a common waterbox, as shown in Figure 5. Since there are three waterboxes for each Salem unit, this gives six local models that will be combined into a master model via the FL approach (see Figure 17). FL model development is discussed in detail in later sections.

3.2.1 Salem CWS Data

From the CWS-associated plant operational data, the following features, denoted as X, are extracted for each M&P set:

- DT is calculated as the difference between the outlet water temperature associated with the M&P set and the inlet river temperature
- The measured *MIB temperature*, *MOB temperature*, and *motor stator temperature*
- From historical CWS M&P replacement/refurbishment dates; the M&P run-hours from one replacement to the next are considered in calculating the *motor age* (M_{Age}) and *pump age* (P_{Age})
- To consider the seasonal effects on the data, *week of the year* is calculated for every timestamp, and is used as a feature.

Thus a total of seven features are extracted from the CWS plant operational data for each M&P set. Detailed information on feature extraction from plant operation data—as well as from vibration data—can be found in [12]. For model development, plant operational data after 2016 were considered because the Salem plant adopted a new six-year CWP replacement PM at that first time. Since 2016, each unit of the Salem NPP has periodically replaced their CWPs as per the updated PM strategy. Based on the date of replacement of each CWP, the age of the M&P set is estimated. If any faults in the M&P are identified after their replacement, the data corresponding to that fault and time period is labeled as *unhealthy*, or else labeled as *healthy*.The samples were then grouped based on CWP combinations and split into training and test samples in accordance with an 80:20 ratio, as shown in Table 2. Figure 18 shows a sample plot of the distribution of each extracted feature in the *healthy* and *unhealthy* classes for group 11. The figure makes it evident that the most significant feature for the classification algorithm is DT. This makes sense because most of the fault data captured in the *unhealthy* class are associated with waterbox fouling, which is best reflected by DT information rather than the other six features discussed above. Also, since only data collected after 2016 are considered for the FL model, only CWP diffuser and waterbox fouling faults are captured for the *unhealthy* class. There are other faults in CWP data prior to 2016 and are not discussed here for clarity; however, the approach is extendable to those faults too.

Table 2. Data split into training and test sets per each of the selected groups for CWP condition prediction.

Data Group	Training samples	Test Samples
Group_11 (CWP 11A and CWP 11B)	6174	974
Group_12 (CWP 12A and CWP 12B)	8303	1309
Group_13 (CWP 13A and CWP 13B)	4366	822
Group_21(CWP 21A and CWP 21B)	1720	288
Group_22 (CWP 22A and CWP 22B)	2356	476
Group_23 (CWP 23A and CWP 23B)	1496	358

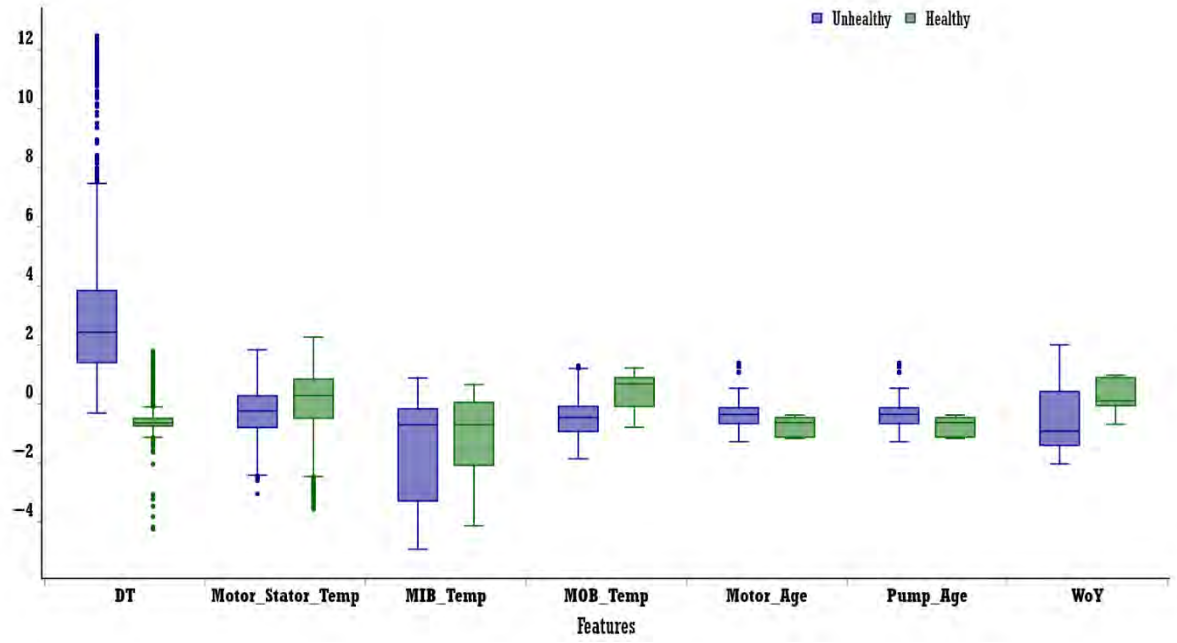

Figure 18. Distributions of *healthy* and *unhealthy* class labels for features from group 11.

3.2.2 Kernel Selection

The SVM [18] model performance is mainly driven by the selection of a kernel function and its associated parameters. Conventional SVM algorithms are based on a single kernel for all features in the entire data set. The most popular kernels used for SVMs are linear, polynomial, and radial basis functions. The heterogeneity of the data collected at the component, system, and plant levels makes single-kernel SVM infeasible for the FL and TL frameworks. Hence, MK-based SVM models are the selected approach. In MK-based methods [17], the features are grouped based on measurement type, and each group has its own kernel/parameter settings. The predicted condition of the CWP is the weighted sum of the contributions from each kernel, as defined by:

$$f(x) = \sum_{i=1}^{n} \alpha_i y_i K(x_i, x_j) + b \tag{1}$$

$$s.t. K(x_i, x_j) = \sum_{m=1}^{M} \beta_m K_m(x_i, x_j)$$

$$\sum_{m=1}^{M} \beta_m = 1$$

where f(x) is the prediction, $K(\cdot)$ is the kernel function, M is the total number of groups, x_j is the sample, x_i is the support vector (SV) with true value y_i and weight α_i, and β_m is the weight associated with kernel-m. The detailed mathematical derivation of equation (1) can be found in Appendix C. A schematic of the feature-group-based MK approach is shown in Figure 19.

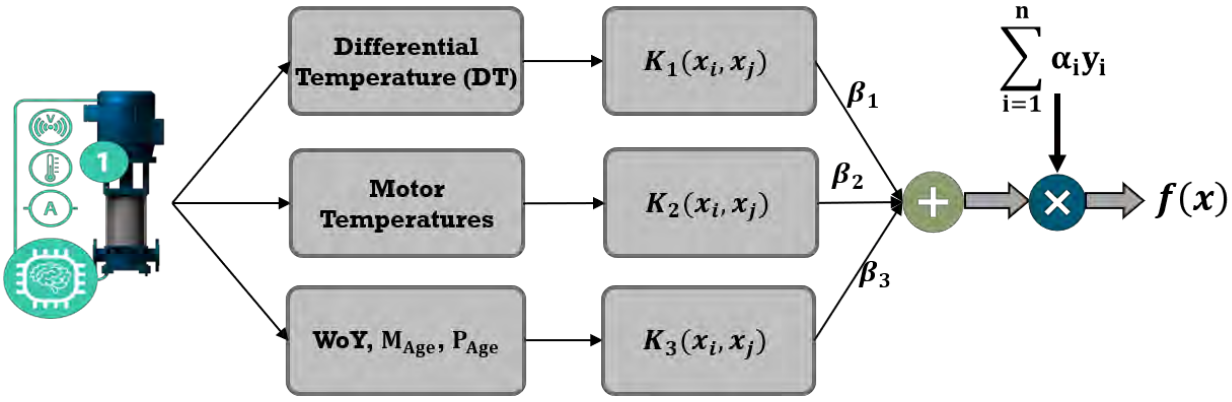

Figure 19. Feature-group-based MK-SVM framework for the Salem NPP.

Thus, in using the MK approach on each CWP-group (see Table 2), six individual MK-SVM models are trained. Each individual model will have three kernels (i.e., one per feature-group), and the net kernel, $K_{net,i}, \forall i \in [1,2,\dots,6]$, is estimated via the weighted sum of the three kernels shown in equation (1). Hence, from six individual models, six net-kernel matrices are extracted, denoted by $K_{Net} = \{K_{net,1}, K_{net,2}K_{net,3}, K_{net,4}, K_{net,5}, K_{net,6}\}$. All the net-kernel matrices, along with their respective performances in terms of accuracy (denoted by $ACC_i, \forall i \in [1,2,\dots,6]$), are shared to the central controller. At the central controller, the weighted aggregation of all the net kernels to a global kernel matrix is calculated as:

$$K_{global} = \sum_{k}^{6} \frac{ACC_k}{\sum_j^6 ACC_j} K_{net,k} \tag{2}$$

As per equation (2), kernel aggregation happens by giving high importance to the most accurate individual model, and lowest importance to the least accurate model. Then, the K_{global} matrix, which has captured patterns from all the individual models, is used to retrain each individual model. After retraining with K_{global}, all groups will have a global model, and the above process of individually updating the kernel matrix and constructing a global matrix from all the net matrices continues.

3.2.3 Hyperparameter Optimization

Selection of optimal hyperparameters C and γ for MK-SVM with radial basis function kernels is performed using grid search cross-validation to predict CWP condition. Since there are three feature groups, the MK-SVM takes three parameters of γ as γ_1, γ_2, and γ_3, each of which must be optimally tuned. In this work, for the sake of simplicity, only one γ parameter is tuned, and it is set as $\gamma = \gamma_1 = \gamma_2 = \gamma_3$. The parameter γ was varied from 1×10^{-3} to 1×10^{3}, and the regularization parameter C was varied from 1×10^{-3} to 1×10^{2}. To predict CWP condition, γ = 100 and C = 0.001 achieved the highest prediction accuracy value (i.e., 95.58%), as shown in Figure 20.

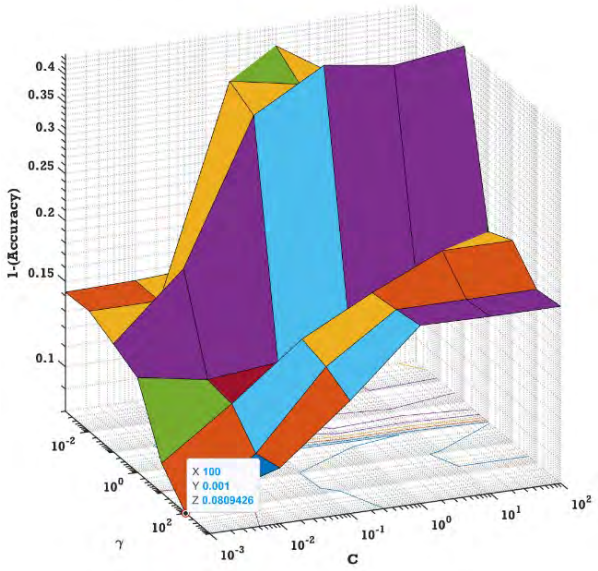

Figure 20. Hyperparameter optimization for the local MK-SVM model for group 11.

3.3 Federated Learning via Neural Networks

As a parallel method to FL via MK-SVM, we also explored the feasibility of using artificial NNs to perform FL on the Salem NPP data. Though development of this approach remains in the initial phase, the early results are promising. Throughout this section, the reader is assumed to have a working knowledge of the methods and terminology associated with NNs. Unlike SVMs, NNs are not inherently reliant on the data being encompassed in a topological metric space. Removal of these underlying geometric conditions allows us to avoid the kernel selection process and the inherent curse of dimensionality. As the number of parameters in the feature space grows, NNs are better equipped than SVMs to determine important features in an agile fashion. We specifically targeted FL via NNs as implemented in the Python library PySyft (https://github.com/OpenMined/PySyft).

3.3.1 Individual NN Model Training

As with the SVM approach, we will be training six different local models, one for each CWP combination. The CWP classification target is *healthy* and *unhealthy*. For consistency, the same full dataset and training/testing splits used for SVMs will be used again here. One of the biggest challenges in NN development is the determination of network architecture. While likely not a final approach, we began with a fully connected feed-forward NN with the following layers:

- Initial layer of seven (7) neurons
- Three (3) hidden layers of sizes 32:16:16
- An output layer of two (2) neurons.

Each hidden layer uses ReLU as its activation function. The output layer uses the log-softmax activation. The implementation is in PyTorch. This same NN architecture is used for each of the six local models. Over time, it may be necessary to create architectures unique to each CWP combination. Such a possibility emphasizes the benefit of the ensemble learning approach induced by FL.

The individual models are all trained using backpropagation coupled with the Adam optimizer. The same set of hyperparameters are used in each instance. More specifically, we use the following hyperparameters:

- Batch size = 16
- Learning rate = 0.001
- L_2 regularization weight = 0.001
- Adam (β_1, β_2) = (0.9, 0.999)
- Epochs = 50

Determining the optimal hyperparameter values (and moreover the architecture of individual models) is currently an open question. Due to the time series aspects of this dataset, there is auspicious potential for recurrent NNs to provide higher CWP health classification accuracy in an ensemble setting.

3.3.2 Federation of the Models

After developing the individual NN models, we entered the federation and ensemble step of our model building process. Initial approaches used unweighted model blending, which aggregated the six individual models and trained a post-hoc NN. Using a variety of iterations on simple, fully connected NNs as the post-hoc classifier, we were unable to find a convergent solution. As such, we focused specifically on the NN approach dictated by the PySyft library. The NN architecture is the same as that used in the individual model development phase; however, for training, we used a batch size of 32 and a stronger L_2 normalization weight of 0.01. All other hyperparameters remained the same. The results of both the individual and FL processes are given in Table 3.

3.4 Results and Discussion

Table 3. Local training and FL performance on Salem NPP data using MK-SVM and NN.

CWP Combination	MK-SVM				Neural Network			
	Individual Learning		FL		Individual Learning		FL	
	Train	Test	Train	Test	Train	Test	Train	Test
11A and 11B	97.11%	95.58%	98.32%	93.73%	100%	88.30%	97.96%	96.30%
12A and 12B	100%	99.92%	100%	99.92%	93.75%	97.33%	98.71%	96.02%
13A and 13B	100%	98.90%	100%	98.90%	100%	97.57%	100%	94.28%
21A and 21B	100%	99.30%	100%	99.30%	100%	75%	100%	96.88%
22A and 22B	100%	98.94%	98.64%	91.80%	100%	75%	100%	98.118%
23A and 23B	100%	98.32%	99.26%	99.16%	100%	82.12%	98.54%	99.72%

3.4.1 MK-SVM Federated Learning

From Table 3, it is seen that individual models from each group achieved a performance of close to 100% in most of the MK-SVM models. This is a clear indication of overfitting in individual models, with the models being unable to predict other datasets or unseen data with the same accuracy. In addition, for some models, the accuracy of the test samples is higher than that of the training samples, since the test data were sometimes easier for the model to predict than the training data. After applying FL-based model aggregation and retraining each individual model, the accuracy levels came down for most of the models, but the performances remained at acceptable levels. FL aggregation over several iterations can further improve overfitting, while maintaining acceptable performance of the diagnostic model. This exemplifies that FL-based model aggregation enables aggregation of diagnostic models from the component level to the plant level. Besides, the fact that the models are trained with limited datasets also impacts the performance of FL. It is anticipated that FL performance will improve with larger training data sets.

3.4.2 Neural Network Federated Learning

The high training accuracies of the individual models suggest that several of the current individual models are overfit to the training data. Future iterations should focus on further regularization techniques. Such overfitting is at least partly reflected in the low-test accuracy displayed by many of the models. (Note that an extremely high individual test accuracy can indicate a high level of model bias and poor generalizability of the model to new observations.) Further work must be done to build more robust individual models that generalize more readily to previously unseen data.

For the FL approach, we see much stronger test set performance on the CWPs that previously showed low accuracy in the individual phase. The added information afforded by examining all pump data *en masse* provided clear advantages to the federated-model building process.

3.5 Transfer Learning

TL aims to train a model on data from one domain (Salem NPP) and adapt that model to another (Hope Creek NPP).

3.5.1 Hope Creek CWS Data for MK-SVM

From the Hope Creek CWS-associated plant operational data, the following features, denoted as X, were extracted for each M&P set:

- The DP associated with each CWP
- *DT* as an average of the DTs measured at the north and south condensers (the DT at each condenser is calculated as the difference between the respective condenser inlet and condenser outlet temperatures)
- The measured *MIB thrust temperature, MOB temperature,* and *motor winding (stator) temperature*.

Thus, five features were extracted from the Hope Creek plant data. To match the features used in the FL model, the DP was dropped, leaving only four features for TL. The features were again grouped based on measurement type for kernel selection, as discussed in Section 3.2.2. Thus, only two kernels were used in the TL for MK-SVM. For the demonstration of TL on Hope Creek data, binary classification was considered, with the *healthy* and *unhealthy* class labels being considered based on plant operation data. For the *unhealthy* state, waterbox fouling fault data were extracted; data prior to the occurrence of waterbox fouling were considered *healthy*. *Healthy* and *unhealthy* samples extracted from CWPs A and C are shown in Table 4. For the extracted samples, the master model from FL is used (both with and without retraining for comparison) in order to predict the CWP's condition using the Hope Creek data. Note that, for TL without retraining, the extracted data are not split into training and test data; instead, all the data are considered test data, and the FL model (see Section 3.1) will be used to predict the labels on whole data.

Table 4. Hope Creek data for TL.

CWP	Date	# of Samples	
		Healthy	Unhealthy
A	November 01, 2017–March 01,2018	1916	966
C	April 01, 2017–April 01, 2018	6502	2558

3.5.2 Hope Creek CWS Data for Neural Networks

The same overall Hope Creek CWS dataset was used as the starting point for TL with NNs. However, to further match the FL model given by the Salem CWS data, we added a fifth feature: *week of the year*. This is calculated in the same manner as was previously applied to the Salem data. The classification target of *healthy* or *unhealthy* is the same as was described in the above subsection. Unlike with the MK-SVM approach, the NN approach to TL amounts to more than merely applying the raw FL model from the Salem plant to the new data. Furthermore, no model is fit solely to the Hope Creek data. This affords us the benefit of truly transferring knowledge from one domain to another. After examining the initial results from the FL model developed above, we then further trained the FL-associated NN by using some of the Hope Creek data. We used a standard 80:20 train-test split of the Hope Creek data.

3.5.3 Results and Discussion

The master models from the FL framework for both the MK-SVM and NN approaches were used on Hope Creek data. The performance of the models on CWP A and CWP C data is shown in Table 5. For MK-SVMs, TL was applied without retraining, then compared with the individually trained model. For NNs, TL without retraining was performed first, followed by TL with retraining using the FL model weight parameters as initial parameters.

Table 5. TL performance on Hope Creek data, using MK-SVM and NN from FL.

CWP Combination	MK-SVM						NN			
	Individual Learning		TL w/o Retraining		TL w/ Retraining		TL w/o Retraining		TL w/ Retraining	
	Train	Test	Train	Test	Train	Test	Train	Test	Train	Test
CWP A	99.9%	66.1%	-	80.74%	81.1%	80.8%	-	80.43%	93.93%	94.01%
CWP C	99.92%	93.1%	-	79.92%	97.3%	95.7%	-	76.90%	97.38%	97.35%

3.5.3.1 MK-SVM Transfer Learning

For MK-SVM-based TL, the overall performance on both CWP A and CWP C data is around 80%. The approach involves using all the samples from CWP A and CWP C as test data in order to classify health using the master model from the FL framework. The performance dictates that the MK-SVM parameters must be further optimized to improve the prediction accuracy. Typically in TL, a small set of sample data is used to retrain the transferred model in order to finetune the model parameters for the new environment (i.e., the Hope Creek plant). For example, only 10–20% of the total number of samples will be used to retrain the model and optimize the parameters of the MK-SVM for the Hope Creek data. After retraining with 20% of the data, CWP A's performance did not improve, whereas CWP C's performance significantly improved—to higher than 95% accuracy. The performance of CWP A with TL indicates there were insufficient samples for building the ML model.

For comparison with TL, individual models were also trained on the Hope Creek data, with an 80:20 split between the training and test data. Individual model performance—particularly for CWP A—clearly shows the same overfitting trend as seen in the FL case. More samples for training are required in order to generalize the model and avoid overfitting.

3.5.3.2 NN Transfer Learning

We first applied the FL model developed on the Salem data to the Hope Creek data. No further training was done on the FL model for this step; it was "raw," and was employed as though the Hope Creek data were merely yet unseen: the overall average accuracy was just above 79%. Wanting to take advantage of the benefits of TL, we then used the above FL results as a weight initialization (initial model), then further trained the NN by using the following hyperparameters:

- Batch size = 16
- Learning rate = 1E-5
- L_2 regularization weight = 0.001
- Adam (β_1, β_2) = (0.9, 0.999)
- Epochs = 20

These hyperparameters resemble those that came before, though we use a smaller learning rate and fewer epochs. The NN architecture remains the same. This was the extent of our process for CWP C. The training and testing accuracies (Table 6) for CWP C result from this TL step. CWP A proved much harder to develop a strong model for. After the initial TL step shown above, we obtained an 82.15% testing accuracy (80.00% training accuracy). While this is an improvement over the raw FL model, the jump in accuracy we saw with CWP C was not replicated. The MK-SVM individual learning model from CWP A suggests this to be a much more challenging ML problem than was presented by CWP C. After training for another 640 epochs on the Hope Creek CWP A data, we obtained an accuracy of around 92% for both testing and training. The fact that hundreds of epochs are needed to achieve sufficient accuracy indicates that our learning rate is too small to escape the bias of the weight initializations of the raw FL model. Therefore, we set the L_2 regularization weight to 0 and the learning rate to 0.001. This means that we should, roughly speaking, learn about 100 times as quickly as before. Once again beginning with the raw FL model, we retrained the NN on the CWP A data from Hope Creek. After 40 epochs, we obtained the accuracies presented in Table 5.

3.6 Summary

An FL approach using Salem Unit 1 and 2 data, and a TL approach using Hope Creek data, were verified using the MK-SVM and NN models. For MK-SVM, the features were grouped based on measurement type, and trained with separate kernel functions. While the performance of MK-SVM for FL is satisfying, the performance of TL can be further improved by adopting a partial retraining approach that optimizes the transferred model parameters without undergoing comprehensive training. The performance of NNs in conjunction with FL is comparable to that of MK-SVM. But, when TL was performed with retraining, TL for NNs performed better than MK-SVMs. This performance can be improved using more training samples.

So far, discussions and results on the development of predictive models using the fault signatures from real-time plant process data are presented. However, there are a few M&P set faults for which no real-time data exists for the PSEG-owned plants. To expand the development of predictive models and fault signatures to cover most of the CWS faults across the fleet, simulated data can be used via M&S of the CW M&P set. In the following chapter, computational model of the CW M&P set is developed to generate simulated data for the misalignment fault, specifically.

4. COMPUTATIONAL MODEL OF CIRCULATING WATER SYSTEM

This section documents the M&S efforts for the CWS M&P set, using the multipurpose finite element software COMSOL Multiphysics [19]. The goal of this task was to develop a detailed, physics-informed model of a CWS M&P set to capture the dynamics of CWS operation. This modeling approach provides the ability to simulate data associated with fault modes for which minimal or no evidence is available in historical plant process data, thus enabling the generation of comprehensive fault signatures to achieve robust predictive models.

Section 4.1 lists the M&S assumptions, while Section 4.2 describes the modeling approach applied in COMSOL Multiphysics. The simulation results are discussed in Section 4.3 and summarized in Section 4.4.

4.1 Modeling Assumptions

One of the most frequent vibration problems in rotating machinery, misalignment in shaft coupling significantly impacts CWS M&P vibrations. Such misalignment may lead to high levels of vibration in the vicinity of the coupling, potentially precipitating bearing degradation, coupling block wear, bolt breakage, and driver overheating due to increased electrical power consumption. It is necessary to correct misalignment before it causes considerable damage to the CWS M&P.

The resulting numerical model for the CWS M&P was developed to provide sufficient simulation vibration data to support the development of a hybrid, physics-informed ML model to capture the signatures of faults caused by shaft misalignment. Currently, a simplified numerical model was built for predicting CWS behavior under good alignment conditions; this model will be applied as a healthy baseline for shaft misalignment analysis in the near future. Figure 21 shows the current numeric model of the CWP M&P, which includes the following four elements:

1. Motor cover (including casing cover, motor casing, and motor stand)
2. Motor shaft and other motor components
3. Pump shaft and other submersible parts of the CWP
4. Shaft coupling.

Due to the unavailability of some geometry data from the manufacturer's manual, some assumptions were made during M&S. More details on this model and the relevant modeling assumptions are discussed in later sections. The geometries of the motor casing, casing cover, and motor stand are determined using the manufacturer's manual for the CWP motor, then incorporated into the numerical model. Table 6 lists the main geometry parameters used for the CWS M&P modeling. A homogenous material with the properties of standard constructional steel was used for the numerical modeling (see Table 7).

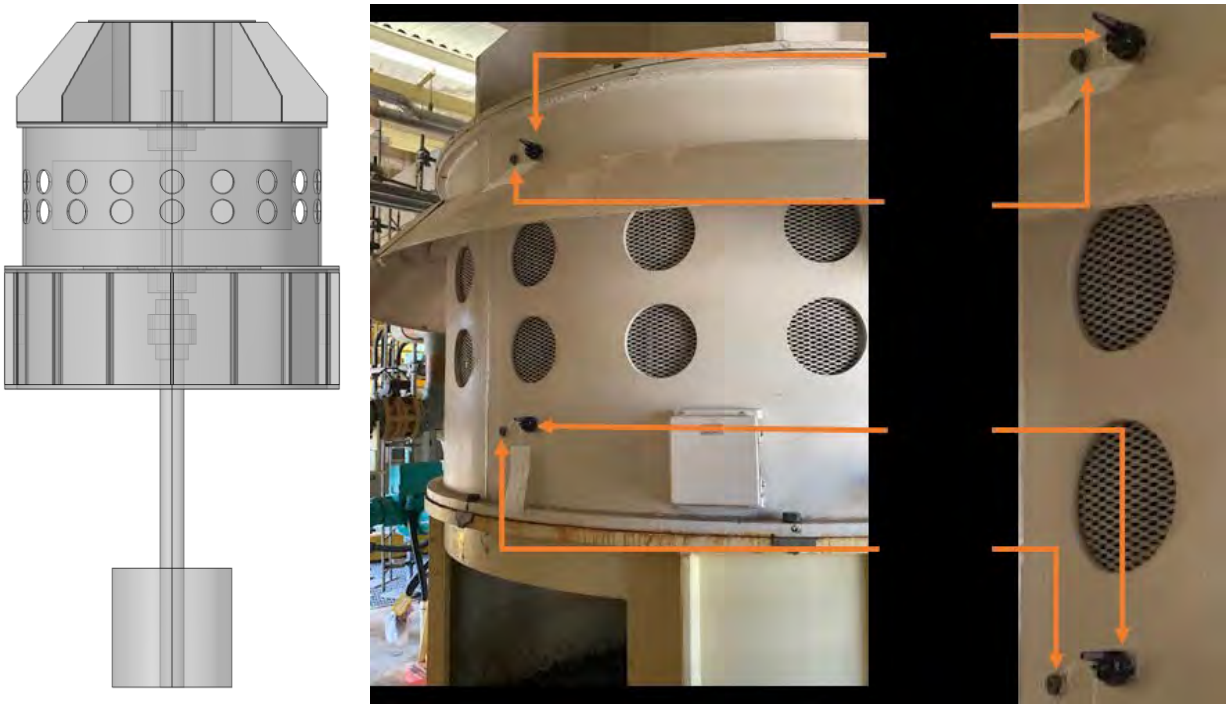

Figure 21. The CWP M&P numerical model for alignment/misalignment analysis.

Table 6. Main geometry parameters for CWS M&P modeling.

Component	Description	Value	Unit
Motor	Motor shaft diameter	7.875	in
	Length	80	in
	Distance between rotor and lower shaft end	45	in
	Stator height	23	in
	Stator outer diameter	80	in
	Height of fin on motor shaft surface	10.5	in
	Depth of fin on motor shaft surface	4.35	in
	Width of fin on motor shaft surface	1.5	in
Pump	Pump shaft diameter	7.875	in
	Length	122.75	in
	Diameter of pump submersible parts	40	in
	Height of pump submersible parts	40	in
	Height of fin on pump shaft surface	10.5	in
	Depth of fin on pump shaft surface	4.35	in
	Width of fin on pump shaft surface	1.5	in

Component		Description	Value	Unit
Rigid flanged coupling	**Coupling nut**	Height of coupling nut	3	in
		Outside diameter of coupling nut	11	in
		Inside diameter of coupling nut	7.875	in
		Number of set screws	3	
		Diameter of set screws	0.5	in
		Diameter of screw location	9	in
	Coupling flange	Height	10	in
		Number of bolts	3	
		Diameter of bolts	1	in
		Diameter of bolt location	14	in
		Length of coupling stand	5	in
		Diameter of coupling stand	16	in
		Outside diameter of coupling center	11	in

Table 7. Main material properties used in CWS modeling and simulation.

Material	Elastic Modulus [GPa]	Poisson ratio	Density [kg/m^3]
Steel	210	0.3	7850

Motor Cover

The geometries of the motor casing, casing cover, and motor stand (see Figure 22) were determined using the manufacturer's manual for the CWP motor, then incorporated into the numerical model. Some other geometry details not available in the manufacturer's manual (e.g., thickness of the casing, vertical stiffeners for the motor stand, size of the motor ventilation holes on motor casing and thickness of the casing cover) were estimated based on discussion and pictures provided by the PSEG CWP motor expert.

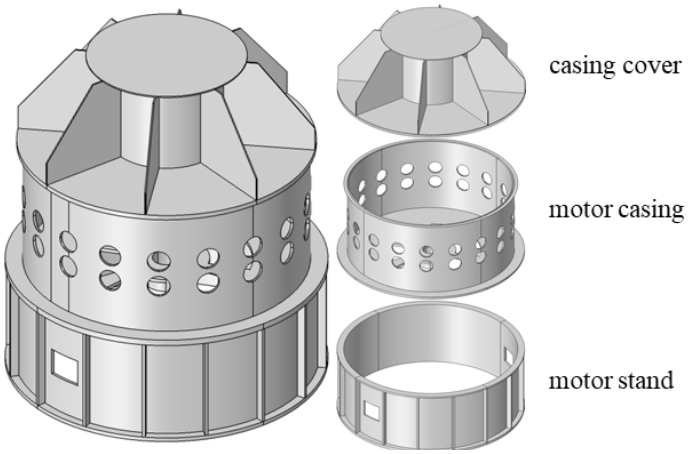

Figure 22. Numerical model for the motor cover, including the casing cover, motor casing, and motor stand.

Since the supporting bolts are equally spaced, the entire supporting surface (between the motor stand and concrete slab) is assumed to be fully constrained (all three displacement components were set to 0). Therefore, the actual bolts or other boundary constraints are not included in the numerical model shown in Figure 23.

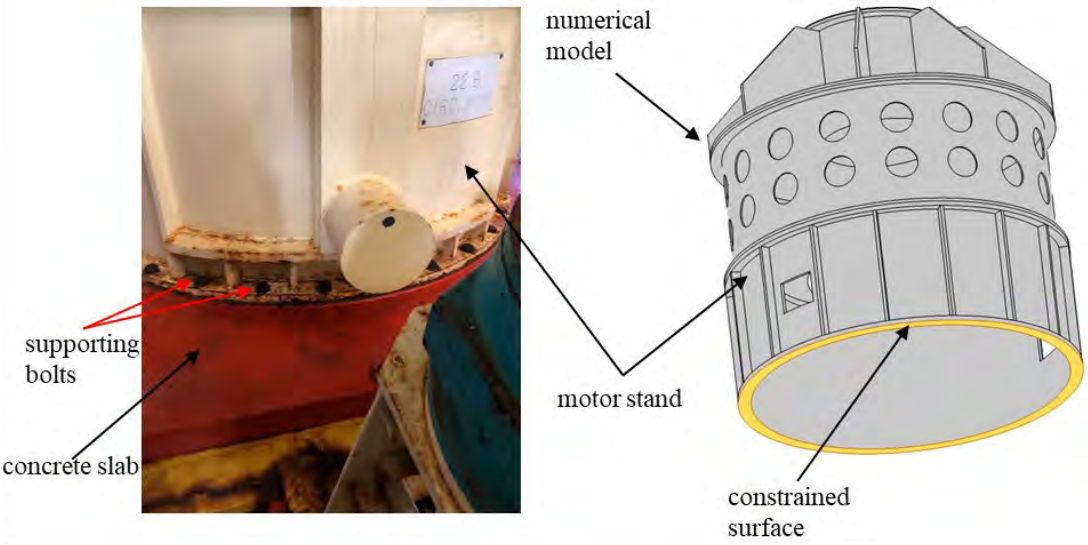

Figure 23. Boundary conditions applied on the motor stand. The bottom surface (in yellow) was fully constrained [20].

Motor Shaft and Other Motor Components

Mounted in the top and lower bearing housings of the motor casing plates, the motor shaft passes through the motor rotor and stator. Figure 24 shows the lower casing bearing plate with a bearing housing outside of the motor shaft. Journal bearings are applied between motor shaft and bearing housing.

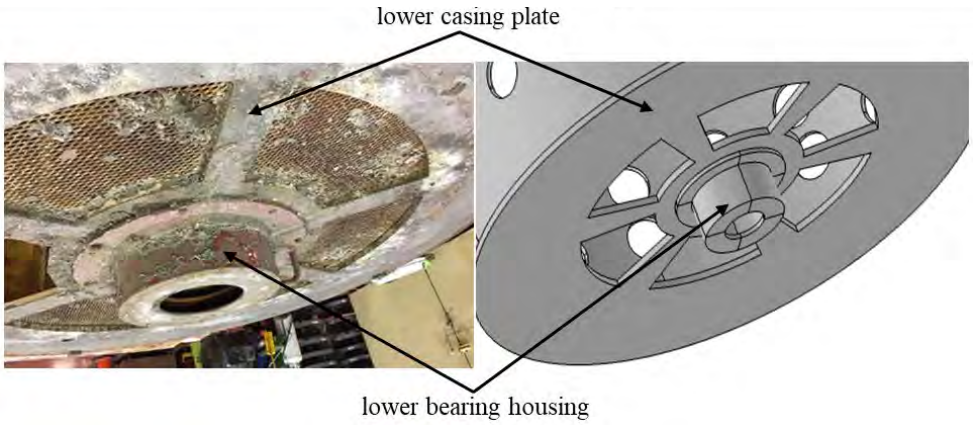

Figure 24. Lower casing bearing plate with bearing housing [20].

Figure 25 illustrates the simplified model of the motor, pump, and shaft coupling. As the driver shaft, the motor shaft is assumed to have a fixed angular speed (30.8 rad/s). It is coupled via two bearings and one shaft coupling. The motor rotor and stator have not yet been modeled in detail; they are combined via the motor shaft in the middle. Their mass may affect the vibration due to shaft misalignment. More details on the motor will be added in future work.

As displayed in Figure 26, two journal bearings are introduced between the motor shaft and the bearing housings on the motor casing plates. Each bearing is supported in its individual bearing housing, and the bearing flange is attached to the bearing housing via bolts that are wired to prevent from working loose. The bearings are water lubricated and contain axial grooves through which water can freely pass. They are made of leaded bronze or cutless rubber, depending on the service conditions.

Figure 26 (a) shows the top and bottom bearing housings, where mechanical loads are introduced from the motor shaft. The shaft bearings attached to the motor shaft are displayed in Figure 26 (b) and are shown separately in Figure 26 (c). Good alignment is assumed between the motor shaft and the motor casing with the journal bearings. In the future, bearing misalignment can also be analyzed based on this model in order to evaluate its impact on CWS M&P vibration behaviors.

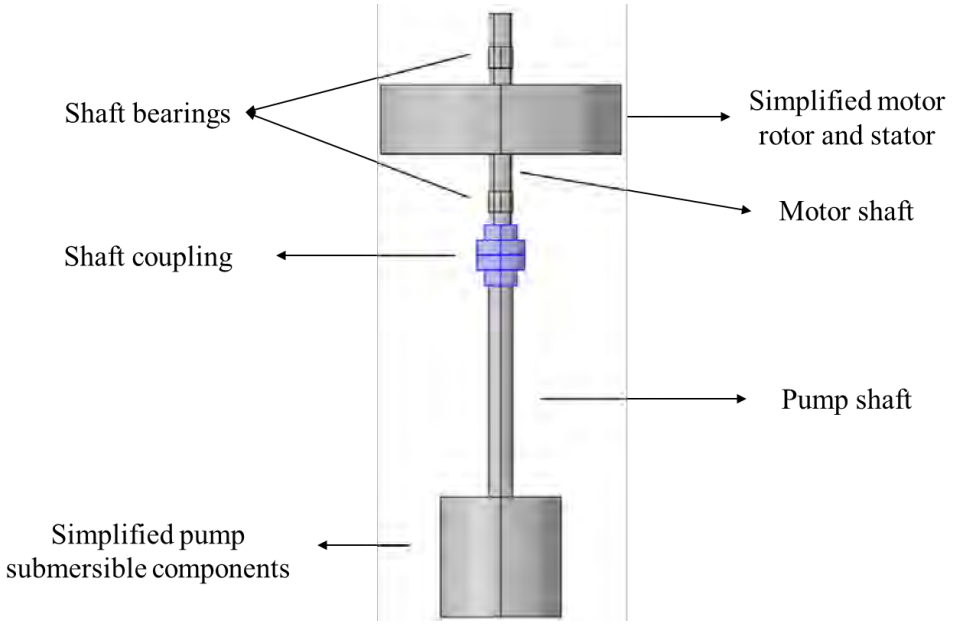

Figure 25. Simplified numerical model for motor, pump, and shaft coupling.

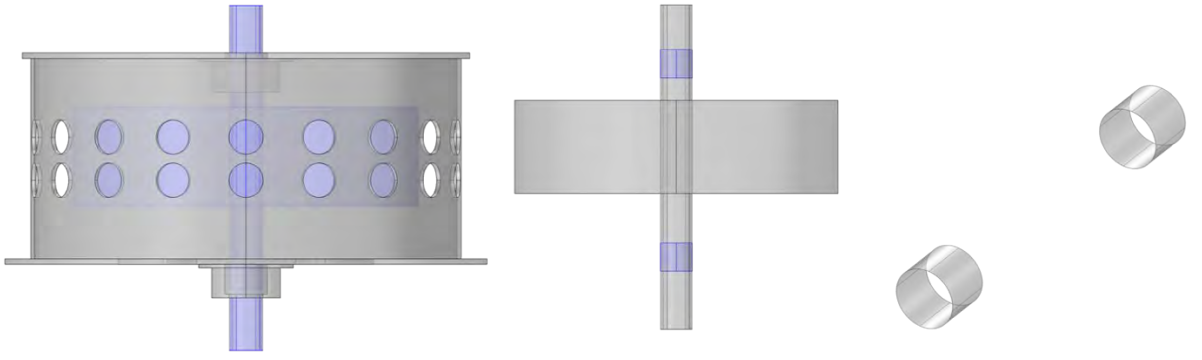

(a) Top and bottom bearing housings

(b) Motor shaft and other components

(c) Motor shaft bearings

Figure 26. Numerical model representation of the top and bottom bearing housings, where mechanical loads are introduced.

Pump Shaft and Other Submersible Parts of the CWS Pump

Considering that the focus of this work is to analyze misalignments among shafts, the complex pump structure is simplified using a pump shaft and a cylindrical component representing the submersible part of the CWP, as shown in Figure 25. The mass of this submersible part is considered and added to the pump shaft, since it may affect the M&P vibration. All potential hydraulic-induced vibration of fluid and fluid-structure interaction—including mechanical interactions between the pump shaft and impeller (below the mounting surface)—are not considered.

Shaft Coupling

Shaft coupling is a component for connecting a driver shaft and a driven part in order to transfer power. The main roles of a coupling include:

- Connecting the driver shafts of motors, etc., with the driven shafts of ball screws, etc., to transmit power
- Providing tolerance for errors (misalignment) between the cores of the driver shaft and driven shaft
- Absorbing equipment impacts and vibrations
- Improving equipment performance
- Introducing mechanical flexibility to compensate for misalignment of the shafts.

Shaft couplings are an important link in minimizing impacts and vibrations, allowing for smooth rotation to be transmitted. According to [21], rigid flanged couplings are normally used to connect the driver to one or more pump shafts. A tapered fit is provided between shafts and couplings to facilitate dismantling or assembly when replacing bearing bushings or shaft sleeves. Fitted bolts and a rabbet fit are used in the coupling to ensure positive alignment and a rigid assembly capable of transmitting high thrust and torque.

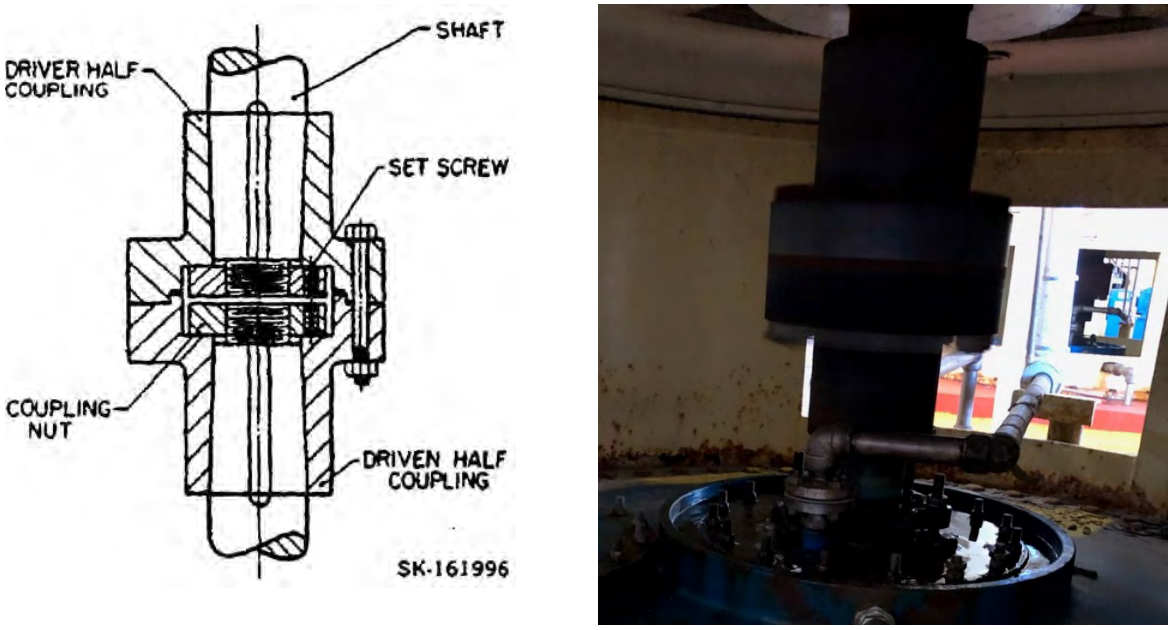

Figure 27. A rigid flanged coupling as taken from [21] (left) vs. a picture of the CWS shaft coupling (right).

Figure 27 compares the rigid flanged coupling from [21] with the CWS shaft coupling. This rigid flanged coupling consists of six parts: driver/driven half-coupling flanges, bolts and bushings for connecting two flanges, the two coupling nuts inside, and set screws that connect the coupling nuts. In the absence of relevant measured data, it is assumed that three bolts and set screws are used for this rigid flanged coupling. Figure 28 displays the structure of the rigid flanged shaft coupling in the current numerical model. For analysis under good alignment conditions, coupling nuts and flanges in the current numerical model are assumed to be tightly connected and combined together. Fins on the shaft surfaces are also modeled to fit with the coupling nuts and flanges. Figure 29 shows how the coupling connects M&P shafts.

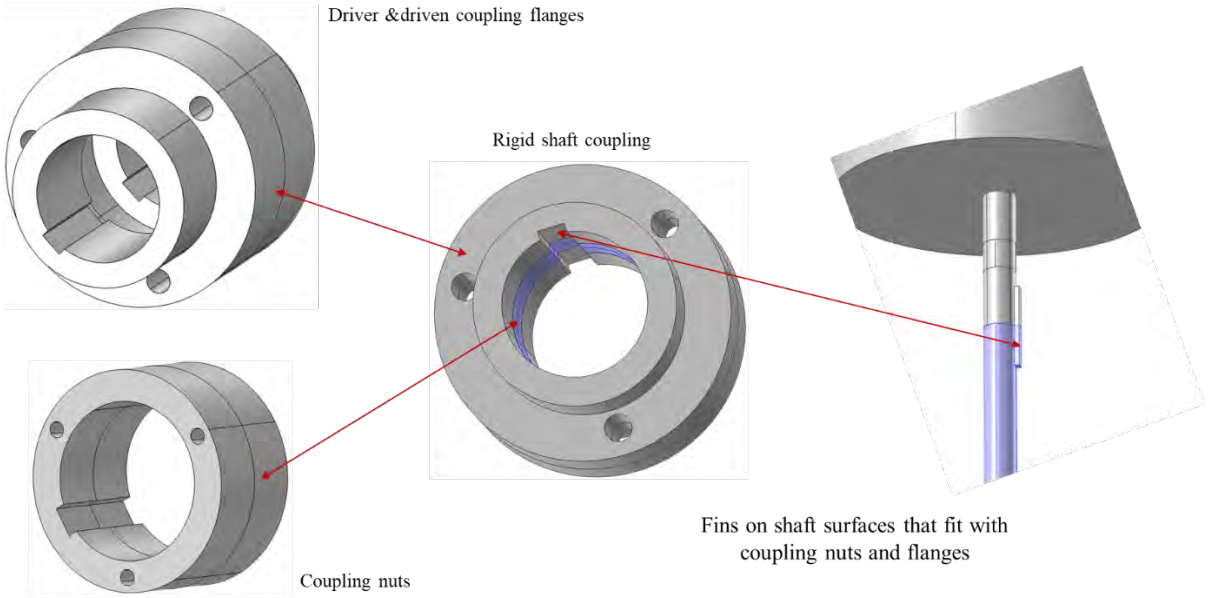

Figure 28. Numeric model of the rigid flanged shaft coupling.

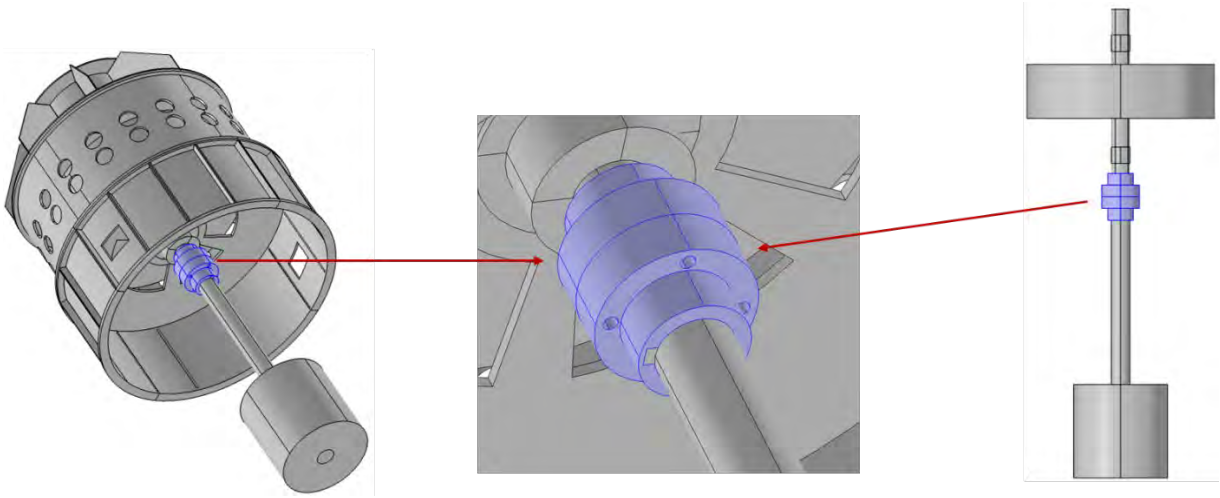

Figure 29. Connection of the rigid flanged shaft coupling with M&P shafts.

4.2 Modeling Approach

All geometry parts were generated and assembled in COMSOL Multiphysics, a cross-platform finite element analysis, solver, and multi-physics simulation software that allows conventional, physics-based user interfaces and coupled systems of partial differential equations. COMSOL Multiphysics encompasses all the steps in the modeling workflow (from defining geometries, material properties, and the physics that describe specific phenomena to solving and postprocessing models) in order to produce accurate, trustworthy results. To create models for use in specialized application areas or engineering fields, users can augment COMSOL Multiphysics with any combination of add-on modules.

In this work, the Multibody Dynamics Module, an optional add-on package for the COMSOL Multiphysics simulation software, was applied to CWS M&P modeling and simulation. The Multibody Dynamics Module is designed to perform static or dynamic analysis for a system of flexible and rigid components connected via a set of joints, springs, dampers, gears, chains, and cams, each with certain degrees of freedom. The components can then undergo complex combinations of translational and rotational motions with respect to one another. Major application areas include the automotive industry, aerospace engineering, biomechanics, biomedical instruments, robotics, and general dynamic simulations [22].

Next, the modeling approach for the Multibody Dynamics interface features is briefly introduced.

Multibody Dynamics Model and Meshing

One big advantage of the Multibody Dynamics Module is the ease with which it enables you to combine rigid and flexible parts. In this work, most of the parts in a multibody simulation are rigid; thus, they are represented by only the degrees of freedom of a rigid body. In the Multibody Dynamics Module, the material model for a rigid part is Rigid Domain. Figure 30 displays the computational domains of the numerical model.

A rigid domain is only represented by a set of ordinary differential equations, covering the equations of motion for a rigid body. The mesh on a rigid domain is only used for integrating properties such as mass, center of gravity, and moments of inertia. This means that the mesh can be much coarser than is usually the case in a finite element model. Since each element still involves a computational and memory consumption cost, one should strive for a very coarse mesh in rigid domains [22].

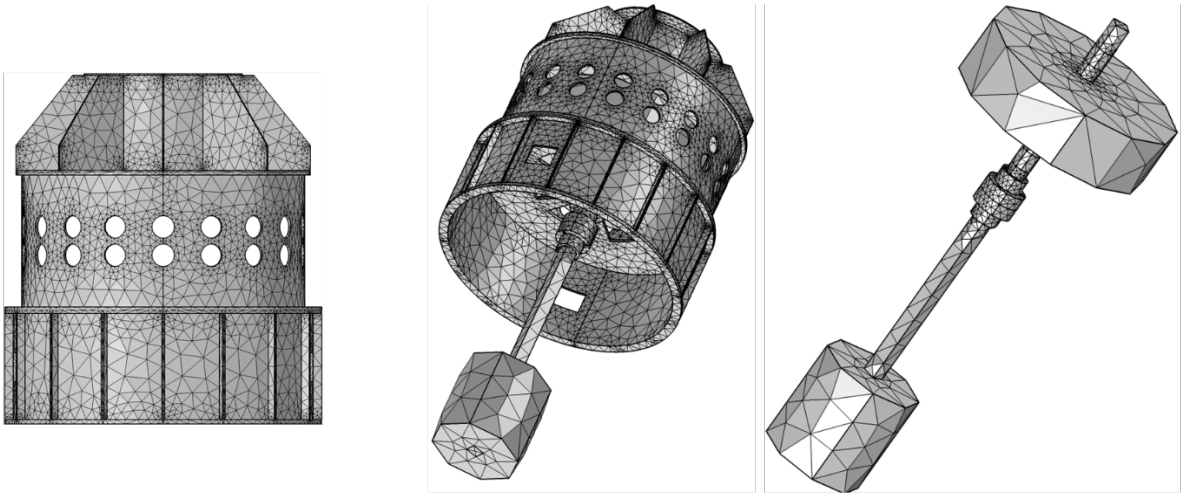

(a) Computational domain for motor cover (b) Entire computational domain (c) Computational domain for Simplified motor and pump

Figure 30. Meshing representation of the numerical model.

Bearings

Bearings are common in multibody systems, as they are necessary to support the relative rotation between two components. The CW M&P have journal bearings, which are widely used to carry radial loads (e.g., to support a rotating shaft).

A simple journal bearing consists of two rigid cylinders: the outer one (bearing) wraps around the inner rotating journal (shaft). The small annular gap or clearance between the shaft and bearing is filled by lubricant. The amount of eccentricity of the shaft with the bearing is determined by the pressure generated in the bearing to balance the radial load. The pressure in the lubricant is governed by the Reynolds equation. For an incompressible fluid with the no-slip condition, the stationary Reynolds equation in the continuum range is given by [23]:

$$\Delta_T \cdot \left[\frac{-\rho h^3}{12\mu}\Delta_T p + \frac{\rho h}{2}(v_a + v_b)\right] - \rho(\Delta_T b \cdot v_b - \Delta_T a \cdot v_a) = 0 \quad (3)$$

where ρ is the density, h is the lubricant thickness, μ is the viscosity, p is the pressure, a is the location of the channel base, v_a is the tangential velocity of the channel base, b is the location of the solid wall, and v_b is the tangential velocity of the rotating shaft. Because the pressure is constant throughout the lubricant film thickness, COMSOL uses the tangential projection of the gradient operator, Δ_T, to calculate the pressure distribution on the lubricant surface. In this case, $(\Delta_T b \cdot v_b - \Delta_T a \cdot v_a) = 0$, so the governing equation simplifies to [23]:

$$\Delta_T \cdot \left[\frac{-\rho h^3}{12\mu}\Delta_T p + \frac{\rho h}{2}(v_a + v_b)\right] = 0 \quad (4)$$

The lubricant thickness, h, is defined as [23]:

$$h = c(1 + \varepsilon \cos\theta) \quad (5)$$

where $c = R_B - R_s$ is the difference between the bearing radius and the shaft radius, ε is the eccentricity, and θ is the polar angular coordinate of a point on the lubricant. The pressure at the ends of the cylindrical journal bearing is assumed to be similar to the ambient pressure.

4.3 Simulation Results

This section presents the COMSOL simulation results showing vibration responses for both the MIB- and MOB-measuring locations, and both the axial and radial directions. These simulation results of acceleration [g] are compared with the vibration measurements after data normalization, with mean value of 0 and standard deviation of 1. A time span of 2 seconds (i.e., seconds 8 to 10 in the simulation data) was selected for the comparisons, as shown in Figure 31–Figure 34.

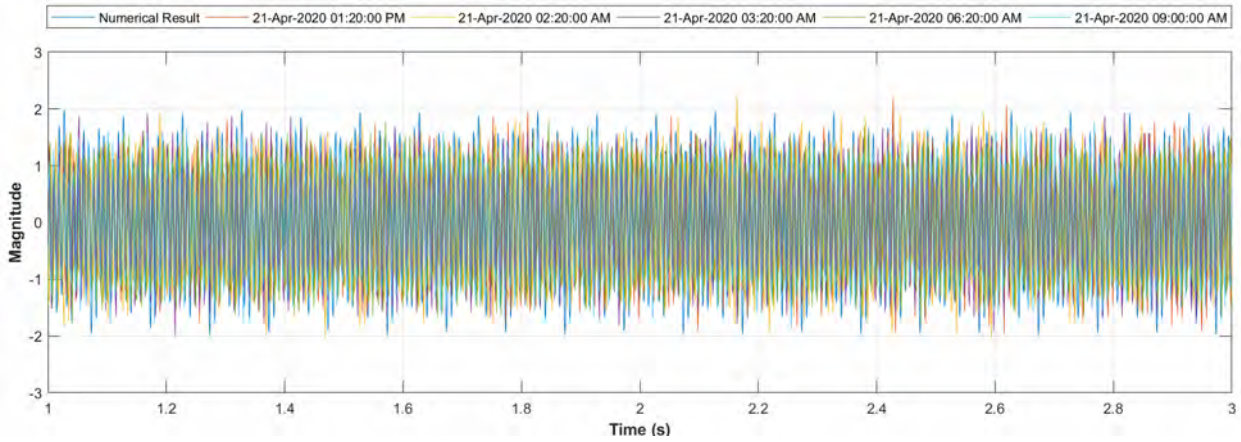

Figure 31. Simulated vibration data vs. measurement data at five different time instances for the vertical (axial) acceleration at the MIB location.

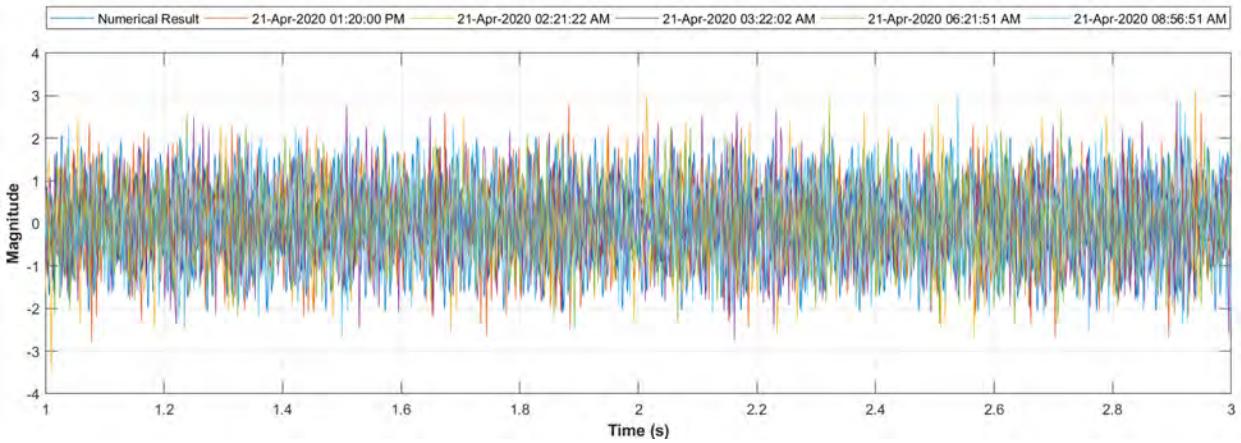

Figure 32. Simulated vibration data vs. measurement data at five different time instances for the radial acceleration at the MIB location.

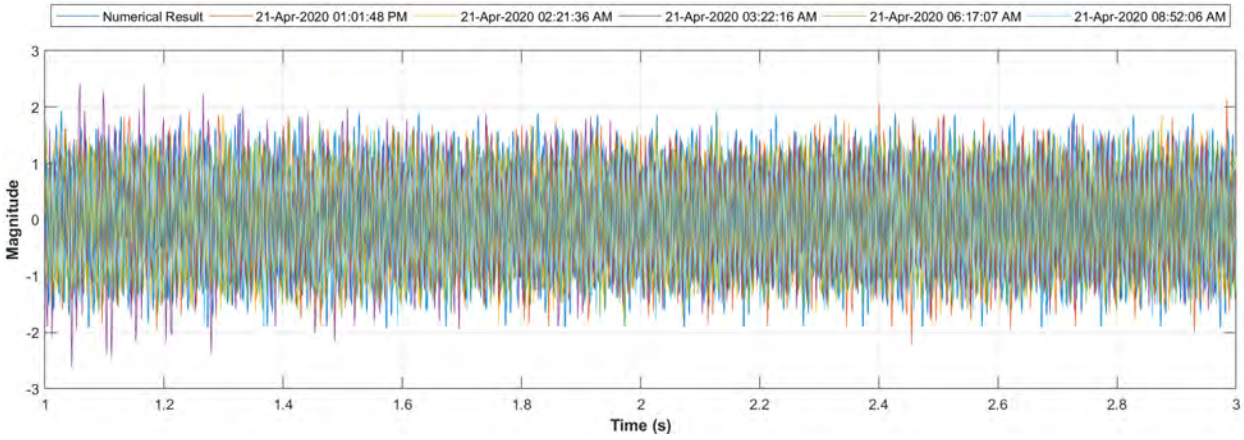

Figure 33. Simulated vibration data vs. measurement data at five different time instances for the vertical (axial) acceleration at the MOB location.

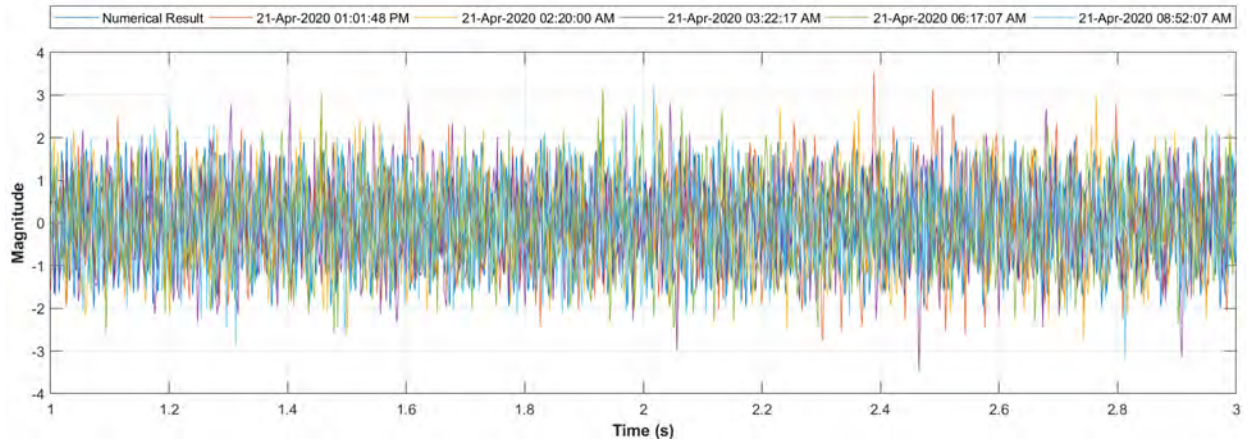

Figure 34. Simulated vibration data vs. measurement data at five different time instances for the radial acceleration at the MOB location.

The vibration signals obtained from the COMSOL simulation were also transferred to power spectral density (PSD) plots for better quantitative comparison with the actual vibration. Results show that the dominant frequencies appear at about 30, 100, and 120 Hz. Figure 35–Figure 38 compare the PSD plots of numerical results with the measurement data at five different time instances. Table 8 lists the root mean square errors (RMSEs) between PSDs of numerical results with PSDs of measurement data using the following equation:

$$RMSE = \sqrt{\frac{1}{n}\sum\left(PSD_{num,i} - PSD_{mea,i}\right)^2} \tag{6}$$

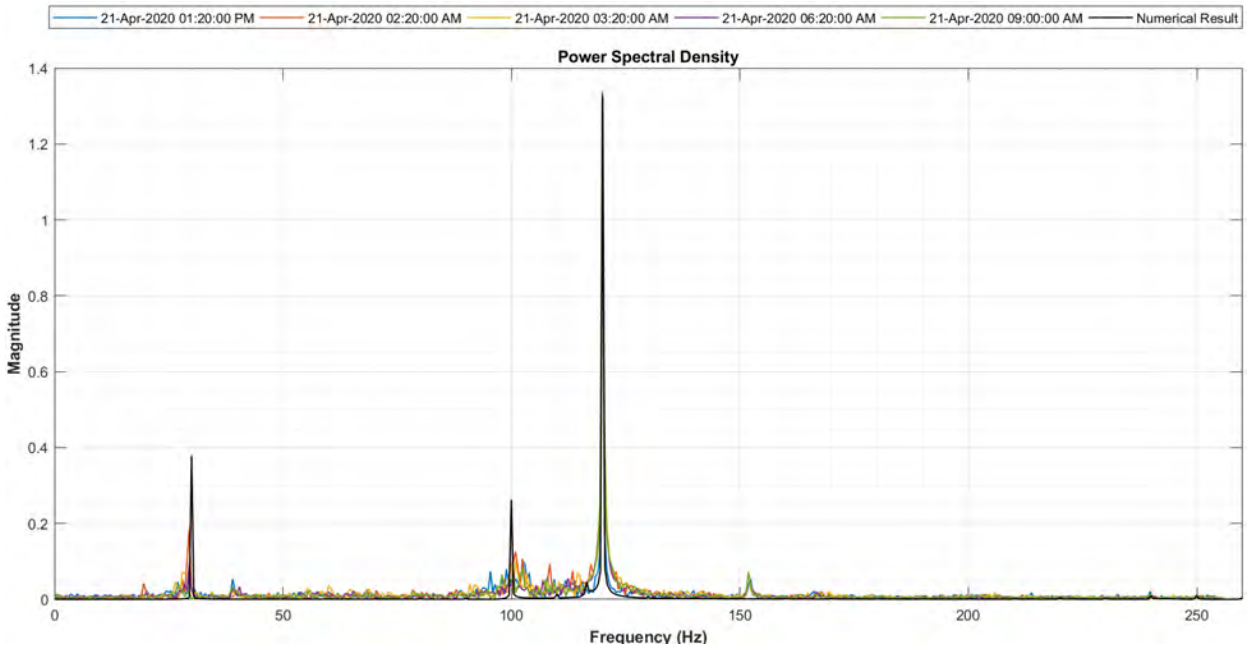

Figure 35. PSD plot for the vertical (axial) simulated vibration waveform at the MIB location.

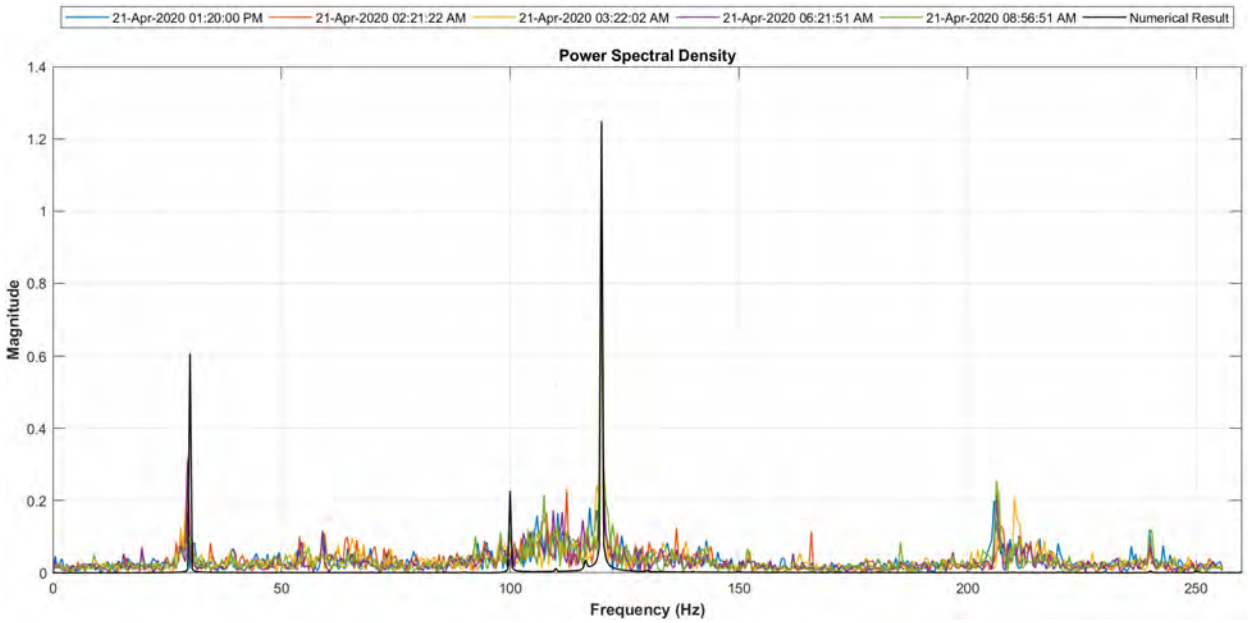

Figure 36. PSD plot for the radial simulated vibration waveform at the MIB location.

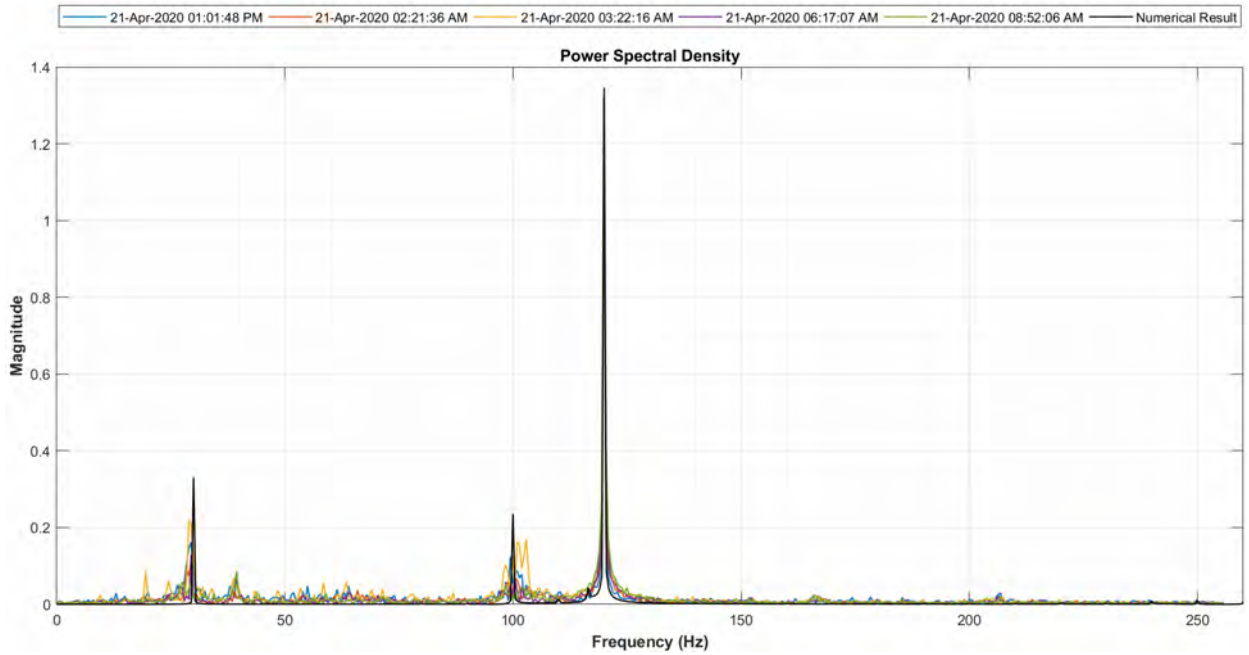

Figure 37. PSD plot for the vertical (axial) simulated vibration waveform at the MOB location.

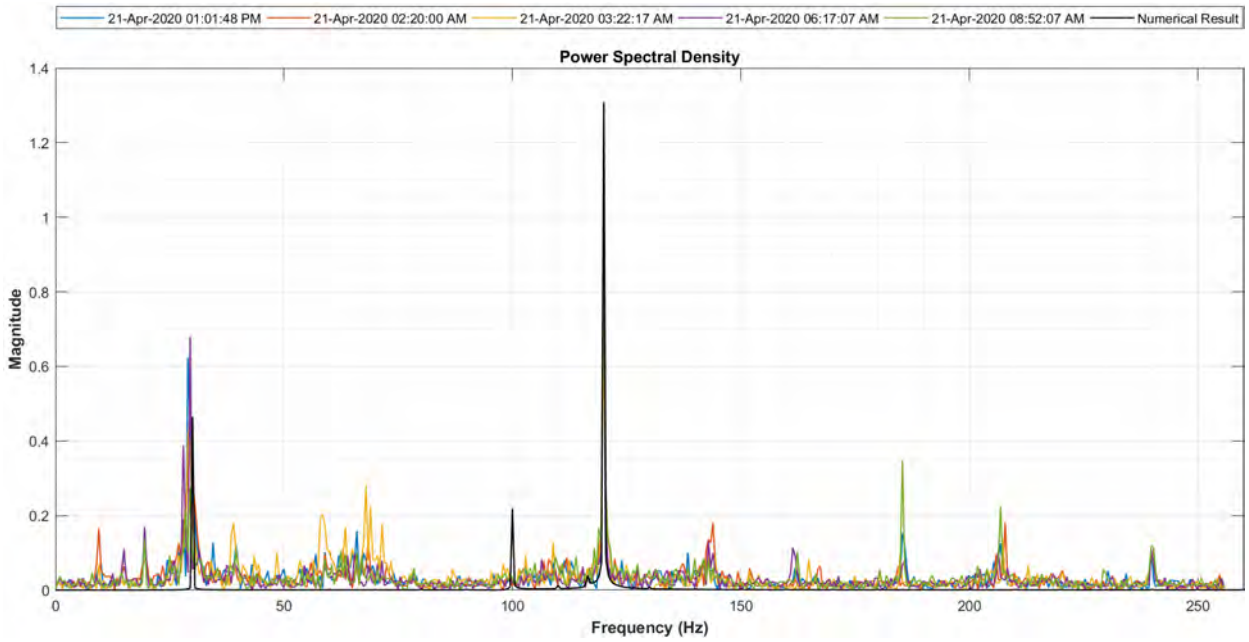

Figure 38. PSD plot for the radial simulated vibration waveform at the MOB location.

Table 8. Comparisons of PSDs of numerical results with PSDs of measurement data.

MIB: axial direction		**MIB: radial direction**	
Data (time instance)	**RMSE**	**Data (time instance)**	**RMSE**
D1: 21-Apr-2020 01_20_00 PM	0.0244	D6: 21-Apr-2020 01_20_00 PM	0.0526
D2: 21-Apr-2020 02_20_00 AM	0.0325	D7: 21-Apr-2020 02_21_22 AM	0.0504
D3: 21-Apr-2020 03_20_00 AM	0.0308	D8: 21-Apr-2020 03_22_02 AM	0.0520
D4: 21-Apr-2020 06_20_00 AM	0.0277	D9: 21-Apr-2020 06_21_51 AM	0.0483
D5: 21-Apr-2020 09_00_00 AM	0.0293	D10: 21-Apr-2020 08_56_51 AM	0.0496
MOB: axial direction		**MOB: radial direction**	
Data (time instance)	**RMSE**	**Data (time instance)**	**RMSE**
D11: 21-Apr-2020 01_01_48 PM	0.0237	D16: 21-Apr-2020 01_01_48 PM	0.0573
D12: 21-Apr-2020 02_21_36 AM	0.0230	D17: 21-Apr-2020 02_20_00 AM	0.0575
D13: 21-Apr-2020 03_22_16 AM	0.0323	D18: 21-Apr-2020 03_22_17 AM	0.0603
D14: 21-Apr-2020 06_17_07 AM	0.0240	D19: 21-Apr-2020 06_17_07 AM	0.0547
D15: 21-Apr-2020 08_52_06 AM	0.0284	D20: 21-Apr-2020 08_52_07 AM	0.0491

4.4 Summary

Simulation results show that the current numerical model using COMSOL Multiphysics can accurately capture the dominant vibration frequencies for both MIB and MOB locations in the vertical and radial directions. Continuing work in FY-22 will focus on improving the current numerical model by:

- Collecting more real geometry and material data
- Releasing modeling assumptions about structure and geometry
- Calibrating with more measurement data collected under good shaft alignment conditions.

Furthermore, the improved numerical model will be applied for providing sufficient simulation vibration data and supporting the development of a hybrid, physics-informed ML model to capture the signatures of faults caused by shaft misalignment. Typical misalignment types will be considered and studied, including angular misalignment (i.e., shaft centerlines intersect not parallel), parallel misalignment (i.e., shaft centerlines are parallel but do not intersected), and a combination of angular and parallel misalignment.

5. RISK AND ECONOMIC MODELING

In this chapter, details on the risk, proportional hazard, and economic models are presented. The three states of the Markov chain risk model are determined based on scale (i.e., component-, state-, or plant-level). This chapter explores how a state-level Markov model scales up to a plant-level model, and vice versa. The proportional hazard model is used to integrate prognostic model outputs with the Markov chain risk model via the state transition rate parameter, λ. The integration informs the estimation of each state probability, which is then used to estimate the profit based on the plant asset's state of health (i.e., CWS, in this research).

5.1 Three-State Markov Model

This section deals with the scalability of continuous Markov models when applied to a risk-benefits analysis of operating assets in NPPs. For the CWS, the scalability of the Markov chain model is demonstrated from the component- to the plant-level.

5.1.1 Component-Level Three-State Markov Model

The component-level three-state Markov chain model of a CW M&P set assumes that most maintenance performed on the set (or any plant asset) is divided into two categories: corrective and preventive. Corrective maintenance (CM), sometimes referred to as repairs, occurs when a component randomly fails during operation or standby. In such situations, CM is necessary for returning the component to an operational state. On the other hand, PM is normally performed when a component is operational but requires some service. Often, PM is performed when the component is online; however, PM may require derating the unit. In addition, PM is mostly performed at fixed time frequencies (with some variance due to operating schedules). A transition diagram of the three-state model is shown in Figure 39.

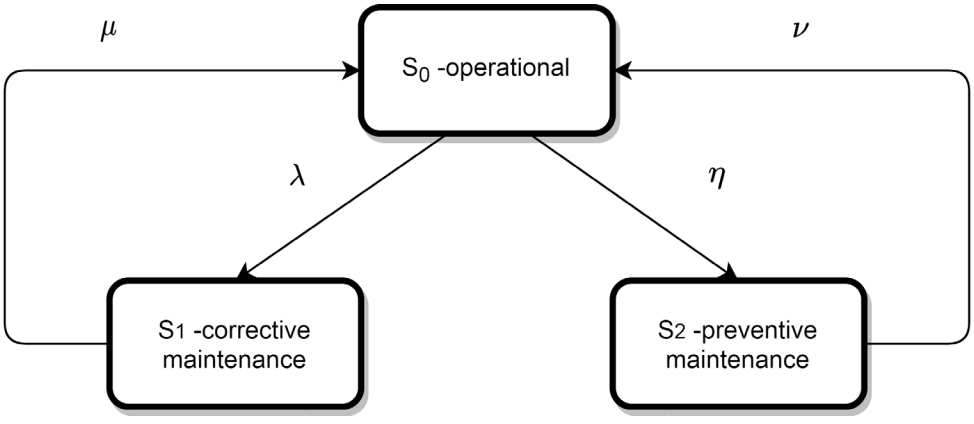

Figure 39. Transition diagram for the three-state model.

The three-state model is completely defined by four parameters: λ represents the failure rate, μ represents the CM rate, η represents the PM scheduling rate, and ν represents the PM rate and its initial conditions. The system of differential equations governing the evolution of the three-state model can be written as follows [24]:

$$\frac{dp_{S_0}}{dt} = \mu \cdot p_{S_1} - \lambda \cdot p_{S_0} + \nu \cdot p_{S_2} - \eta \cdot p_{S_0}$$

$$\frac{dp_{S_1}}{dt} = \lambda \cdot p_{S_0} - \mu \cdot p_{S_1} \quad (7)$$

$$\frac{dp_{S_2}}{dt} = \eta \cdot p_{S_0} - \nu \cdot p_{S_2}$$

$$p_{S_0}(0) = 1, p_{S_0}(t) + p_{S_1}(t) + p_{S_2}(t) = 1$$

where p_{S_0}, p_{S_1}, and p_{S_2} represent the probabilities of the component being in the corresponding state. Using the normalization requirement and two of the three differential equations, the steady-state probabilities can be written as [24]:

$$p_{S_1} = \frac{1}{1+\frac{\mu}{\lambda}+\frac{\mu \cdot \eta}{\lambda \cdot \nu}}; p_{S_0} = \frac{\mu}{\lambda} p_1; p_{S_2} = \frac{\eta}{\nu} p_1 \quad (8)$$

The three-state model in Figure 39 can be represented as a birth-death model. The steady-state solution is guaranteed to exist when represented as the birth-death model and for situations in which all four parameters are time-independent (i.e., they are constants) and [25]. In this research, both time-independent and -dependent parameters are considered. For time-independent parameter estimation and results, see [9]. The component-level three-state Markov chain model in Figure 39 can also be transformed or scaled to a two-state model by combining PM and CM into a single state and adding the corresponding rates. For details, see [4].

5.1.2 Plant-Level Three-State Markov Model

A plant's CWS has more than one M&P set. Recall from Chapter 2 that PSEG's Salem and Hope Creek NPPs have six and four CWS M&P sets per unit, respectively. It was observed that if a plant or unit has even a single CWP unavailable, its power generation is impacted (i.e., derated); and if a plant or unit has a certain number of CWPs unavailable at a given time, it could lead to a trip (i.e., the power generation falls to zero).

This generalization of the Markov chain model for the plant/unit level is obtained by considering a three-state Markov model in which each node represents the state of the whole plant/unit under different conditions, as shown in Figure 40.

In this model (Figure 40), S_0 is the fully operational state in which all plant systems are available and running, with no loss of power generation. S_D is the derated state in which some loss in power generation occurs due to the unavailability of one or more plant systems (including CWS M&P sets). λ_D is the a compound rate of transferring from the operational state to a derated state. λ_T is the hourly rate of transferring from a derated state to the trip state. Each downtime rate (λ_D or λ_T) is compound, meaning that it includes a superposition of transition rates from several plant subsystems. μ_D and μ_T are maintenance rates that reflect how quickly the plant can recover from a derated or tripped state, respectively. The maintenance rates μ_D and μ_T are assumed identical, can be represented as μ without any loss of information, and do not depend on the plant's state. Note that, for the model in Figure 40, an additional rate covering the direct transition from S_T to S_0 is introduced to account for the possibility of different maintenance scenarios at different utilities. The parameter p is the probability of the utility choosing to go online in a derated state as soon as some plant systems become partially available, while $1 - p$ is the probability that the utility will wait to go online until a fully operational state has been reached in which all plant systems are available. Here, "plant system" refers to the CWS and other systems that impact plant or unit generation without affecting plant or unit safety. Both recovery scenarios are possible, and this model provides additional scalability to specific utility maintenance practices. While the transition from S_T to S_0 delays the recovery to fully operational, it provides a safety margin in case a plant system goes down again. Due to the additional edge connecting S_T and S_0, this mixed-scenario model is not a birth-death model, and no analytical solution is available for steady-state probabilities.

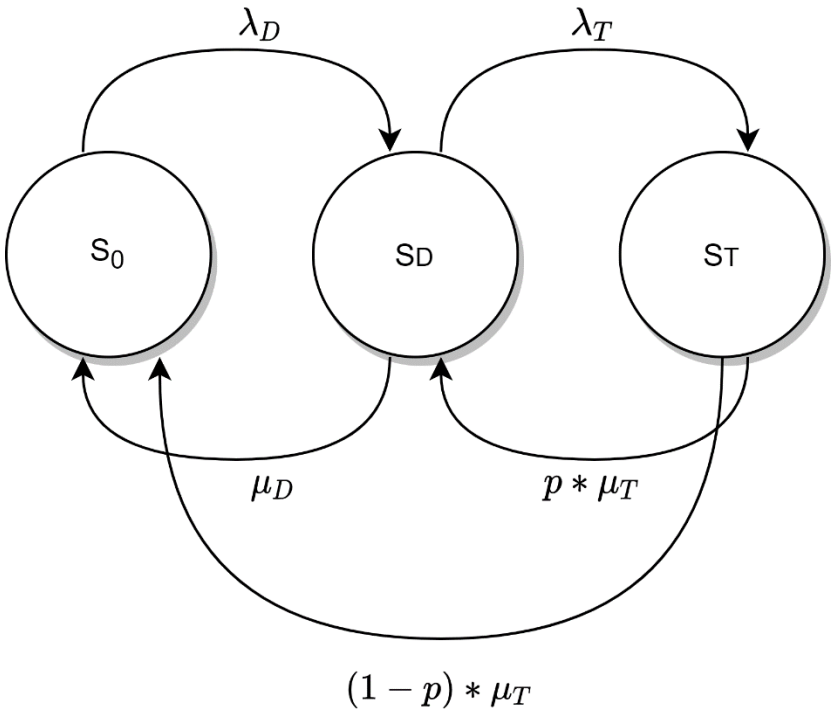

Figure 40. Plant-level mixed scenario model for derated and trip states.

Instead, the following system of differential equations must be solved, along with normalization conditions:

$$\begin{gathered}\frac{dp_{S_D}}{dt} = \lambda_d \cdot p_{S_0} + (\mu_T \cdot p) \cdot p_{S_T} - \mu_D \cdot p_{S_D} - \lambda_T \cdot p_{S_D} \\ \frac{dp_{S_0}}{dt} = \mu_D \cdot p_{S_D} + (\mu_T \cdot (1-p)) \cdot p_{S_T} - \lambda_D \cdot p_{S_0} \\ \frac{dp_{S_T}}{dt} = \lambda_T \cdot p_{S_D} - (\mu_T \cdot p) \cdot p_{S_T} - (\mu_T \cdot (1-p)) \cdot p_{S_T} \\ p_{S_0}(t) + p_{S_D}(t) + p_{S_T}(t) = 1\end{gathered} \tag{9}$$

In this system of equations, the first three differential equations describe the time evolution of the probabilities of three states, while the last equation is the normalization that enforces the condition that the system must be in one of the three states at any given time. Notice that by setting the parameter p to 1, the model in Figure 40 can be transformed into a pure birth-death model with an available analytical solution for steady-state probabilities:

$$p_{S_0} = \frac{1}{1+\frac{\lambda_D}{\mu_D}+\frac{\lambda_D \cdot \lambda_T}{\mu_D \cdot \mu_T}} ; p_{S_D} = \frac{\lambda_D}{\mu_D} \cdot \ p_{S_0} ; p_{S_T} = \frac{\lambda_D}{\mu_D} \cdot p_{S_D} \tag{10}$$

where p_{S_0}, p_{S_D}, and p_{S_T} are the probabilities of corresponding states S_0, S_D, and S_T, respectively.

To use compound rates in Markov chain modeling, a few underlying assumptions govern the flow of events in Markov chains. The most important assumption is that the event flows are ordinary, stationary, and memoryless. Stationarity implies that the rate does not change over time, memorylessness means that

future events are not dependent on previous events, and the flow is called ordinary if two events cannot occur simultaneously [26].

To calculate compound transition rates for a complex system such as a CWS, two approaches exist, each with its own advantages and disadvantages. The first approach will separately evaluate the transition rates for each subsystem, then use the above-postulated assumptions to superimpose the transition rates of different subsystems into a single compound rate. This approach requires information on transition failure/downtime rates for different systems—data not always readily available. An alternative approach is to analyze some aggregate parameter of a plant's performance (e.g., gross load). Since this parameter reflects overall plant performance, it is a compound variable that can be analyzed to obtain compound rates. The second approach is adopted in this report (see Section 5.2), as information on failure rates for different plant subsystems is unavailable.

5.2 Parameter Estimation

For the plant-level Markov model, this section estimates the parameters λ_D, λ_T, μ_T, and μ_D. The parameters for the component-level Markov model were estimated using the WO data, along with some information from the CWS plant process data (i.e., CWP status and gross load). For details on the component-level Markov model parameter estimation, see [4]. In this research, the parameters of the plant-level Markov model were estimated solely from the CWS process data. It is important to note here that derates and trips of the plant or unit as a result of other plant systems are not used in the parameter estimation. However, it is a straightforward extension of the presented parameter estimation approach.

The CWP status, the time instances in which a CWP is unavailable, the number of CWPs unavailable, and the duration of unavailability are all used for parameter estimation. The number of CWPs unavailable is used to estimate the transition rate from the operational state, S_0, to the derate state, S_D, and from the derate state, S_D, to the trip state, S_T. The duration of unavailability is used estimate maintenance rates and is also used in the profit calculation (see Section 5.3). The steps involved in extracting transition and maintenance rates for the plant-level Markov model for both the Salem and Hope Creek NPPs—using their respective CWS information—are presented as follows:

1. From the CWS plant process data on both the Salem and Hope Creek NPPs, the CWP status and gross load data are extracted after filtering out the instances in which the gross load equals zero. A gross load of zero indicates that the plant or unit has either tripped or is in an outage. A non-zero gross load indicates that either the plant or unit is in a derated or fully operational state.
2. From the filtered data, the number of CWPs that were down at each time instance is calculated.
3. For derate cases, the instances when CWPs were unavailable are determined (along with their duration) and used to estimate λ_D and μ_D. For each Salem unit, the number of unavailable CWPs ranges from one to three, and for the Hope Creek NPP, it ranges from one to two.

$$\lambda_D = \frac{1}{P}\sum_{K_D} \frac{Count(CWPs\ down==K_D)}{Total\ CWP\ run\ hour} \tag{11}$$

$$\mu_D = \frac{1}{P}\sum_{K_D} \frac{Duration(CWPs\ down==K_D)}{Total\ CWP\ run\ hour} \tag{12}$$

4. Also, the trip parameter, λ_T, is calculated as:

$$\lambda_T = \frac{1}{P}\frac{Count(CWPs\ down==K_T)}{Total\ CWP\ run\ hour} \tag{13}$$

In equations (11)–(13), P is the total number of CWPs in a plant/unit. For each Salem unit, $P = 6$ and $K_D = \{1,2,3\}$ for the derated state. For $K_T = 4$, the Salem unit is in a trip state. For the Hope Creek NPP, $P = 4$ and $K_D = \{1,2\}$ for the derated state. For $K_T = 3$, the Hope Creek plant is in a trip state. Annual run hours of each CWP from 2008 to 2020 for the Salem and Hope Creek NPPs are shown in Figure 41,

Figure 42, and Figure 43, respectively. These annual run hours are used to calculate the total CWP run hours in equations (11)–(13).

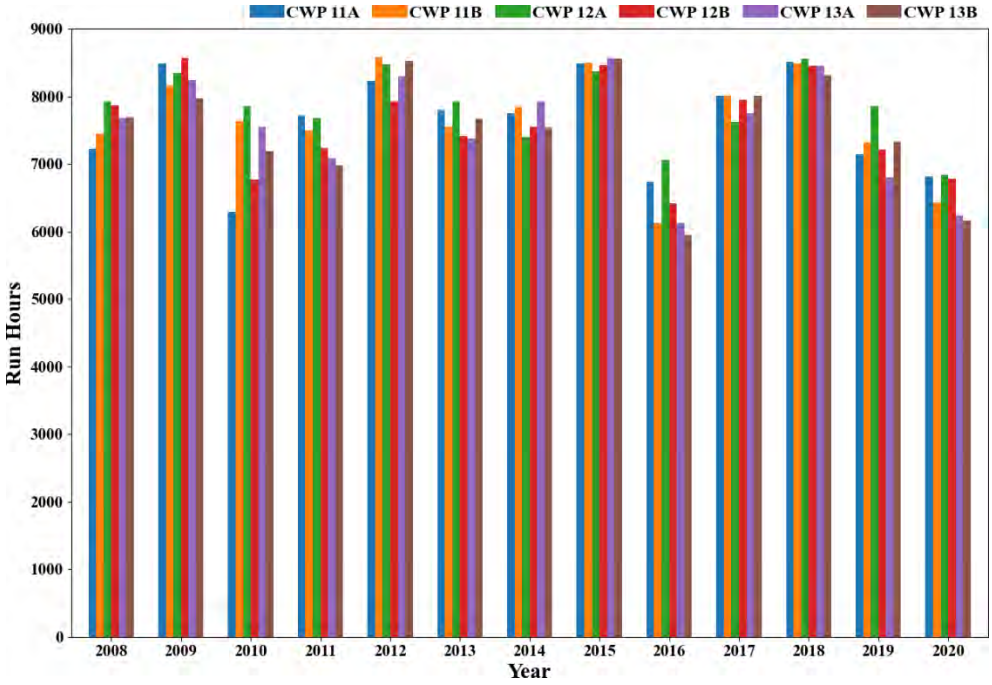

Figure 41. Annual run hours for each CWP from 2008 to 2020 for Salem Unit 1.

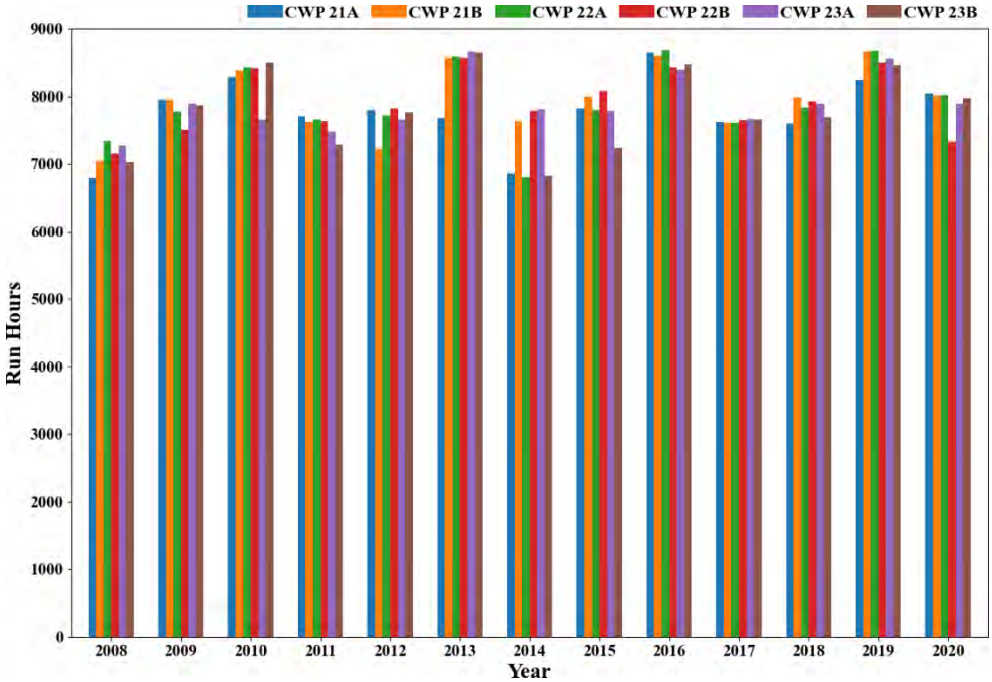

Figure 42. Annual run hours for each CWP from 2008 to 2020 for Salem Unit 2.

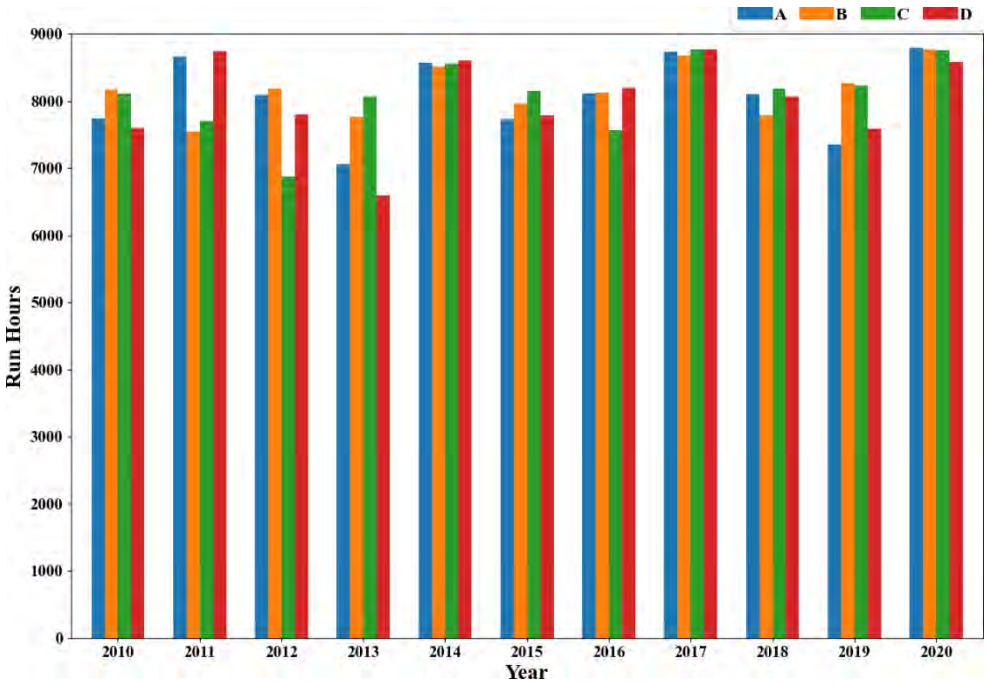

Figure 43. Annual run hours for each CWP from 2010 to 2020 for Hope Creek.

In the case of the Hope Creek plant, the derates are not usually due to problems in the CWS. Also, Hope Creek CWS operation is influenced by seasonal effects; thus, to calculate μ, a different approach using gross load information is considered. In a derated state, there will be, at minimum, a 5% drop in the gross load compared to its maximum value when the plant is fully operational. Thus, accounting for both CWS and other system maintenances, μ is calculated as follows, using the gross load:

$$\mu = \frac{Duration(0<Gross\ load<95\%*\max(Gross\ load))}{Total\ operational\ duration\ of\ plant} \tag{14}$$

The calculated values of λ_D, λ_T, and μ for the Salem and Hope Creek NPPs are shown in Table 9 and Table 10, respectively. The estimated values are compared against those obtained using the WO data in [4].

Table 9. Estimated parameters for Salem Units 1 and 2.

Parameters	Unit	From real-time plant process data	From work order data ([4])
λ_D	1	2.767×10^{-3}	2.04×10^{-3}
	2	1.49×10^{-3}	1.64×10^{-3}
λ_T	1	7.30×10^{-6}	-
	2	2.39×10^{-5}	-
μ	1	4.392×10^{-2}	2.037×10^{-2}
	2	3.553×10^{-2}	1.761×10^{-2}

Table 10. Estimated parameters for Hope Creek.

Parameters	From real-time plant process data
λ_D	4.25×10^{-4} (from pump status)
μ	9.102×10^{-2} (from gross load)
λ_T	1.41×10^{-4} (from pump status)

Given the stationary transition rates and probabilities of different states (interpreted as a percentage of time spent in a given state), the hourly profit is estimated for different p values by using the plant-level model (Figure 40) for a 1200 MWe unit. The hourly profit is calculated via the following formulation:

$$Hourly\ Profit = Hourly\ Revenue\ at\ Full\ Power \cdot p_{S_0} - [(LR + FR_1 + MC)T_1 + (LR + FR_2 + MC)T_2 + \mathbb{I} \cdot (LR + FR_3 + MC)T_3] \cdot p_{S_D} - (LR + Hourly\ Revenue\ at\ Full\ Power + MC) \cdot p_{S_T} \quad (15)$$

where FR_1, FR_2, and FR_3 represent the hourly foregone revenue whenever 1–3 CWPs are unavailable, respectively. LR is the hourly labor rate, and MC is the hourly cost of materials. T_1, T_2, and T_3 are the proportions of time in which 1–3 CWPs are unavailable, respectively, out of the total number of run hours at the time of hourly profit estimation. The indicator $\mathbb{I} = 0$ is for the Hope Creek NPP, and $\mathbb{I} = 1$ is for the Salem NPP. The hourly profit equation reflects the fact that the derated state is compound with possibly 1–3 CWPs unavailable. The values of T_1, T_2, and T_3 are obtained from operational data for both the Salem and Hope Creek NPPs. The results of applying the Markov chain model, along with the corresponding benefits to the Salem and Hope Creek NPPs, are shown in Table 11–

Table 13 for different values of p. The tripped state is also compound; however, the loss in the tripped state is assumed identical, as the plant is offline regardless of how many CWS M&P sets are down. Additionally, the cost of maintenance in this case is small compared to the hourly foregone revenue.

Table 11. Stable probabilities of different states and hourly profit values for Markov chain models of different units, with $p = 0.5$.

Parameter	p_{S_O}	p_{S_D}	p_{S_T}	Profit, \$/hour	λ_D	λ_T	μ	p
Salem Unit 1	0.940733	0.059262	5.05E-06	115615.6	0.002767	7.30E-06	0.0439	0.5
Salem Unit 2	0.959751	0.040234	1.36E-05	128694.1	0.00149	2.39E-05	0.0355	0.5
Hope Creek	0.9968998	0.003097	2.49E-06	154229.5	0.000283	0.000141	0.0910	0.5

Table 12. Stable probabilities of different states and hourly profit values for Markov chain models of different units, with $p = 0$.

Parameter	p_{S_O}	p_{S_D}	p_{S_T}	Profit, \$/hour	λ_D	λ_T	μ	p
Salem Unit 1	0.940737	0.059257	5.27E-06	115618.6	0.002767	7.30E-06	0.0439	0
Salem Unit 2	0.959764	0.040222	1.36E-05	128702.0	0.00149	2.39E-05	0.0355	0
Hope Creek	0.9969021	0.003095	2.52E-06	154231.1	0.000283	0.000141	0.0910	0

Table 13. Stable probabilities of different states and hourly profit values for Markov chain models of different units, with $p = 1$.

Parameter	p_{S_O}	p_{S_D}	p_{S_T}	Profit, $/hour	λ_D	λ_T	μ	p
Salem Unit 1	0.940728	0.059266	5.03E-06	115612.4	0.002767	7.30E-06	0.0439	1
Salem Unit 2	0.959738	0.040247	1.36E-05	128685.2	0.00149	2.39E-05	0.0355	1
Hope Creek	0.9968976	0.003099	2.57E-06	154228.0	0.000283	0.000141	0.0910	1

Analysis of Table 11–Table 13, reveals that the highest hourly profit for all three units is achieved for $p = 0$ (in other words, going from the tripped state directly to fully operational state is the most economical strategy). The Hope Creek NPP has the highest hourly profit, due to featuring the lowest transition rate to the derated state, λ_D, and also due to having the highest maintenance rate, μ. For the currently used model, it assumed that $\mu = \mu_D = \mu_T$—namely, the maintenance rates are the same when transitioning from tripped or derated states. Also, due to lower downtime rates and higher maintenance rates, the Hope Creek NPP has the highest probability of being in a fully operational state for all three values of the parameter p.

5.3 Hazard Model

The hazard function (or instantaneous failure rate) is a function of t, the time reached/survived without failure [27]. It is not a legitimate probability density function (PDF), since its integral diverges. The hazard function (instantaneous failure rate) is a conditional PDF calculated at survival time t.

Since the exponential distribution is inappropriate for modeling aging and degradation, other distributions must be explored to describe ongoing degradation. One such widely used distribution is the Weibull distribution [27]:

$$f(t;\alpha,\beta) = \frac{\beta}{\alpha}\cdot\left(\frac{t}{\alpha}\right)^{\beta-1}\cdot e^{-\left(\frac{t}{\alpha}\right)^{\beta}};\alpha,\beta>0,t\geq 0 \quad (16)$$

The Weibull distribution, which can be considered an extension of the exponential distribution, has two parameters: α and β [27]. β controls the shape of the distribution, while α controls the scale or variance, as is evident from Figure 44. The parameters of the Weibull distribution shown in Figure 44 are used to demonstrate the parametric dependency of the distribution, and are not obtained by fitting plant-specific data.

As seen from the top panel in Figure 44, if α is fixed and β is varied, the PDF of the distribution is changing shape. If β is fixed and α is varied, as shown in the bottom panel, the PDF's shape remains the same, but the spread of the PDF changes, indicating changes in scale or variance. For the Weibull distribution, different values of β produce different distributions. For example, for $\beta = 1$, the Weibull distribution becomes an exponential distribution, while for $\beta = 2$, it corresponds to the Rayleigh distribution. The hazard function for the Weibull distribution can be written as [27]:

$$h(t) = \frac{\beta}{\alpha}\left(\frac{t}{\alpha}\right)^{\beta-1} - power\ of\ t \quad (17)$$

The Weibull hazard function for different values of parameter β is shown in Figure 45. The figure shows the hazard rate behavior for 900 hours; however, the behavior is retained if the time scale is extended to thousands of hours or days. For example, for $\beta = 1$, the hazard rate will be a constant, while for $\beta = 2$ it will be a linear function of time, regardless of time scale.

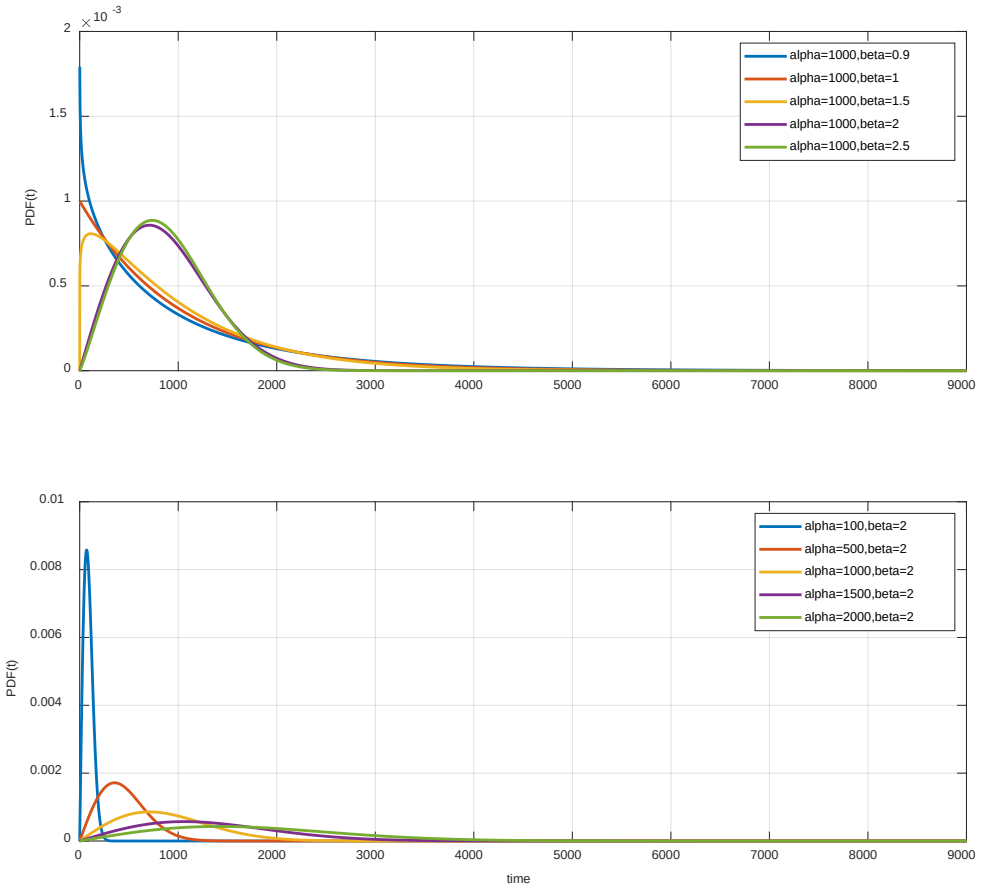

Figure 44. Weibull PDF for different values of parameters α and β.

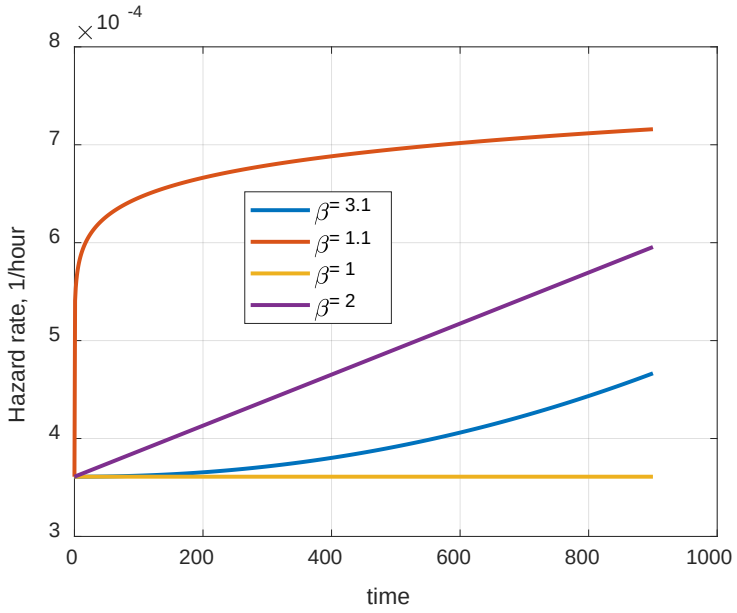

Figure 45. Hazard rate for the Weibull distribution with different values of parameter β, and parameter $\alpha = 2.7 \cdot 10^3$.

In contrast to the exponential distribution, the Weibull distribution can be used to model aging and degradation, as its conditional PDF differs from its unconditional PDF, as is shown in Figure 46, which demonstrates the dependency regardless of time scale.

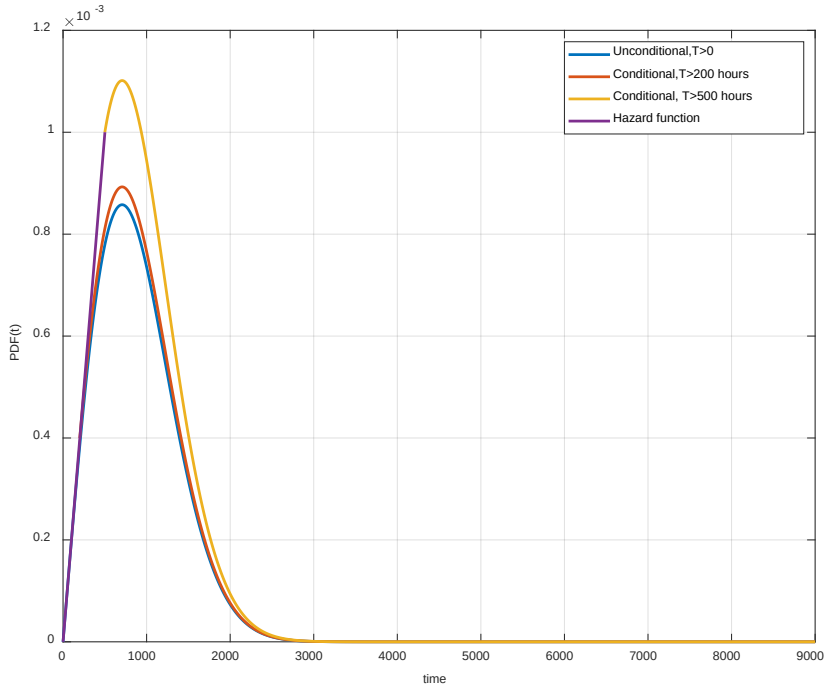

Figure 46. Unconditional/conditional PDFs and hazard function for a Weibull distribution with α = 1000 and β = 2.

The Markov chain model, however, can be generalized to time-dependent transition rates—for example, to account for equipment degradation. Equipment degradation is normally detected via a degradation variable (e.g., temperature, vibration, strain, or a combination thereof). Having obtained the degradation variable, a time-dependent transition rate, λ(t), can be represented through a proportional hazard model [28]:

$$\lambda(t|\beta) = \lambda_0 \cdot e^{\beta(t)} \tag{18}$$

where λ_0 is the stationary downtime rate in the absence of any degradation and β is the degradation variable that reflects the deterioration of a piece of equipment.

In this report, the Salem Unit 1 CWP diffuser degradation determined via the vibration data is used to demonstrate how degradation information is captured using the proportional hazard model. For details on the CWP diffuser degradation and the computation of the degradation variable, β, see [12,29]. The time evolution of the degradation variable for the CWP diffuser is shown in Figure 47. As seen in this figure, after a time stamp of 200 hours, the degradation variable starts to increase, reflecting the deteriorating condition of the CWP. For this report, the proportional hazard model was only used for parameter λ_D.

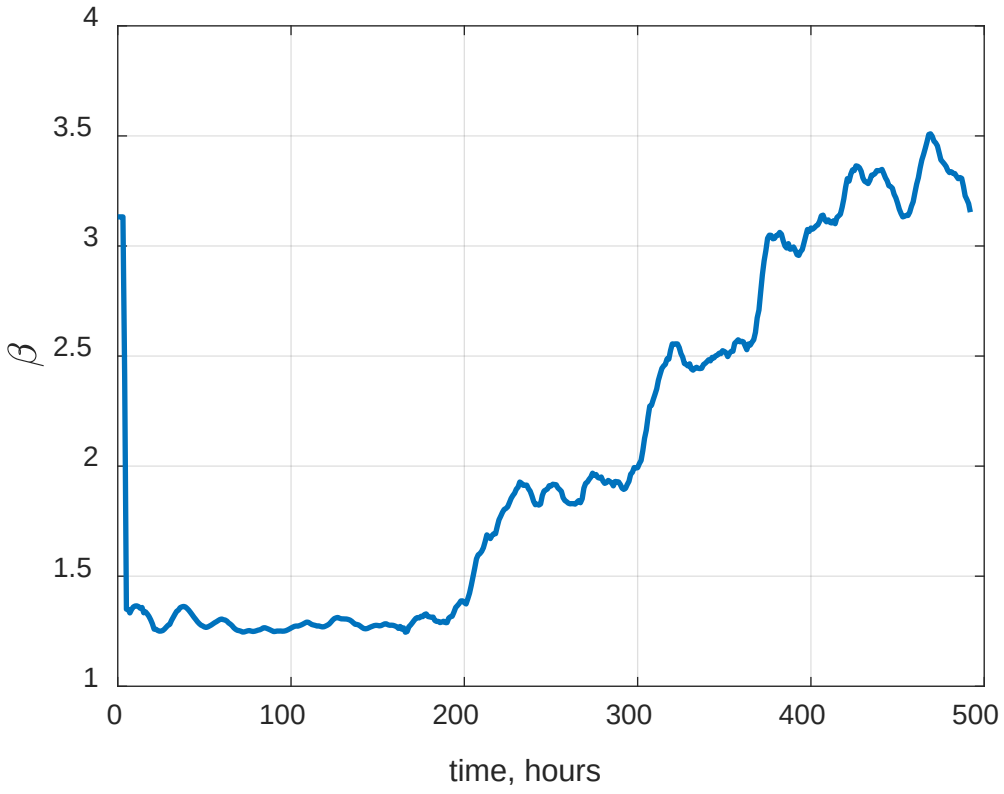

Figure 47. Time dynamics of degradation variable β for Salem Unit 1.

The time evolution of state probabilities and hourly profit for the proportional hazard model is shown in Figure 48. As seen in the figure, the probability of being fully operational, p_{S_0}, starts to decrease at a time stamp of around 200 hours. At the same time, the probabilities of two other states (i.e., the derated state, P_{S_D}, and the tripped state, P_{S_T}) starts to increase, reflecting the degradation of a CWS M&P set. The bottom panel in Figure 48 shows the changes in expected hourly profit for the unit, revealing that, under this degradation scenario, the unit quickly starts losing money unless the degradation process is reversed or fixed. It should be emphasized that, while economic analysis of the system performance is beneficial for foreseeing economic losses and gains, it can only be meaningfully applied in the case of long-term operations (e.g., the duration of the fuel cycle). In a quickly developing situation such as the CWS M&P set degradation described above, the profit calculations are only useful for indicating how rapidly the system is moving toward economic losses.

The rate of financial losses, as described by the hourly profit equation, depends on parameter values obtained from plant operational experience. For example, the derate levels of different plants may differ significantly based on time of year and the number of M&P sets. The proportion of time that the plant spends in a certain derated state also affects its hourly profit. While the parameters of the hourly profit equation (i.e., equation [15]) are plant-dependent, they can be adjusted to accommodate the operational practices of different plants, thus demonstrating the scalability of the hourly profit equation and economic analysis to a variety of operation conditions and plant types.

The proportional hazard Markov chain model uses forecasted values for the degradation variable; the profit curve in Figure 48 shows the time window of opportunity for the plant to return to profitability before it suffers financial losses. This provides plant management with the forecasting opportunity to plan PM and CM.

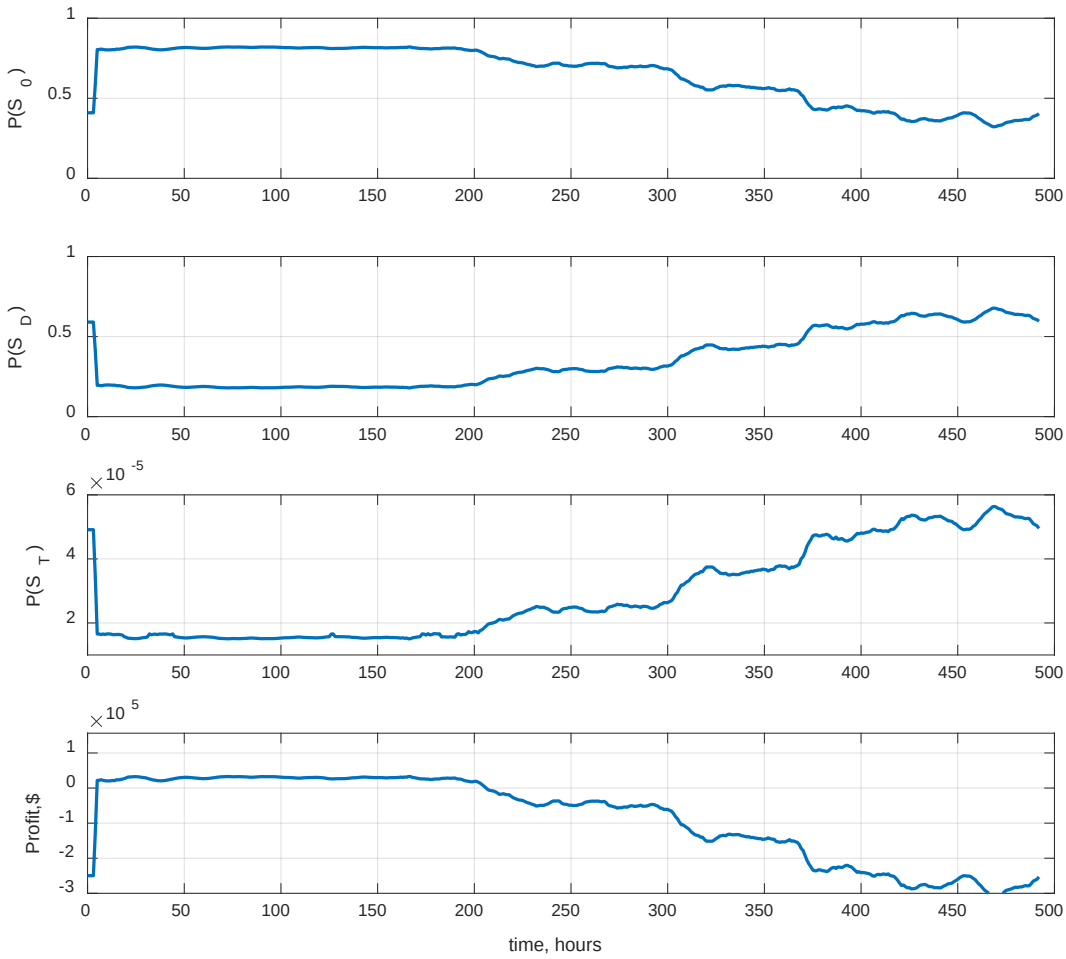

Figure 48. Markov model probabilities of state and profit for the proportional hazard model for Salem Unit 1.

The example shown in Figure 48 is for a single-variable proportional hazard model. This model can also be scaled to multiple degradation variables representing different subsystems of the plant:

$$\lambda(t|X) = \lambda_0 \cdot e^{(\beta_1+\beta_2+\cdots+\beta_n)} \tag{19}$$

where β_1, β_2, …., β_n are degradation variables for the different subsystems of the plants. The Markov chain model can also be scaled in order to add a PdM system to a plant's subsystems. In this case, the benefits equation can be modified as follows:

$$Hourly\ Profit = Hourly\ Revenue\ at\ Full\ Power \cdot p_{S_0} - \big((LR + FR_1 + MC)T_1 + (LR + FR_2 + MC)T_2 + \mathbb{I} \cdot (LR + FR_3 + MC)T_3\big) \cdot p_{S_D} - (LR + Hourly\ Revenue\ at\ Full\ Power + MC) \cdot p_{S_T} - Total\ Hourly\ Cost\ of\ PdM\ Ownership \tag{20}$$

where $Total\ Hourly\ Cost\ of\ PdM\ Ownership$ includes the capital and operational expenditures of the PdM system**.**

For the purposes of demonstration, assume the total cost of the PdM is approximately $135K for 9,000 hours of operation, resulting in an hourly cost of PdM of $15/hr. Further, assume that the hourly O&M labor is $100 and the hourly operational cost of materials is $333. The PdM system does not directly affect the failure/downtime rate, though it does affect maintenance rates, as it enables

maintenance to be performed more quickly and efficiently. Table 14 shows the change in profit after simply introducing PdM and assuming that the PdM increased the maintenance rate μ by 10%.

Table 14. Stable probabilities of different states and hourly profit values for Markov chain models of different units, with $p = 0$ and a PdM system introduced at an hourly cost of $15, and with μ increased by 10%.

Parameter	p_{S_O}	p_{S_D}	p_{S_T}	Profit, $/hour	λ_D	λ_T	μ	p
Salem Unit 1	0.9458327	0.054163	4.25E-06	119106.4	0.002767	7.30E-06	0.0483	0
Salem Unit 2	0.9632867	0.036701	1.13E-05	131108.7	0.00149	2.39E-05	0.0390	0
Hope Creek	0.9971827	0.002815	2.10E-06	154408.9	0.000283	0.000141	0.1001	0

The profit column in Table 14 should be compared with the one in

Table 12. Introducing PdM at a cost of $15 an hour and increasing μ by 10% as a result of using PdM is already beneficial to the plant's bottom line. This example demonstrates how utilities can use the proposed economic modeling to make decisions on introducing new technologies or implementing new maintenance policies. For example, prior to purchasing a new PdM system, the utility may want to investigate how much it will affect its maintenance rates and whether the benefits justify the spending. The economic modeling is scalable to different monitoring equipment, the different subsystems in the plants, and the different costs of ownership.

6. USER-CENTRIC VISUALIZATION

6.1 Introduction

Prior research has demonstrated that a risk-informed PdM strategy requires a carefully designed visualization scheme to plainly communicate the information from the risk-informed models and predictions to analysts and other plant personnel. Visualizations comprised of graphical representations are an effective means of conveying complex system statuses and supporting data processing for abnormality diagnoses. Graphical representations of large datasets leverage the immense innate processing power of the human visual system to communicate trends, complex patterns, outliers, or other data characteristics. This enables users to quickly ingest, process, and make decisions on large, complex datasets in order to support business and operations strategies. Within the context of risk-informed PdM, these visualizations serve several key functions for maintenance, engineering, operations, and management personnel. First, since the visualizations (particularly the health status of components) are driven by ML algorithms designed to predictively identify abnormalities across different operational contexts, they provide alerts indicating potential equipment degradation. Second, the visualizations serve as power data aggregation and synthesis representations to support personnel in diagnosing a potential degradation in order to yield an understanding of its root cause and make informed decisions concerning the amount of risk the degradation poses to the overall operation of the plant. The capability to detect potential degradation and support analysts in focusing their efforts on monitoring these flagged components is, and will continue to be, a critical piece of the broader operational posture for NPPs, as these facilities are now reaching 40, 50, or 60 years of age. In many instances, these plants use parts no longer in production. Due to the important place these plants occupy in our nation's power supply, having real-time clarity and transparency into these systems' performance is imperative, and well-designed visualizations can support these goals.

In developing the visualization front-end for this risk-informed PdM system, some key differences with other standard visualizations or dashboards were encountered. This project sought to establish an interface system and data interaction structure for the broader diagnosis, monitoring, and engineering organizations in order to support a better understanding of component health. PdM is an important goal

for nuclear power, and this project seeks to develop an ML-informed interface that leverages the facility's high levels of data maturity and the novel ML approaches developed for the project. The interfaces designed here extensively rely on state-of-the-art visualization techniques, but these visualizations are not the central focus of the interface. Indeed, utilities already challenge their staff with numerous complicated software systems, and this project strives to avoid being just another new system that staff must contend with to perform their tasks. Instead, the philosophy driving the interface design is that the interface and all accompanying visualizations serve as vehicles to convey the ML output in an intuitive, effective manner. The design team's primary goal was to collect user needs and requirements in order to inform the design of an interface structure that would enable them to immediately perceive and understand plant data as well as interact with the underlying ML model and its predictions—all within a functional, usable structure to assist plant personnel in maintaining the systems efficiently.

6.1.1 Research Problem

The nuclear power industry is made unique by the incredibly variegated systems, facilities, and deployments involved. Companies or organizations involved in managing these facilities continually work to employ a maintenance and operation standard for the plants within their portfolio, and the immense variety of systems can be a large obstacle to that goal. While these plants cannot all be standardized across a given company's fleet, the approach instead attempted to develop a scalable visualization scheme to enable cross-facility users to understand the states of these systems without having to remember and use entirely separate pieces of software. Organizational costs to train on multiple software platforms—as well as the potential for human error introduced as users try to juggle different applications—render the older paradigm unsustainable. The solution is to explore whether visualization concepts exist that could be employed in a way that allows different user types from different facilities to use the same platform in support of their decision making. To achieve this goal, it was hypothesized that a concept termed "user-centered scalability" may be the key to unlocking cognitive design principles in order to develop a standard design to support common cognitive tasks associated with data analytics.

6.1.2 Scalability Across Plants, Systems, and Users

Scalability is commonly applied to software development, with a model or code potentially being scaled to a broader application set or to a significantly larger data landscape. User-centered scalability refers to the process of designing a visualization that is useful to a variety of users across a range of disciplines. This concept is a response to issues involving various types of facilities/personnel and the need for organizations to align information across these different types. Organizations also have significant incentives to align their systems. Expecting personnel to work across many different monitoring systems increases the risk of human error, miscommunication, and poor performance. Difficulties in coordinating and communicating across these systems highlight and further exacerbate these issues. Therefore, the human factors team hypothesized the user-centered scalability concept as a method of aligning all various data sources and visualizations in order to reinforce teamwork and user mental models.

6.1.3 Cognitive Task Design

To design a visualization scheme that can be useful across disciplinary lines, the research team needed to understand the specific cognitive tasks users performed when interacting with visualized information. The misconception to be avoided was that the differences among, for example, engineers, maintenance staff, and management are so stark that no configuration of information could satisfy all parties. It is true that each potential user base has very different end goals for the information they access, but these goals and tasks can be deconstructed into specific cognitive parts and tasks. This deconstruction will be part of ongoing work. Deploying robust cognitive engineering into the design tasking will make this scaling more effective. Figure 49 shows a layout with specific locations allocated to user queries and where on the visualization the answers could be found. The cognitive tasks are collected through user

research methods, including operating experience review, task analysis, and informal allocation of functions. The initial collection of cognitive tasks is explained in greater detail in Section 2.

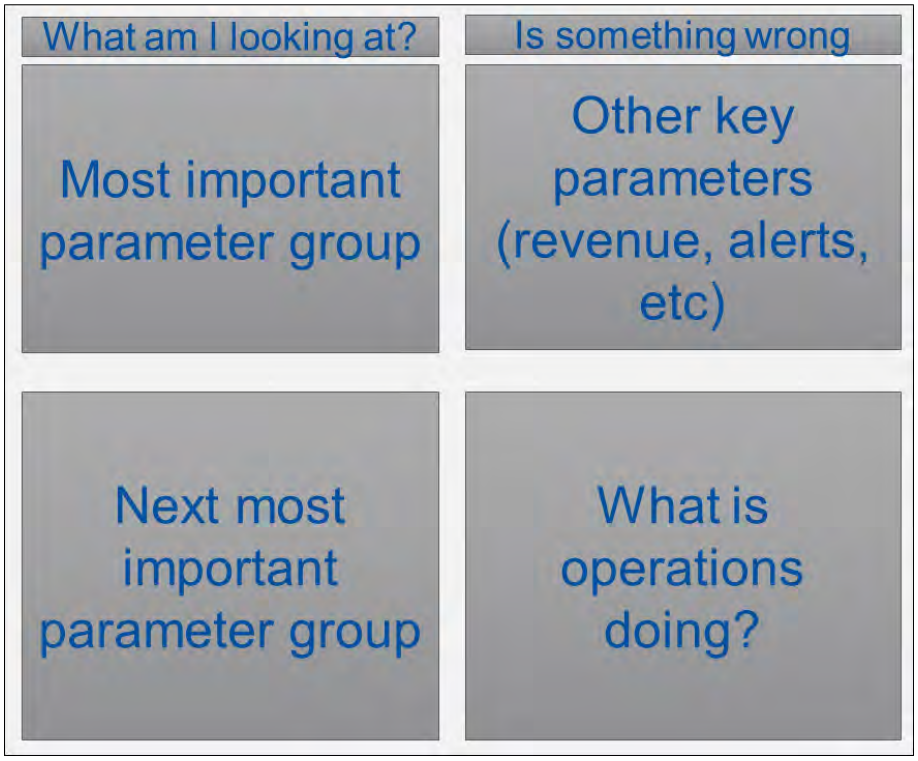

Figure 49. Cognitive layout example.

6.1.4 Design and Evaluation Process

To fully capture the specific cognitive tasking and validate different design concepts, the design team planned an initial three-round interview process with two rounds of prototype iteration, as shown in Figure 50. The participant roster included seven individuals with varying ranges of experience in the nuclear field, roles at nuclear facilities, and technical backgrounds. During round one, participants were asked to explain their approach to PdM tasks, the information they look for to understand a system's state, and what challenges they have experienced. This operating experience review was intended to capture the specific issues that users have with the current approach. The result of this initial round was a list of design requirements and user needs derived from these interviews. The second round saw users experiencing an initial mockup of some of the designs that satisfied the previously identified user needs, and critiquing the designs to support further iterations. The third round will be very similar to the second round, as user requirements are updated and another iteration of the design is shown to the users. The iterative loop process ensures continual refinement of both the user requirements and the prototype design. The goal is to design a visualization that is deemed useful by each participant, thus validating the hypothesis of user-centered scalability.

During the interview sessions, the team adopted a semi-structured interview format in which some questions were pre-determined and the remaining time was spent exploring the interface and allowing for freeform questions and discussion. Repeated iteration and refinement of user needs is critical for the human factors design process, in that it helps ensure that the best design endures (see Figure 50). The design project was composed of multiple interview rounds, with participants representing various across the maintenance, engineering, and diagnostic organizations. The prototype evaluation rounds are a critical component of the evaluation loop. Any design prototype is the culmination of assumptions made by

designers working from the user requirements, and is an attempt to manifest the requirements into the interface components. It is critical to involve users in this process, however, as the designers will never truly capture the most useful design option on the first attempt. Therefore, the evaluative interviews are key for adjusting the design and requirements to capture user needs more closely.

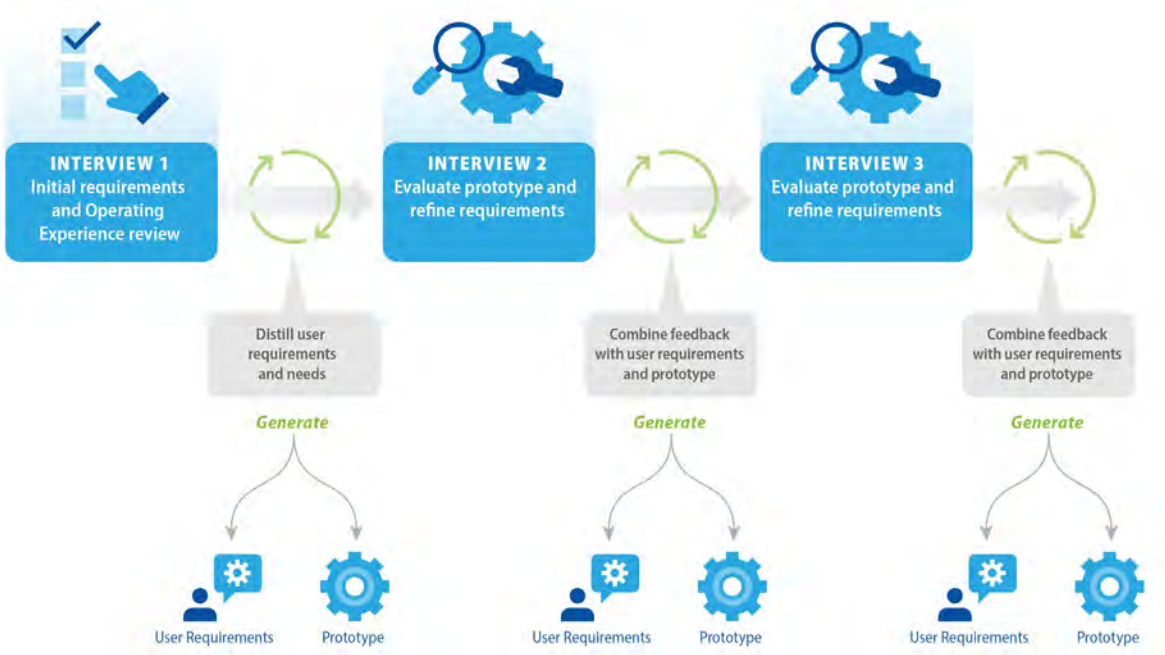

Figure 50. Interview and iterative process flow.

6.1.5 Prototype Approach

The prototype was designed within PowerBI, as per customer request, and that PowerBI file was connected to a database of parameter values and ML model outputs. A simple data model was constructed to ensure a quickly iterative process, and the overall dashboard layout was designed in a manner consistent with the cognitive task design principles shown in Figure 51. This initial prototype was developed from a limited dataset to test initial assumptions and enhance the responsiveness of the dashboard file. Following the second round of interviews, the design team will iterate on the designs and update the user requirements. Additionally, the next iteration will expand the datasets and ML model interpretability. The iterative process means that each interview stage will be followed by refinement and modification to the prototype design. It is critical that multiple iterations be performed during a design project in order to ensure triangulation [30] and thorough refinement of the user requirements. To some, certain iterative steps may appear redundant, but they are key to the overall process. It often takes multiple iterations and evaluations to design something that truly meets the user requirements, and to manage the modes and interactions in a usable manner.

Figure 51. User-centered design process [31].

6.2 Operating Experience Review and User Requirements Generation

Capturing and analyzing the current practices and workflow of the M&D analysts was an important step in the overall HSI development process. In accordance with good human factors practices within the nuclear domain and others, understanding the tasks performed by users is critical in developing HSI requirements to ensure that the HSI effectively supports and enhances users' abilities to perform those tasks. The human factors members of this research team conducted a series of interviews to identify M&D analysts' current workflow. The workflow described by the analysts aligned with their expertise-driven approach to evaluating data streams used to support their M&D tasks. Furthermore, the tools and techniques they described with positive utility during the interviews were invaluable for benchmarking features to include in the specification for the proposed risk-informed PdM HSI. Enhancements and additions requested by the analysts were then reviewed and synthesized into the developed specification. This specification was, in turn, used to develop an HSI prototype, and the operators were provided an opportunity to give feedback on the design. This section reports the approach, methodology, and outcomes of the initial investigation into the M&D personnel's current practices and the users' needs for a visualization to support a more efficient and robust risk-informed PdM concept of operation. The human factors team has an extensive research record in developing HSIs for nuclear process control. The development approach included a variety of iterative design activities and techniques, all adhering to the central user-centered design philosophy that considers the user to be the centerpiece of the system design.

6.2.1 Operating Experience Review

Central to the user-centered design approach is gathering information from the system end users, who are often licensed operators. But for the proposed system, the analysts and system engineers are the primary user base. Gathering user information is standard human factors practice, and various techniques can be found under a variety of different terms. In the nuclear domain terminology, this information-gathering activity is referred to as operating experience review, as per the Nuclear Regulatory Commission's guidance in "Human Factors Program Review Model" [32]. To this end, the human factors team performed a series of semi-structured interviews with M&D and system engineering personnel to capture the state of current practices and gather features to enable a more streamlined, efficient work process for analysts and the operations group as a whole. The collaborating nuclear utility provided access to several plant experts involved with diagnostic and maintenance activities at two NPP sites.

A total of eight individuals were interviewed by two human factors experts. The eight plant personnel included systems engineers, the M&D group manager, and M&D analysts. All the personnel had at least two years of experience in diagnostics and maintenance, while most had significantly more. The plant personnel were knowledgeable of the project's purpose and aware of the diagnostic capabilities of the ML algorithms under development. The semi-structured interviews included questions aimed at capturing how personnel currently perform M&D, issues they encounter regarding their current practices and tools, and how their current practices could be improved using the envisioned HSI diagnostic capabilities. Care was taken to ensure that participants had realistic expectations for what the algorithm could detect and convey within the proposed new system.

6.2.2 User Requirements Generation

For the first round of interviews, the human factors research team did not generate a mockup or initial design for users to provide feedback on. Typically, designers wait to begin designing any components of a mockup until initial discussions with users can be undertaken. This is due to the tendency of designers to become attached to specific features or components they feel add value to the task at hand. However, it is critical for designers to remember the adage "you are not the user" and avoid presupposing user needs. This decision was extremely valuable for these initial interviews, as users did not have to both describe operation experiences and pain points, as well as cognitively try to combine those pieces of information with the mockup being presented to them. As a result, the team could explore, via hour-long interviews, different scenarios, challenges, opportunities, and expectations regarding the extremely complex tasks that underlie diagnostic operations in complex NPP facilities. The result was an initial set of user requirements to inform the visualization design, as well as collaboration with the ML model team in terms of back-end feature sets that would be needed to support the user requirements. Table 15 shows the initial requirements collected from these interviews. The requirements were fairly high level and oriented on task rather than specific visualization element. This is predictable, as the design team would be expected to apply their expertise to the user needs and attempt to create the best option to satisfy those specific needs.

A unique characteristic of visualization design and mockups—one that differs from application or web design—is the need for a data model to populate the visualization software. A graph with obviously false (i.e., dummy) values produces an odd effect in which users cannot express preferences as well. Human understanding of these digital data visualizations has become so solidified that the specific element designs operate in parallel with the data. As such, if the design does not have the specific data or information to populate a feature, that feature will not be included in the mockup. Table 15 shows this by highlighting that most of the requirements were not added to the initial iteration. This was not generally due to any issues or limitations, but rather because the data model developed for the initial iteration was a specific vertical slice of one system over a specific period of time, and was not built with all the logic and external connections the users requested. However, future iterations will feature an expanded dataset and greater model development, resulting in more of these advanced requirements being integrated into the

design. The initial interviews succeeded in better capturing the operating experience and user postures that the design needed to support. They also succeeded in eliciting specific needs or feature options from the diverse sets of users interviewed by the team.

Table 15. Initial user requirements and disposition.

Requirement	Description	Disposition
Narrative Log Immediate Access	Most of the users interviewed discussed the need for quick access to the logs from operations in order to cross-check system states and conditions with potential operator actions in the control room.	Added to first iteration
Risk and Priority Communication	All users discussed the need to understand the relative risk of system or component degradation, as well as decision support in priority determinations for maintenance actions.	Not in current iteration
Smart Alert Generator	Currently, system alerts are defined manually by the M&D center staff. Users requested a model-based, data-informed alert generation engine that can detect different anomalous conditions and communicate them to users.	Not in current iteration
Smart Diagnostic Pathing	Users requested a recommended “first step” or actionable suggestion from the system. For example, instead of just alerting the users of specific deviant conditions, users requested a recommendation engine to assist them with what further action to take, value to verify, or process to look further into.	Not in current iteration
Contextual Grouping	Users requested that abnormal values be grouped or contextualized within the system, along with the identification of other values that may be linked or impacting/impacted by the abnormal value. This orientation is important in trying to actively diagnose slight degradations that may be predictors of larger issues.	Added to first iteration
Advanced Sharing Function	A specific interaction that came up in most interviews was the need for precise visualizations seen by one analyst to be quickly shared with the team at large. Currently, the more manual process of printing screens and emails could potentially be replaced by the generation of a hyperlink with a specific time and feature selection sharable with other team members, thus facilitating better communications.	Not in current iteration
Model Explainability	Users were skeptical of using a ML model to determine the health status of a specific system or component. The users require a way to easily see and understand the model’s decision-making process, and see other potential options.	Added to first iteration

6.3 Visualization Concept

The human factors team initially determined the layout of some of the specific areas that would be needed and would legibly fit within the canvas area. The team was aware that certain specific requirements would be implemented into this initial mockup, due to model and data limitations. However, the most important request was for clear access to the operations narrative log readouts. This was one requirement that the team ensured was present in the mockup, and that the data was valid. The design had to function within the standard PowerBI framework to ensure easy adoption by the utilities, without requiring customized integration for a given utility or site.

6.3.1 Initial Mockup Design

The initial draft layout is shown in Figure 52. Six may seem a low number of sections, but with the use of advanced graphing techniques, the team could mockup the key parameters found in the data at hand. Additionally, one concern with the existing operating experience of these diagnostic tasks is that the graphing of multiple parameters can become messy, creating a visualization that is difficult to parse. The team wanted to avoid that with the initial mockup, and tried to place only the absolute minimum necessary numbers of parameters onto the canvas, under the assumption that it is always easier to add items than remove them.

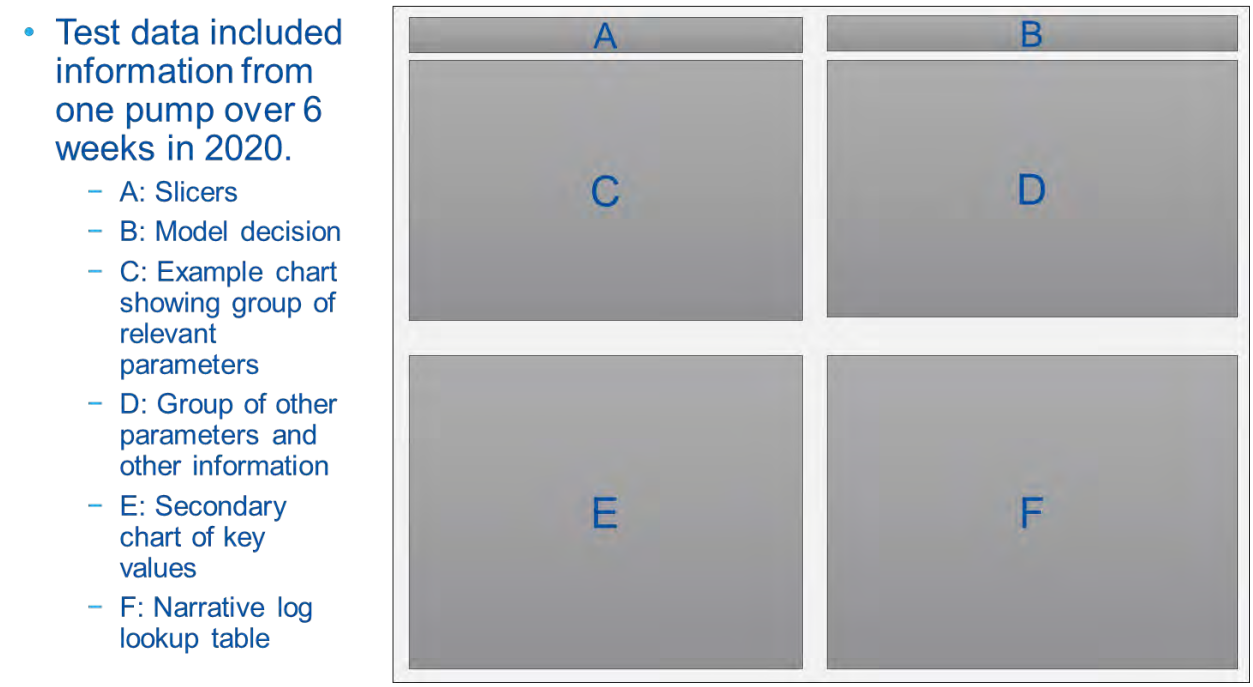

Figure 52. Initial mockup draft layout.

As described previously, this initial mockup was created using a smaller, demonstration dataset to fully test some of the concepts without having to manage the large computational loads incurred when using a full dataset. NPP systems and components generate incredibly detailed—and thus large—datasets that can cause lagging issues in the demonstration if the platform and model are not well optimized. As such, the initial mockup tested some specific assumptions in a smaller venue.

Section A houses the current slicers for this dataset. This includes options to select a time range, different facilities, or pumps. All displays and calculations within the visualization are driven by these selections, so its placement in the upper-left corner makes it the primary location that users interact with when first opening the dashboard.

The tools available to M&D personnel in current operations do not provide the users with a visualization tool to persistently display key parameters. Rather, they must select specific datasets and parameters to input into a specific graph. This prototype interface was intended to capture consistently referred-to parameters, and group them near each other to support a simple perception and understanding loop for the users of the visualization. In Figure 52, the two primary sections for this task are C and E, and these were intended as the landing positions for orienting users to the current state/status of these items. It was assumed that if the primary parameters were in a single section of a shared graph, this could quickly orient users to specific concerns or issues, and drive deeper, more targeted analysis, as needed. This was largely viewed positively, and the general concept was satisfactory, though the second-round interviews featured some recommendations on which specific parameters to include.

Figure 53 shows these sections with some completed graphing present. The specific sections included are meant to show how the user sees the dashboard; however, steps were taken to mockup and anonymize the visualizations to prevent the release of any participating utility partner's proprietary information. The initial mockup was received positively by the users, and further iterations will follow the interview process; those displays will be likewise included in the next round of user interviews, with the goal of refining and capturing requirements until all are present and performing to users' satisfaction.

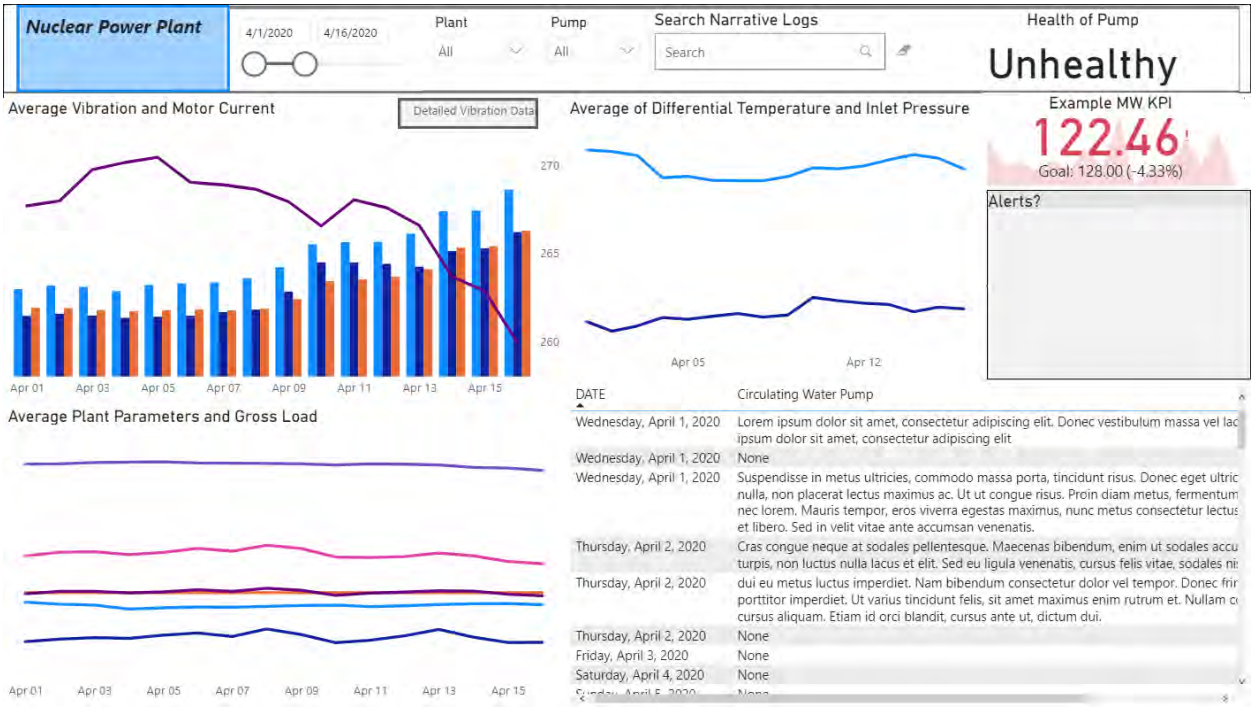

Figure 53. Anonymized dashboard design.

6.3.2 Human-Centered Artificial Intelligence (HCAI) and Supporting Explainability

A large focus of AI/ML technologies is ensuring that their functioning and logic are transparent and explainable to human users. As a field, explainable AI (XAI) has experienced significant growth in recent years, and is often considered a core feature of these systems. There are reasonable, prudent concerns in implementing inscrutable (i.e., black-box-style) systems, particularly if they are working in a key aspect of society, such as the criminal justice system, mortgage approvals, or, in this case, critical energy infrastructure. The ML model in this visualization project is no exception, and the human factors and ML teams worked closely from the outset to ensure that both the visualization and the ML model were symbiotic, and that each supported the goals of the other. The team further sought to delineate the perhaps

more common term of XAI from what has been defined as HCAI [33]. HCAI brings the user-centered approach from design and applies it to the AI/ML space. Specifically, the concept of HCAI differentiate itself from other similar fields by resisting attempts to automate humans out of various roles. Often, automation is considered a component that functions at the same level as a human; thus, human operators could have their tasks or entire roles replaced by automated systems or machines. HCAI, on the other hand, suggests that advancements in automation (or computation [e.g., AI/ML]) should instead be viewed as supplementary to—and empowering of—human capabilities. These dashboards are intended, both in function and design, to help enhance the effectiveness and efficiency of human operators and users by designing graphical elements that align with information processing research, and ensuring that ML-informed components are clear and transparent to the user. This explanation of the system aligns far better with the notions of HCAI than with other XAI-focused fields.

One explicit requirement that users had was driven by a healthy skepticism of trusting an ML model to determine the health of an item and—more specifically—make a decision based on that determination, without further validation. To solve this, the human factors team worked closely with the ML model team to understand how the model functioned and how its decision process could best be captured for the users. The goal was to ensure that the model did not become a black box and that the users had transparency into the model and oversight into its decisions. Windowpane B in Figure 52 is a simple readout of the determination of *healthy* or *unhealthy* for users to see immediately. While the user hovers a cursor over the text, a tooltip popup expands to show the feature importance values that various parameters had on the decision. For example, the model tells the user the top three contributing factors to the determination of a pump as being *unhealthy*. This enables the user to supervise and dig deeper into identified parameters if further analysis is needed before taking a subsequent diagnostic action. This feature was received very positively in terms of how the concept of explainability was captured, as well as its ease of use. However, there were some concerns in using feature importance and how it truly translates into something the user can readily understand. This is a valuable piece of feedback for the next iteration—as the dataset and model grow, additional opportunities may be available to communicate these values.

6.3.3 Narrative Log Feature Set

One of the final components to mention was the inclusion of narrative logs into the visualization interface. As mentioned earlier, in many instances, 50% or more of the specific alerts or abnormal parameters that users see are due to an action taken by the control room. The ability to quickly determine a specific situation's link to these operations actions is important to the broader ability to perform diagnostic and monitoring oversight to the broader systems. The human factors teams included narrative logs in three places in the interface, due to its high priority for users. First, in section F of Figure 52, a table showed the entire set of narrative logs for the time scale selected in section A, enabling users to explore the entries as needed. Next, the narrative logs were included into the on-hover tooltips for the other chart visualizations. This enabled users to hover over a specific data point and have a window pop up with some additional details or information. The inclusion of these narrative logs gave the users a way to immediately link the data point at hand with operations actions, speeding up the overall process of monitoring these situations. Lastly, the human factors team also included a search function that allows users to input a specific text string and search within the table for a narrative log that includes that specific text. An additional feature of the search box is that it acts as a slicer and will isolate the data points that relate to the searched-for text. This can help users if there is a need to explore what data points look like when operations notes specific actions.

6.4 Second-Round Interview Process

The second interview process was less structured than the initial requirements gathering. This was a conscious choice made by the human factors team to employ a more exploratory "think aloud"-style process and facilitate a more freeform discussion regarding the interface. The same participant roster was used, save for one change due to a previous participant switching roles and being replaced. The new analyst was added to the roster to give some fresh insights into the design. Another reason to allow for a more exploratory approach was to facilitate each user exploring and asking their own questions. Typically in design projects such as this, there is a common theme in your user base, or an ideal "customer" for commercial applications. However, this project's primary focus is on the differences among users, rather than on any commonalities that may be present. The goal of the project is to have an individual place where multiple departments and disciplines can get the needed information to perform predictive diagnostics and maintenance tasks. While some areas of the dashboard caught every user's interest, each user had unique contributions to the insights gathered and helped reinforce some early requirements, as well as provide some new opportunities for the design.

The second-round interview involved some limitations to be discussed, particularly the robustness of the initial dashboard design. Ultimately, this project seeks to show CWS data and status across three different NPPs (one boiling-water reactor and two pressurized-water reactors), yet this initial dashboard was only loaded with one pump from one location across a narrow slice of time. As mentioned above, this decision was made partially due to the selected data being the most prepared and ready for visualization, but also to explore some initial conceptions and assumptions without having to bring in a massive dataset. This choice does insert some limitations to findings from this round, as many different interactions and representations of the data were not present in the iteration and thus could not be tested. This does not undermine the validity of any findings or the feedback received, but will likely lead to a more conservative iteration between the second and third rounds as more datasets are added and those interactions are available to test.

Another limitation is the requirements in Table 15 that are not present in this iteration of the design. As such, some features or aspects have not been designed out and tested with the user base. These components generally describe more advanced functionalities that will likely interact with other systems and thus necessitate more care in designing interactions that suit the entire user base. This will be a large challenge as the project moves forward, and the human factors team will need to consider these external connections and guiding the user appropriately as they explore the data and problem space. Recall that each user requirement is derived from explicit pain points elicited during the initial user requirements evaluation; as such, they are all key components of the design that will be implemented into future iterations.

6.4.1 Results

Overall, participant feedback regarding the prototype was positive, and the participants were able to clearly understand the visualization design and system layout. The narrative log inclusion was a very positively received feature; the search function and the filtering interaction were both reviewed as being helpful in their daily tasks. As an initial prototype, and considering the limitations discussed above, the overall impression was positive.

Several issues and criticisms arose from the evaluations. More specifically, these involved the parameter selection in the graphs and the ML-model explainability. Broadly speaking, the integration of expanded datasets will support a filtering mechanism that enables users to select from certain options regarding parameter sets. Beyond this selection interaction, more research will be undertaken during the next iteration to better understand the relations of specific parameters and how they should be displayed to maximize usability for the user base. Another interesting issue that was discovered pertained to disciplinary differences among the various fields of engineering—specifically mechanical and electrical. Two participants were electrical engineers and mentioned that the standard plant parameters in the design

were not usable for them and not indicative of the problems they manage. This novel criticism will require additional research to better understand the data posture of the parameters needed by the electrical engineering teams at the site.

6.4.2 Refining User Requirements

If prototype development is one side of the iterative coin, the refinement of user requirements is the other, and the second round of this project provided more detailed requirements than did the initial set. This is not uncommon, as initial user requirements are often broader and at a higher level than the design implementation or development scope. As such, the results section above highlights some of the specific feedback received and captures some of the more granular requirements that will be added to the requirements document and addressed in the next iteration. At the time of this writing, the user requirements table has not been fully refined, but will be demonstrated in a future report.

Some specific requirements will be parameter-specific selections, filters, or other orientation components in the dashboard. Different ways will be considered to understand the ML model's decision process, and a method will be developed to drill down into this data to better understand how the model is working. Additional engineering focuses and a possible selection pane or filter for specific engineering disciplines are also needed, as mentioned by the electrical engineer participants. Additional R&D work will be required in order to better understand the current data posture of those parameters and ensure that their inclusion is technically feasible from a data perspective.

6.5 Summary and Discussion

This chapter explores a design project that is unique in terms of the notion that there is no ideal user. The challenge of this visualization design is also the hypothesis being tested by the human factors team: that an interface could be designed that is grounded on the cognitive tasks of the users and is responsive to those needs. Several limitations have been discussed, some technical and some hypothetical; however, the evaluative interview steps showed promise in regard to the hypothesis. The notion of cognitive task design was understood and well received by users, and future iterations that expand some of the design characteristics are expected to be similarly well received.

The design and evaluation process followed human factors best practices and employed several methods such as think-aloud, user-guided exploration and semi-structured interviews. The iterative process has been successful in refining user requirements and prototype designs. The human factors team will begin working on the next prototype iteration and design of the visualization, following completion of the second round of interviews. This process is also well suited to solving a variety of challenges such as designing a visualization platform that can support different staff, plants, and disciplines across the incredibly variegated landscape of nuclear power facilities and systems.

A key aspect of this project is the close collaboration between the human factors design team and the ML model development team. From the outset of this project, the two sides were engaged in discussions about the datasets, user requirements and needs, and model specifics. This enabled the teams to share needs and ensure that the model and design were both established in consideration of each other. A key concern voiced by users was strong skepticism of the capabilities and reliabilities of the ML model and the trustworthiness of this new system. Many of our users are completing complex diagnostic and exploratory tasks that involve navigating many different systems and compiling information from these disparate systems to support decision making and support for the nuclear power facilities that are critical for the communities they serve. As such, there is a high expectation of performance of the tools these groups rely on, and ML models can often drift into spaces or methodologies that are extremely complex and inscrutable. This possibility was not an option for the project, and the users expected full transparency into the ML model's decision-making process and the ability to affect the model's learning and development. XAI has become a term for this consideration of how users will access and understand the model, whereas "interpretable AI" focuses on ensuring that the ML model performs in a manner easily

understood by human users. However, the term HCAI better captures the expectations and challenges faced with increasing use of AI systems by human users. We are working closely with development teams to ensure that all aspects of the model are human-centered just as the interface design is, which can be a novel concept in ML modeling. The results from the second interviews showed that recognizing the users' needs and expectations and working to develop a solution to those initial concerns built significant trust in the ML model broadly, simply because the users could access the model's decision making and understand how it arrived at its conclusion. The notion that, by involving users as early as possible in any system design, the system will be made better at the end is not a novel concept; however, it was demonstrated in this project, as specifically related to ML model development and a very skeptical user population.

7. CONCLUSIONS AND PATH FORWARD

This report presented the R&D performed by INL in collaboration with the PSEG-owned Salem and Hope Creek NPPs to scale a risk-informed PdM strategy across different plant assets at the plant site and across the nuclear fleet.

To support the R&D, heterogeneous data collected on both the Salem and Hope Creek CWSs were received and analyzed by INL. Analysis of the CWS data was supported by information on maintenance logs, notifications, and WO documents, as well as interaction with both Salem and Hope Creek plant site engineers. As part of the data analysis, fault signatures were developed for specific CWS faults modes for both NPPs.

The Salem CWS fault signatures were used to develop two types of FL: the first based on an MK-SVM and the second based on NNs. The federated models developed for Salem were then used to estimate the state of health of the Hope Creek CWS (this process is referred to as TL). The results obtained were comparable to predictive models individually trained on Hope Creek data. This demonstrated the significance of the federated-transfer learning approach, and avoided building exclusive predictive models for each NPP and each system.

The scalability of three-state Markov chain risk models developed at the component-level, system-level, and even plant-level was demonstrated on the Salem and Hope Creek CWSs. Integration of state of health and time into static risk models using a proportional hazard model was used to derive probabilities reflecting NPP states. These state probabilities were used to understand the *economics of automation* achieved by transitioning from a time-consuming, labor-intensive, cost-prohibitive PM program to a risk-informed PdM strategy.

Given the variety of information generated—ranging from fault signatures, diagnostic/prognostic outcomes, probabilities of state, and hourly profit—an HSI design was created based on user-centric visualization guided principles, using the design inputs provided by users from the PSEG-owned Salem and Hope Creek NPPs. The HSI focused heavily on ensuring that the ML models were transparent and explainable to skeptical users by implementing HCAI concepts. The inputs were collected via a series of structured virtual interviews, and an initial prototype was evaluated in a second round of similar interviews. A representative user-centric HSI was developed using the Microsoft PowerBI platform.

The scientific accomplishments achieved under this notable outcome stem from developing innovative scalable technological solutions that signify advancements in (1) online asset monitoring, (2) data analytics, (3) modeling and simulation, (4) risk assessment methodologies, and (5) user-centered design strategies. These advancements are leading the transformation of the nuclear industry to adopt risk-informed PdM strategies. This adoption would drive automation, efficiency gains, enhanced reliability of plant systems, and substantial cost savings via dramatic reduction or elimination of unnecessary time-consuming, labor-intensive maintenance activities, helping nuclear power to achieve economic competitiveness in the energy market. Transferring the scalable technologies to an industrial partner such as PKMJ Technical Services LLC would enable their implementation in a cloud-based digital platform and broaden the possible implementation of technologies for use by industry in order to achieve the greatest return on investment based on economies of scale.

The scalable risk-informed PdM research summarized in this report will continue through further efforts planned activities under the TERMS project. Specifically, future work will focus on the explainability and trustworthiness of ML and AI-based technologies. These important, challenging aspects need to be addressed prior to adoption by the nuclear industry. In parallel, LWRS researchers, in collaboration with industrial partners, will develop the technical requirements needed for an AI/ML data architecture, as well as analytics capabilities that support implementation of the necessary trustworthy, explainable methodologies within a centralized digital platform.

8. REFERENCES

1. T. McJunkin, V. Agarwal, and N. J. Lybeck. 2016. “Online Monitoring of Induction Motors,” Idaho National Laboratory, INL/EXT-15-36681, Rev. 0. https://doi.org/10.2172/1239881.
2. V. Agarwal, N. J. Lybeck, and B. T. Pham. 2014. “Diagnostic and Prognostic Models for Generator Step-up Transformers,” Idaho National Laboratory, INL/EXT-14-33124, Rev. 0. https://doi.org/10.2172/1166054.
3. V. Agarwal, N. J. Lybeck, L. C. Matacia, and B. T. Pham. 2013. “Demonstration of Online Monitoring for Generator Step-up Transformers and Emergency Diesel Generators,” Idaho National Laboratory, INL/EXT-13-30155, Rev. 0.
4. N. Goss, et al. 2020. “Integrated Risk-Informed Condition Based Maintenance Capability and Automated Platform: Technical Report 1,” PKMJ Technical Services, PKM-DOC-20-0013, Rev.0.
5. V. Agarwal, et al. 2019. “Deployable Predictive Maintenance Strategy Based on Models Developed to Monitor Circulating Water System at the Salem Nuclear Power Plant,” Idaho National Laboratory, INL/LTD-19-55637, Rev. 0.
6. Idaho National Laboratory. 2020. “Light Water Reactor Sustainability Program, Integrated Program Plan,” INL/EXT-11-23452, Rev. 8.
7. V. Agarwal. 2018. “Risk-Informed Condition-Based Maintenance Strategy: Research and Development Plan,” Idaho National Laboratory, INL/LTD-18-51448, Rev. 0.
8. “Scalability of Risk-Informed Predictive Maintenance Strategy,” Light Water Reactor Sustainability Newsletter, Issue 13, May 2021. https://lwrs.inl.gov/Newsletters/LWRS_Newsletter_December_2013.pdf.
9. V. Agarwal, et al. 2020. “Scalability of a Risk-Informed Predictive Maintenance Strategy,” Idaho National Laboratory, INL/LTD-20-58848, Rev. 0.
10. “PSEG Configuration Baseline Document for Circulating Water System,” DE-CB.CW-0028(Z), Rev. 0, 1-1.

11. KCF Technologies, “KCF Wireless Vibration Sensor,” [Online]. Available: https://kcftech.com/hardware/ [Accessed August 2021].
12. V. Agarwal, et al. 2021. “Machine Learning and Economic Models to Enable Risk-Informed Condition Based Maintenance of a Nuclear Plant Asset,” Idaho National Laboratory, INL/EXT-21-61984, Rev. 0. https://www.osti.gov/servlets/purl/1770866.
13. T. Li, A. K. Sahu, A. Talwalkar, and V. Smith. 2020. “Federated learning: Challenges, methods, and future directions,” *IEEE Signal Processing Magazine*, 37(3):50-60.
14. K. Yang, et al. 2020. “Federated learning via over-the-air computation,” *IEEE Transactions on Wireless Communications*, 19.3: 2022-2035.
15. J. Brownlee. 2019. “Deep Learning for Computer Vision: Image Classification, Object Detection, and Face Recognition in Python,” *Machine Learning Mastery*.
16. S. J. Pan, and Q. Yang. 2009. “A survey on transfer learning,” *IEEE Transactions on Knowledge and Data Engineering*, 22.10:1345-1359.
17. J. Yang, J, et al. 2012. “Group-sensitive multiple kernel learning for object recognition,” *IEEE Transactions on Image Processing*, 21.5:2838-2852.
18. H. Drucker, C. J. Burges, L. Kaufman, A. Smola, V. Vapnik.1996. “Support vector regression machines,” *Advances in neural information processing systems*, May 9,9:155-61.
19. The COMSOL Multiphysics® software. [Online]. Available: https://www.comsol.com/ [Accessed August 2021].
20. V. Agarwal, S. Kovacevic, and P. Harry. 2020. “Hybrid Modeling of a Circulating Water Pump Motor,” Idaho National Laboratory, INL/EXT-20-59600, Rev. 0.
21. Worthington Corporation, “Instruction for Installation, Operation, and Maintenance, and List of Parts,” Pump and Heat Transfer Division, Harrison, NJ.
22. The COMSOL Multiphysics® software. Multibody Dynamic Module – User’s Guide. [Online] Available: https://doc.comsol.com/5.4/doc/com.comsol.help.mbd/MultibodyDynamicsModuleUsersGuide.pdf
23. F. Concli. 2020. “Journal Bearing: An Integrated CFD-Analytical Approach for the Estimation of the Trajectory and Equilibrium Position,” *Applied Science* 10, no. 23:8573.
24. W. L. Winston. 1991. *Operations Research: Applications and Algorithms*, 2nd ed., Boston: PWS-Kent Publishing.
25. L. Kleinrock. 1975. *Queueing Systems*, vol. I: Theory, Wiley.
26. W. Feller. 1968. *An Introduction to Probability Theory and Its Applications*, Volume 1, 3rd Edition Wiley mathematical statistics series Wiley.
27. H. F. Martz and R. A. Waller. 1982. *Bayesian Reliability Analysis*, New York: Wiley.
28. R. Nelson. 1995. *Probability, Stochastic Processes, and Queueing Theory*, Springer-Verlag.
29. Yarlett, et al. 2021. “Integrated Risk-Informed Condition Based Maintenance Capability and Automated Platform: Technical Report 3,” PKMJ Technical Services, PKM-DOC-21-0007, Rev.0.
30. M. Resnick, et al. 2013. “Triangulation of multiple human factors methods in user experience design and evaluation,” in *Proceedings of the Human Factors and Ergonomics Society Annual Meeting*, vol. 57,1:404-408.

31. *User-Centered Design Basics.* (n.d.). Usability.gov. Retrieved August, 3, 2021, from https://www.usability.gov/what-and-why/user-centered-design.html

32. J. O'Hara, J. Higgins, and S. Fleger. 2012. "Human factors engineering program review model," NUREG-0711, Revision 3: update methodology and key revisions. In *proceedings of 8th international topical meeting on nuclear plant instrumentation and control and human-machine interface technologies*.

33. B. Shneiderman. 2020. "Human-centered artificial intelligence: Reliable, safe & trustworthy," *International Journal of Human–Computer Interaction, 36*,6:495-504.

Appendix A

Layout of Circulating Water System at Salem Nuclear Power Plant

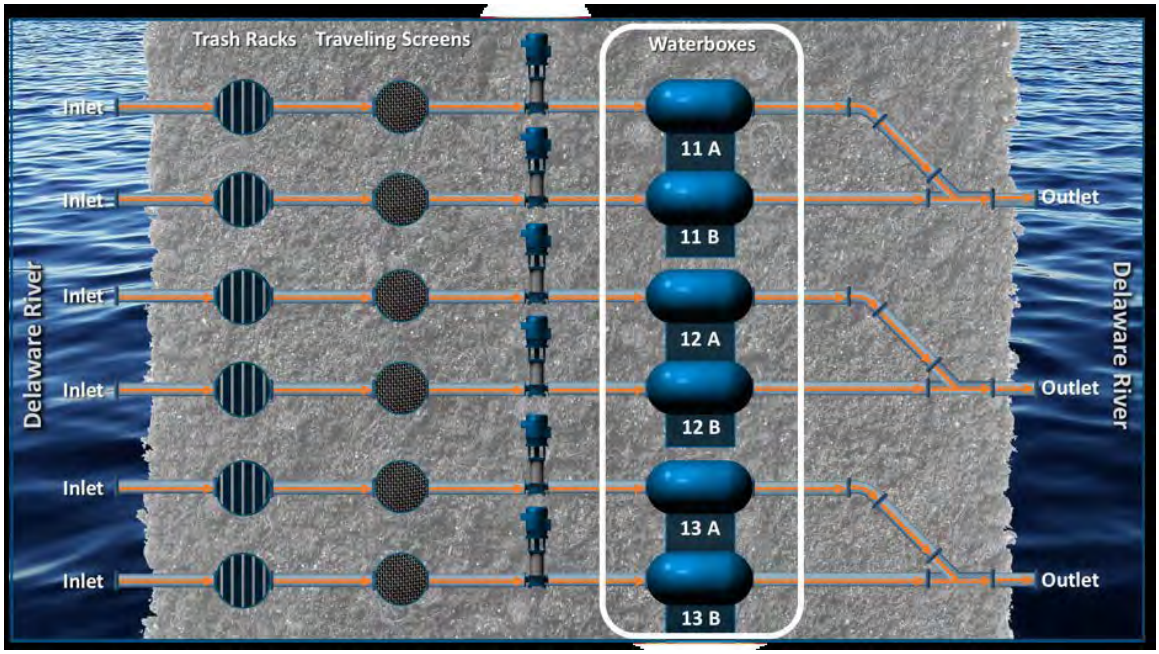

Figure A-1. Salem Unit 1 CWS with main condenser consisting of three pairs of condensers.

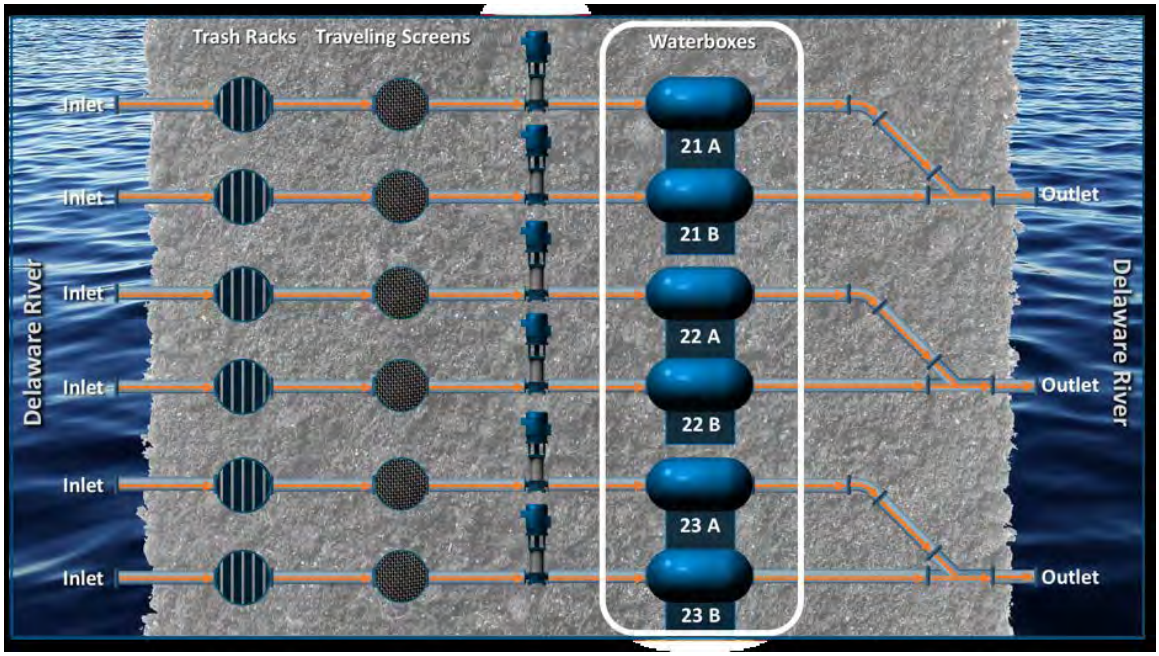

Figure A-2. Salem Unit 2 CWS with main condenser consisting of three pairs of condensers.

Page intentionally left blank

Appendix B

Plant Process Data Comparison of Salem and Hope Creek Nuclear Power Plants

Table B-1. Circulating water pump systems.

Data	Salem NPP	Hope Creek NPP
Pump Status	Y	Y
Inlet Pressure eSOMs	Y	N
AB Outlet Water Temperature	Y	N
Motor Axial Position	N	Y
CWP Discharge Valve Position	N	Y
CWP Basin Level	N	Y

Table B-2. CWP motor vibration and temperature.

Data	Salem NPP	Hope Creek NPP
Motor Inboard Radial (X,X.1, Y)	N	Y
Motor Outboard Radial (X,X.1, Y)	N	Y
Inboard-Bearing Radial (X,X.1,Y)	N	Y

Table B-3. CWP system condenser parameters.

Data	Salem NPP	Hope Creek NPP
Condenser Backpressure	Y	N
Condenser Wide-range Backpressure	N	Y
Condenser Narrow-range Backpressure	N	Y
Hotwell Level	N	Y
Hotwell Temperature	Y	Y
North End Inlet/Outlet Temperature	N	Y
South End Inlet/Outlet Temperature	N	Y
Secondary Condenser Discharge Flow	N	Y
Condenser Pump Discharge Valve Position	N	Y
Condenser North/South End Out	N	Y
Condenser Inlet	N	Y

Table B-4. Main turbine and vacuum parameters.

Data	Salem NPP	Hope Creek NPP
Condenser Backpressure	Y	N
Condenser Wide-range Backpressure	N	Y
Condenser Narrow-range Backpressure	N	Y
Hotwell Level	N	Y
Hotwell Temperature	Y	Y
North End Inlet/Outlet Temperature	N	Y
South End Inlet/Outlet Temperature	N	Y
Secondary Condenser Discharge Flow	N	Y
Condenser Pump Discharge Valve Position	N	Y
Condenser North/South End Out	N	Y
Condenser Inlet	N	Y

Table B-5. CWP maintenance parameters.

Data	Salem NPP	Hope Creek NPP
Gross Load/ Main Generator MW	Y	Y
Time/ Description	Y	Y
Ambient Temperature DEGF- 15 Min Avg	N	Y
Ambient Air Temperature	Y	N
River Level	Y	Y
CWP Inlet River Temperature/River Temperature	Y	Y
Cooling tower Basin level	N	Y
Cooling tower basin water temperature	N	Y
CWP Narrative log entry Text/Timestamp	Y	N
Power Changes Narrative log entry Text/Timestamp	Y	N

Appendix C

Multi-Kernel Support Vector Machine

Support vector machine (SVM) is a discriminative classifier that finds a maximum margin hyperplane in a high dimensional space that has longest distance between data points of both the classes. The orientation and position of the hyperplane are influenced by the data points on the hyperplane called as support vectors (SVs). Figure C- 1 shows the representative diagram of a hyperplane and its components in SVM. For the input feature $x \in X$ with label $y \in Y$, the mathematical expression for a hyperplane is

$$w\phi(x) + b = 0 \tag{C1}$$

Here w is the weight vector, b is the intercept, and $\phi(\cdot)$ is a kernel function (which will be discussed ahead). An i^{th} feature vector, $x_i \in X$ falling on either side of the hyperplane is described as

$$If\ Y_i = +1 : w\phi(x_i) + b \geq 1 - \xi_i$$
$$If\ Y_i = -1 : w\phi(x_i) - b \geq 1 + \xi_i \tag{C2}$$

Parameter ξ_i is a slack variable, which allows certain data points to be within the margin.

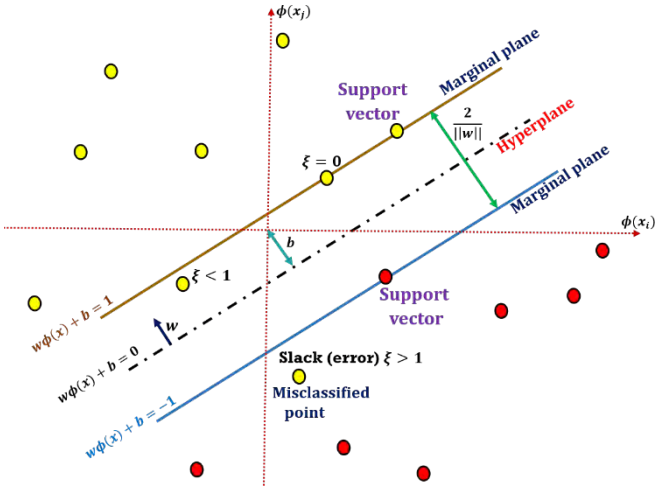

Figure C- 1. SVM hyperplane and its components.

Using (4), the general expression for a soft-margin classifier in dual form with regularization parameter, C is given by:

$$\max_{\alpha} \sum_{i,j} \alpha_i - \frac{1}{2} \sum_{i,j} \alpha_i \alpha_j Y_i Y_j K(x_i, x_j)$$
$$s.t. \sum_{i} \alpha_i Y_i = 0$$
$$C \geq \alpha_i \geq 0, \forall_i, \forall_j \tag{C3}$$

where α is a Lagrange multiplier, and $K(x_i, x_j) = \phi(x_i) \cdot \phi(x_j)$ is a kernel function, where x_i and x_j are ith and jth samples. The kernel function such as Gaussian kernel maps non-linearly separable datapoints to a higher dimension, where data points can be linearly separable. The Gaussian kernel is defined as [8]:

$$K = e^{\left(-\gamma\left||x_i - x_j|\right|^2\right)} \tag{C4}$$

The parameter γ determines the influence of single training data point. With the low value of γ, the data points far from the plausible decision plane are considered calculating hyperplane, otherwise only the datapoints closer to the decision plane are considered. On the other hand, the regularization parameter, C controls the extent to which the datapoint misclassification is avoided. For a large value of C, optimization picks a thin-margin hyperplane if that hyperplane can mis-classify least number of datapoints. Conversely, for a small value of C, the optimization tries to find a large-margin hyperplane even if that hyperplane misclassifies more datapoints.

With the kernel function, the soft margin decision function for SVM is defined by:

$$\mathrm{f(x)} = \sum_{\mathrm{i=1}}^{\mathrm{n}} \alpha_\mathrm{i} y_\mathrm{i} \mathrm{K}(\mathrm{x_i}, \mathrm{x_j}) + \mathrm{b} \tag{C5}$$

Let $[X]_{m \times n}$ is the data matrix with m samples and n features. The sample set can be vertically partitioned based on the feature type. The multi-kernel SVM across vertically partitioned sample set can be determined by computing a net kernel matrix (also called as gram matrix) $K = K(x_i, x_j)$ from individual matrices determined from each vertically partitioned samples. The $[X]_{m \times n}$ data matrix can be vertically partitioned into A^1 and A^2 (assume only 2 partitions). Then X^1 and X^2 will have $K^1 = K(X^1, {X^2}^T)$ and $K^2 = K(X^2, {X^2}^T)$ as the gram matrices, respectively. Then the net gram matrix can be combined as the linear combination of individual gram matrices. Let $(i, j)^{th}$ element of K is $K(x_i, x_j)$ and x_i^1 and x_i^2 be vertically partitioned vectors of x_i from X^1 and X^2, respectively. Accordingly,

$$K(x_i, x_j) = K(x_i^1, x_j^1) + K(x_i^2, x_j^2)$$
$$\therefore \quad K(X, X^T) = K^1 + K^2 = K\left(X^1, {X^2}^T\right) + K\left(X^2, {X^2}^T\right) \tag{C7}$$

The net gram matrix can also be obtained by weighted summation of individual kernels. Hence for M vertical partitions, equation (7) can be generalized as:

$$K(X, X^T) = \beta_1 K^1 + \beta_2 K^2 + \cdots + \beta_M K^M = \sum_i^M \beta_i K\left(X^i, {X^i}^T\right) \tag{C8}$$

where β_i is the weight associated with each local gram matrix and $\sum_i^M \beta_i = 1$. Using the net kernel matrix be applied in equation (3) and SVM model parameters can be obtained by solving a quadratic programming. Note that each gram matrix will be a square matrix. The similar approach can be extended to federated learning across *P* parties, where a global (master) gram matrix can be generated by weighted sum of net kernel matrix K_t(determined in equation [8]), for $t = [1,2, \ldots, P]$. The formulation to generate global gram matrix can be given by:

$$K_g(X, X^T) = \sum_t^P p_t K_t(X, X^T) \tag{C9}$$

where p_t is the weight associated with each net gram matrix and $\sum_t^P p_t = 1$. Substituting equation (8) in (9), we get

$$K_g(X, X^T) = \sum_t^P p_t \sum_i^M \beta_i K_t \left(X^i, X^{i^T}\right) \quad \text{(C10)}$$

The global gram matrix will be shared with each party. Then, using global gram matrix in equation (3), each party can obtain the SVM model parameters by solving a quadratic programming.